Texas Salt Domes--Aspects Affecting Disposal of Toxic-Chemical Waste in Solution-Mined Caverns

S. J. Seni
W. F. Mullican III
H. S. Hamlin

Contract Report for Texas Department of Water Resources
under Interagency Contract No. IAC(84-85)-1019

Bureau of Economic Geology
W. L. Fisher, Director
The University of Texas at Austin
University Station, P. O. Box X
Austin, Texas 78713

TEXAS SALT DOMES--ASPECTS AFFECTING DISPOSAL OF TOXIC-CHEMICAL WASTE IN SOLUTION-MINED CAVERNS

TABLE OF CONTENTS

FIGURE CAPTIONS

Figure 1. Distribution of Texas salt domes and salt provinces in relation to major fault zones and the Stuart City and Sligo reef trends.

Figure 2. Block diagrams of salt domes and structure on top of Cretaceous and Tertiary units in Houston Embayment (modified from Ewing, in preparation).

Figure 3. Block diagram of salt domes and structure of top of Woodbine Group in East Texas Basin (from Jackson and Seni, 1984b).

Figure 4. Structure contour map, Frio Formation around Boling, Markham, and Damon Mound salt domes. Salt-withdrawal basin for Boling dome is closed structural depression southeast of Boling dome. Regional growth faults intercept the northeast flank of Boling dome and the southwest flank of Markham dome.

Figure 5. Cross section, Boling dome and flanking strata. Salt-withdrawal basin has abundant faults in Vicksburg, Jackson, Frio, and Anahuac Formations. Top of Miocene is depressed 500 ft over salt-withdrawal basin owing to post-Miocene (younger than 5 Ma) salt flow into Boling dome.

Figure 6. Cross section, Markham dome and flanking strata. Salt-withdrawal basin is a structural sag north of dome. Major faults are absent in this orientation of cross section.

Figure 7. East-west cross section, Barbers Hill dome and flanking strata. Faulting is common through Frio and Anahuac Formations and at base of Miocene strata. Cap rock is surrounded by Evangeline aquifer.

Figure 8. North-south cross section, Barbers Hill dome and flanking strata. Faulting is common from base of Miocene to deepest control. Faults are typical down-to-the-coast (south) regional growth faults. Salt-withdrawal basin is north of dome.

Figure 9. Isopach map, Miocene and post-Miocene strata, area around Boling, Markham, and Damon Mound domes. Miocene and post-Miocene strata are 2,000 ft thicker in salt-withdrawal basin southeast of Boling dome owing to extensive syndepositional salt flow into Boling dome.

Figure 10. Isopach map, Anahuac Formation, area around Boling, Markham, and Damon Mound domes. Anahuac Formation is approximately 100 percent (600 ft) thicker in salt-withdrawal basin southeast of Boling dome owing to extensive syndepositional salt flow into Boling dome.

Figure 11. Cross section showing map intervals and correlations.

Figure 12. Idealized creep curve depicting behavior of rock salt. Transient (primary), steady-state (secondary), and accelerating (tertiary) stages of creep are separated by inflection points in the curve. The creep curve terminates at the point of brittle (sudden) failure by creep rupture.

Figure 13. In situ creep shown by convergence of floor and ceiling in an underground salt mine (after Empson and others, 1970). Heating of a nearby mine pillar causes acceleration of the rate of convergence.

Figure 14. Creep curve for artificially prepared salt showing the effect of temperature, confining pressure, and axial stress (after Le Comte, 1965).

Figure 15. Creep curves for Avery Island dome salt deformed at temperatures from 24^{o}C to 200^{o}C and stresses from 10.3 MPa to 20.7 MPa. Confining pressures were 3.5 MPa or above (data from Hansen and Mellegard, 1979; Hansen and Carter, 1979, 1980; after Carter and Hansen, 1983).

Figure 16. Stress-strain curve for bedded and dome salt deformed by a differential stress rate of 0.006 MPa to 0.023 MPa s^{-1} and a confining pressure of 3.45 MPa. There is no systematic variation in creep behavior between bedded and domal salt. However, bedded salt from Lyons, Kansas, is the most creep resistant salt of those tested (after Hansen and Carter, 1980).

Figure 17. Creep curve for artificially prepared salt showing the effect of variations in grain size and axial stress on the creep behavior (after Le Comte, 1965).

Figure 18. Strain rate curve for artificially prepared salt deformed at high temperature (1013 K). Strain rates with a constant stress show a significant increase due to increases in grain size and subgrain size (cited by Hume and Shakoor, 1981; after Burke, 1968).

Figure 19. Convergence in Canadian potash mine as a function of time. Long-term convergence is nearly constant (after Baar, 1977).

Figure 20. Borehole closure of (A) Vacherie and (b) Rayburns salt domes (after Thoms and others, 1982).

Figure 21. Strain rate curve for borehole closure at Vacherie salt dome based on borehole closure data from Thoms and others (1982). Linear closure data were converted to strain data base on a nominal hole diameter of 8-3/4 inches. Strain rates were derived using four points for time control (that is, 0, 163, 413, and 890 days after drilling; see figure 20). At a given depth, strain rates were remarkably linear. Differential stresses were derived from the difference between the lithostatic load exerted by the salt and the load exerted by the borehole filled with saturated brine. Note the exponential increase in strain rate with increasing differential stress or depth.

Figure 22. Exponential creep law behavior (after Herrmann and Lauson, 1981a).

Figure 23. Logarithmic creep law behavior (after Herrmann and Lauson, 1981a).

Figure 24. Power law creep behavior (after Herrmann and Lauson, 1981a).

Figure 25. Predicted long-term closures using different creep law forms (after Wagner and others, 1982).

Figure 26. Deformation-mechanism map for salt, including probable repository and storage cavern conditions in cross-hatchured area. Grain size is constant at 3 mm. Solid lines between regimes are confirmed by experimental evidence;

boundaries shown as dashed lines are based on calculations of constitutive equations; boundaries shown as dotted lines are based on interpolation or extrapolation; questions marks on boundaries mean the location is based on conjecture only (after Munson, 1979).

Figure 27. Cross section, Bryan Mound dome, showing core locations and foliation. Angle of foliation decreases from vertical in deepest core to 20 to 30 degrees from vertical (no azimuth orientation) in shallow core. Flow direction is inferred to change from near vertical in deep parts of stock to more lateral flow in upper parts of stock.

Figure 28. Photographs of core, Bryan Mound dome, showing variations in grain size and foliation. Core 1A at -1,848 ft is well bedded with dark anhydrite layers and unfoliated; core 110C at -4,173 ft shows no bedding and vertical foliation.

Figure 29. Photographs of core from cap rock, A. Long Point dome, showing mineralogical variations and fractures, B. Long Point dome showing sulfur and fractures, C. Boling dome showing sulfur and vugs.

Figure 30. Map of cap-rock injection zones, Barbers Hill dome. Injection into shallow cap rock is over central part of dome, whereas injection into basal anhydrite sand is around periphery of dome.

Figure 31. Cross section, Barbers Hill dome, and cap rock showing lost-circulation zones and stylized cavern geometries. Appendix 1C lists cavern and injection well names.

TABLE CAPTIONS

Table 1. Growth rates for Boling salt dome.

Table 2. Strain rates for deformation of rock salt (modified from Jackson, 1984).

Table 3. Analysis of salt core--Bryan Mound salt dome.

APPENDICES

INTRODUCTION

This report is Phase II of a one-year contract to analyze technical issues associated with the proposed isolation of toxic-chemical waste in solution-mined caverns in Texas salt domes. A major goal of Phase II research was characterizing properties of salt domes which could affect this type of waste disposal.

Organization

This report is organized along two parallel themes: (1) investigations of dome-related strata--their stratigraphy, structure, and geohydrology and (2) investigations of dome material--salt, cap rock, and mechanical properties of salt. Each theme begins with a regional focus and continues with increasingly narrow investigations.

In Phase II we have (1) block diagrammed regional structure around domes in the Houston diapir province and the East Texas diapir province; (2) mapped and sectioned the structure and stratigraphy locally around four Texas domes; (3) reviewed published data on mechanical properties of salt, concentrating on creep properties; and (4) analyzed site-specific data on cap rocks and salt in 20 cores from six salt domes.

During Phase I, a statewide dome data base was established (Seni and others, 1984b) and natural resources associated with Texas salt domes were detailed with emphasis on brine and storage-cavern industries (Seni and others, 1984a).

Recommendations

It is not possible to fully evaluate in one year all possible technical issues associated with waste disposal in domes. We have concentrated on those issues with the greatest importance and those which could be completed in the allotted time. A complete characterization of a salt dome for the purposes of waste isolation requires detailed site-specific data on relevant properties of salt, cap rock, and surrounding strata and quantitative data on the hydrogeologic system within the cap rock and the associated strata.

A strong and expanding storage industry is one indication that waste storage in solution-mined caverns in salt is technically feasible. However, long-term (greater than 50 years) containment has not been demonstrated. Critical weak points in a waste-containment system are at the intersection of the cement-casing string and the cap-rock lost-circulation zones. The security of a waste-containment scheme is enhanced by (1) maximizing the number of cemented casing strings, (2) maximizing the safety zone of (a) undisturbed salt around the storage cavern and (b) undisturbed strata around the salt dome, (3) maximizing the viscosity of waste by solidification, (4) minimizing the pressure differential within and outside the cavern, (5) minimizing the contact between the waste-containment system and lost-circulation zones, (6) minimizing contact between the host salt dome and circulating ground water, and (7) choosing a host dome with minimum dome growth rates over the recent geologic span of history.

STRUCTURE, STRATIGRAPHY, AND GROWTH HISTORY

The growth of salt domes typically has a profound influence on the structure, stratigraphy, and depositional systems of surrounding strata. Critical data on the timing of dome growth, rates and volumes of salt flow, and potential for future growth or stability are available through careful analysis of the influence that dome growth has on surrounding strata. Structural, stratigraphic, and depositional systems analysis each provides a part of this information. However, this technique represents only one approach to reliably predicting the future stability of salt domes or interior caverns. Clearly, aspects of hydrologic stability and geomechanical stability must be integrated to reliably predict future stability.

Structure

Dome growth usually distorts both the local and regional structure around a dome. However, the structural distortion can be very minimal during periods of nongrowth, relatively slow growth, or when the salt source layer has been exhausted. Structurally high areas form over the dome crest and flanks owing to relative upward flow of salt and shear-zone drag. Salt-withdrawal basins are structurally depressed areas that form above zones from which salt is flowing to feed rising diapirs.

A single dome may cause both uplift and subsidence of supradomal strata in different areas of the dome crest. Jackson and Seni (1984a) note that the structural attitude of strata on dome flanks is in part a function of the stage of dome growth and the slope of the sides of the salt stock. The dip of strata around domes commonly varies systematically with increasing depth from dip up toward the dome at the shallow horizons, through horizontal dip, to dip down toward the dome for the deeper strata. The plane where strata near the dome are horizontal or at regional dip is inferred to mark the termination of the stage of active diapiric growth owing to exhaustion of the salt source layer. Apart from shear-zone drag, there is no longer a mechanism to cause the dip of surrounding strata to deviate from regional norms when the salt-source layer is exhausted.

Regional structural patterns around salt domes in the Houston diapir province are illustrated in map view and in a block diagram in figures 1 and 2. Figure 3 is a similar block diagram for domes in the East Texas salt diapir

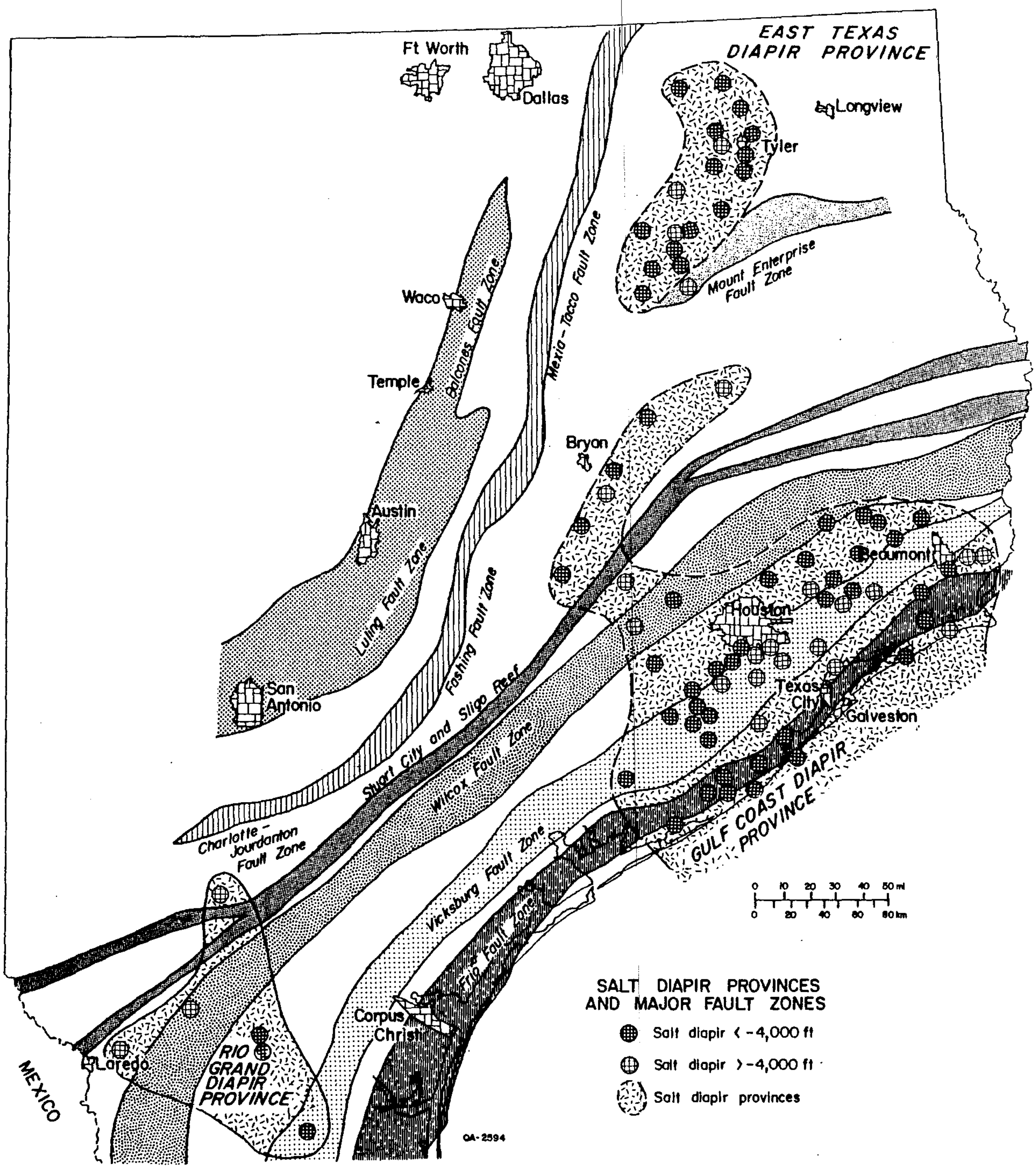

Figure 1. Distribution of Texas salt domes and salt provinces in relation to major fault zones and the Stuart City and Sligo reef trends.

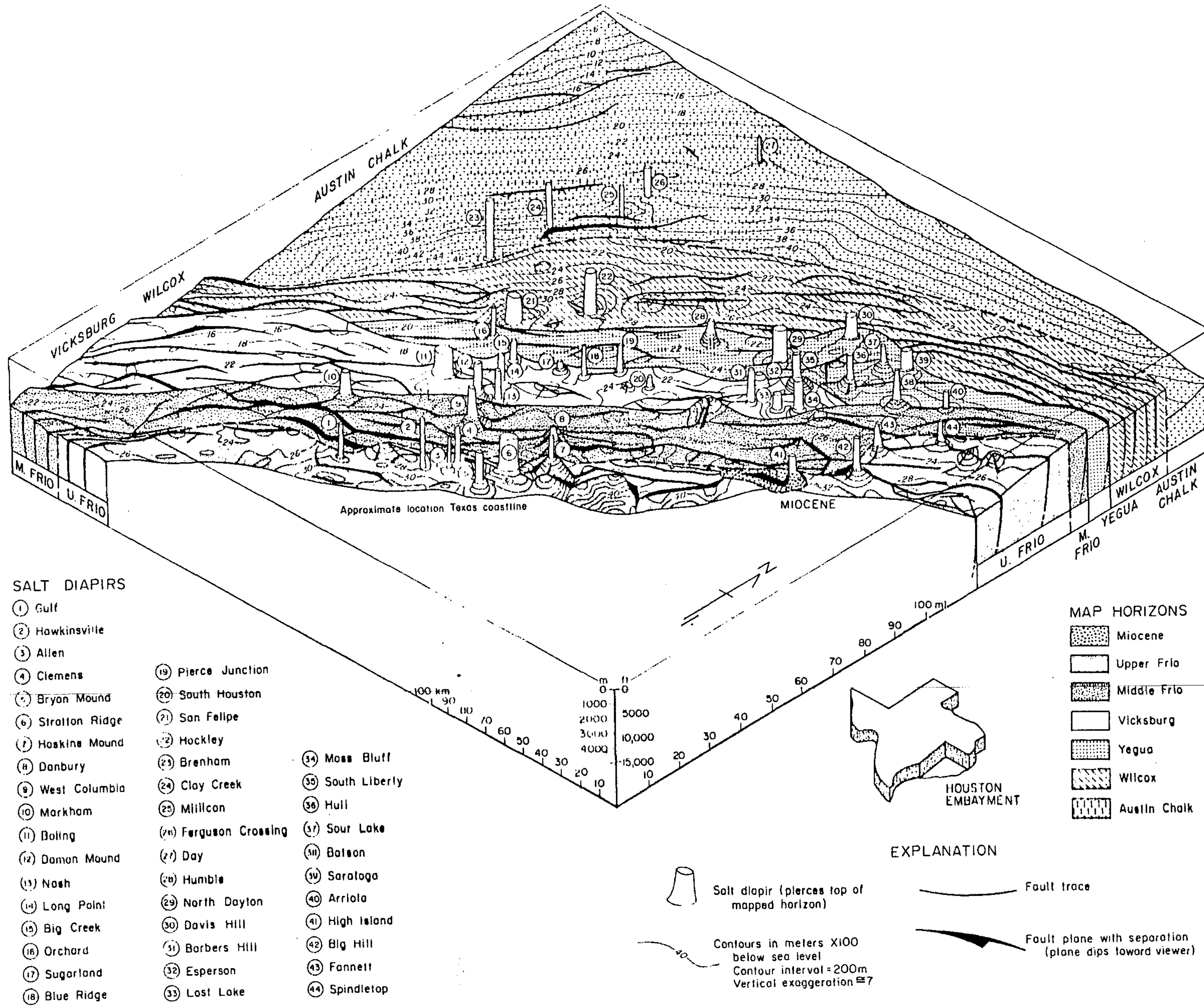

Figure 2. Block diagrams of salt domes and structure on top of Cretaceous and Tertiary units in Houston Embayment (modified from Ewing, in preparation).

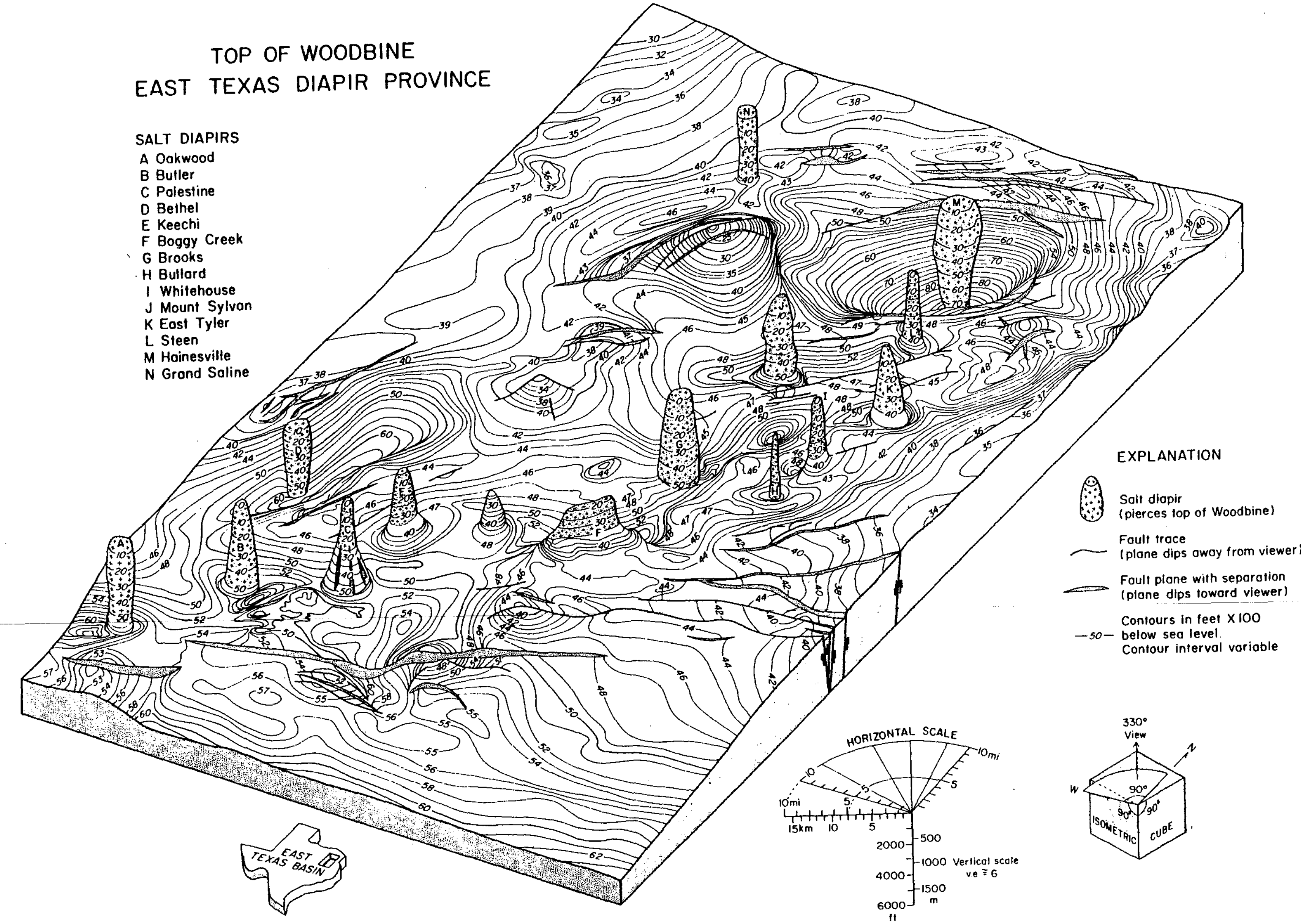

Figure 3. Block diagram of salt domes and structure of top of Woodbine Group in East Texas Basin (from Jackson and Seni, 1984b).

province. Most of the larger faults in the Houston salt diapir province are down-to-the-coast, normal, growth faults. The smaller faults around domes are radial-tear or trap-door faults. The relationship between regional growth faults and salt domes is enigmatic (Ewing, 1983). Whether there is a cause-effect relationship between growth faults and salt diapirism is disputed. Several aspects of salt domes in the Houston diapir province argue against a cause-effect relationship. The regional, parallel, growth-fault trends are highly developed and regularly spaced in the Coastal Bend area, an area without salt domes. But, in the Houston diapir province the fault patterns become more random and fault segments are shorter. There is no strong linear parallel orientation of groups of domes that might be attributed to control of dome distribution by faults or vice versa. The strongest linear arrangement of domes is displayed by the Brenham, Clay Creek, Mullican, Ferguson Crossing, and Day salt domes. These domes are oriented about 30 degrees North of the orientation of regional strike and of the strike of local faults. Note also that these domes have the least effect on the structure of surrounding strata (Austin Chalk). These domes may have terminated the active stage of diapir growth by exhausting their salt source layer in the late Cretaceous.

Major growth faults appear to randomly intercept some domes and to avoid others. Major growth faults intercept Boling, Markham, Hockley, Barbers Hill, Fannett, and Big Hill salt domes. On the other hand, major growth faults are isolated from Damon Mound, Gulf, Allen, Clemens, Big Creek, South Houston, Moss Bluff, Lost Lake, Saratoga, North Dayton, Davis Hill and Arriola salt domes.

The local structure around Boling, Markham, and Damon Mound domes is mapped at the top of the Frio in figure 4. Appendix 1A lists all wells in figures 4, 9, and 10. Major regional faults clearly intercept both Boling and Markham domes but only small radial faults intercept Damon Mound dome. The large oval depression southeast of Boling dome is a salt-withdrawal basin.

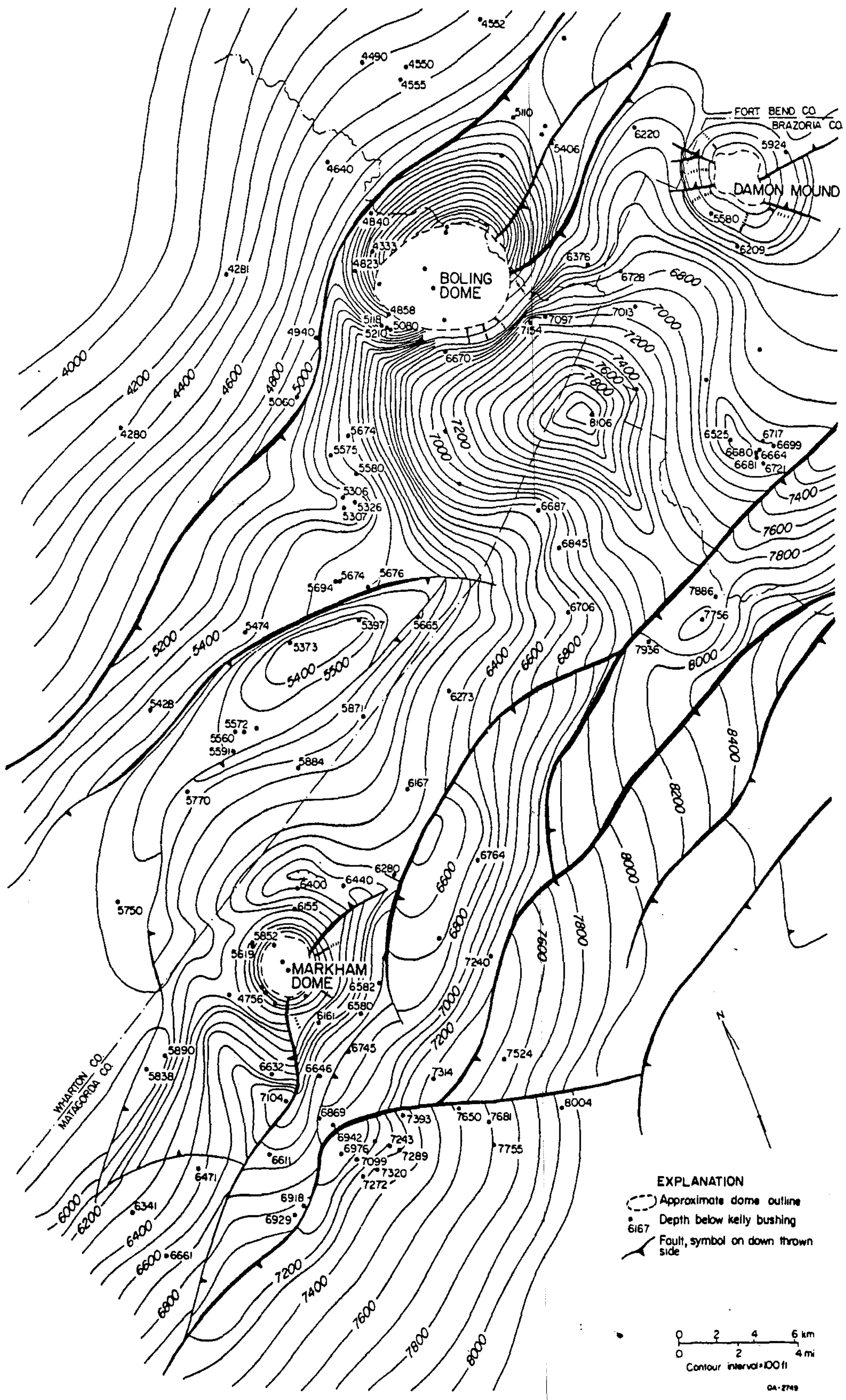

Figure 4. Structure contour map, Frio Formation around Boling, Markham, and Damon Mound salt domes. Salt-withdrawal basin for Boling dome is closed structural depression southeast of Boling dome. Regional growth faults intercept the northeast flank of Boling dome and the southwest flank of Markham dome. Map shows extent of coverage in Fort Bend, Wharton, Matagorda, and Brazoria Counties.

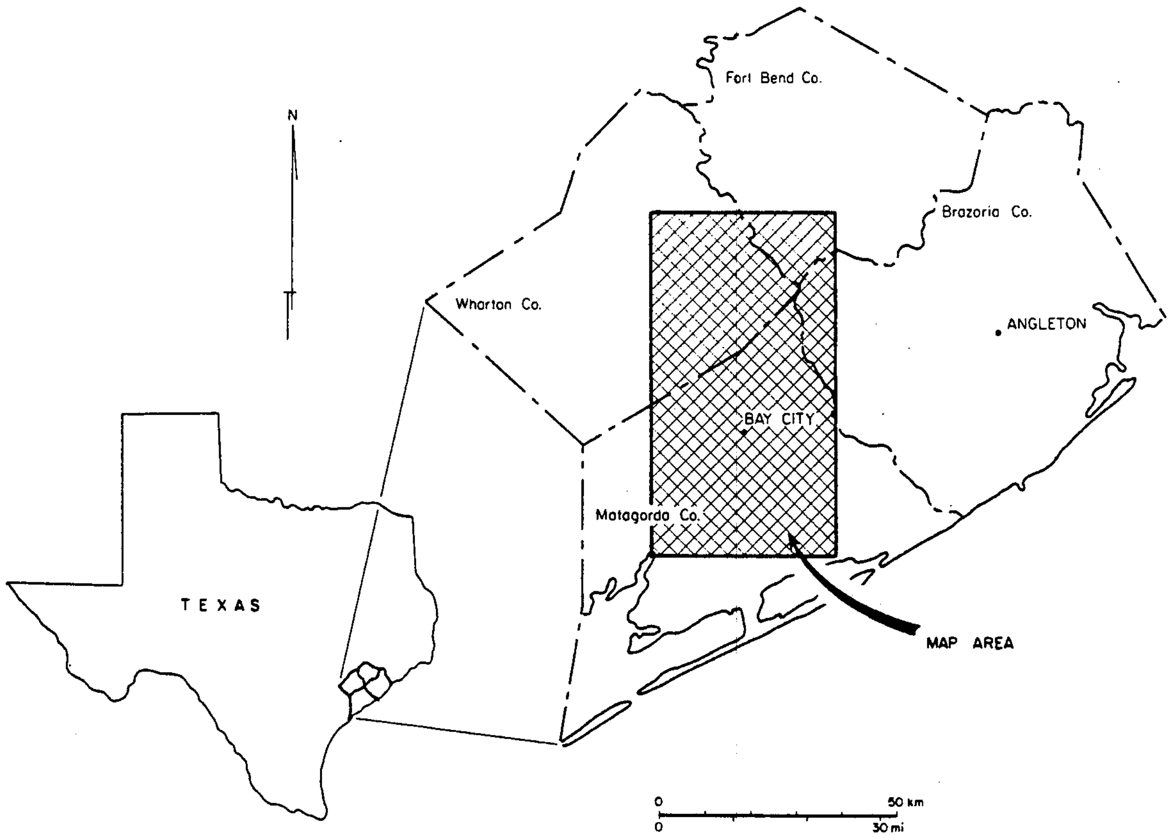

N
Fort Bend Co.
Brazoria Co.
Wharton Co.
ANGLETON
BAY CITY
Matagorda Co.
TEXAS
MAP AREA
0
50 km
0
30 mi

(continued)

Because this structure affects the top of the Frio, the structure must be post-Frio in age.

Radial faults are probably associated with all domes. Only with dense subsurface well or seismic control can the orientation and distribution of these minor faults be determined. Local structure around Boling, Markham, and Barbers Hill domes is also shown in cross section in figures 5, 6, 7, and 8. Appendix 1B lists all wells on cross sections in figures 5, 6, 7, and 8. Salt-withdrawal basins are clearly visible north of Markham, and Barbers Hill domes and southeast of Boling dome. Together with isopach maps, stratigraphic data can be used to help deduce the timing of dome growth.

Stratigraphy

Miocene and post-Miocene strata (fig. 9) and the Anahuac Formation (fig. 10) were mapped around Boling, Markham, and Damon Mound domes. The map interval and correlations are shown in figure 11. Isopach maps are particularly powerful tools for determining the timing of dome growth because syndepositionaly growth directly influences isopach patterns and these thickness patterns are preserved in the stratigraphic record with a minimum of complications (Seni and Jackson, 1983a; 1984). Figures 9 and 10 illustrate a large salt-withdrawal basin covering approximately 130 km^2 (50 mi^2) southeast of Boling dome. The isopachous thickening was active during deposition of Anahuac, Miocene, and post-Miocene strata. In contrast, Markham dome has only minor thickening in an ill-defined salt withdrawal basin north and northeast of the dome. The well-formed basin by Boling dome indicates more vigorous growth of Boling dome than for Markham dome during the same time interval.

VE = 20x

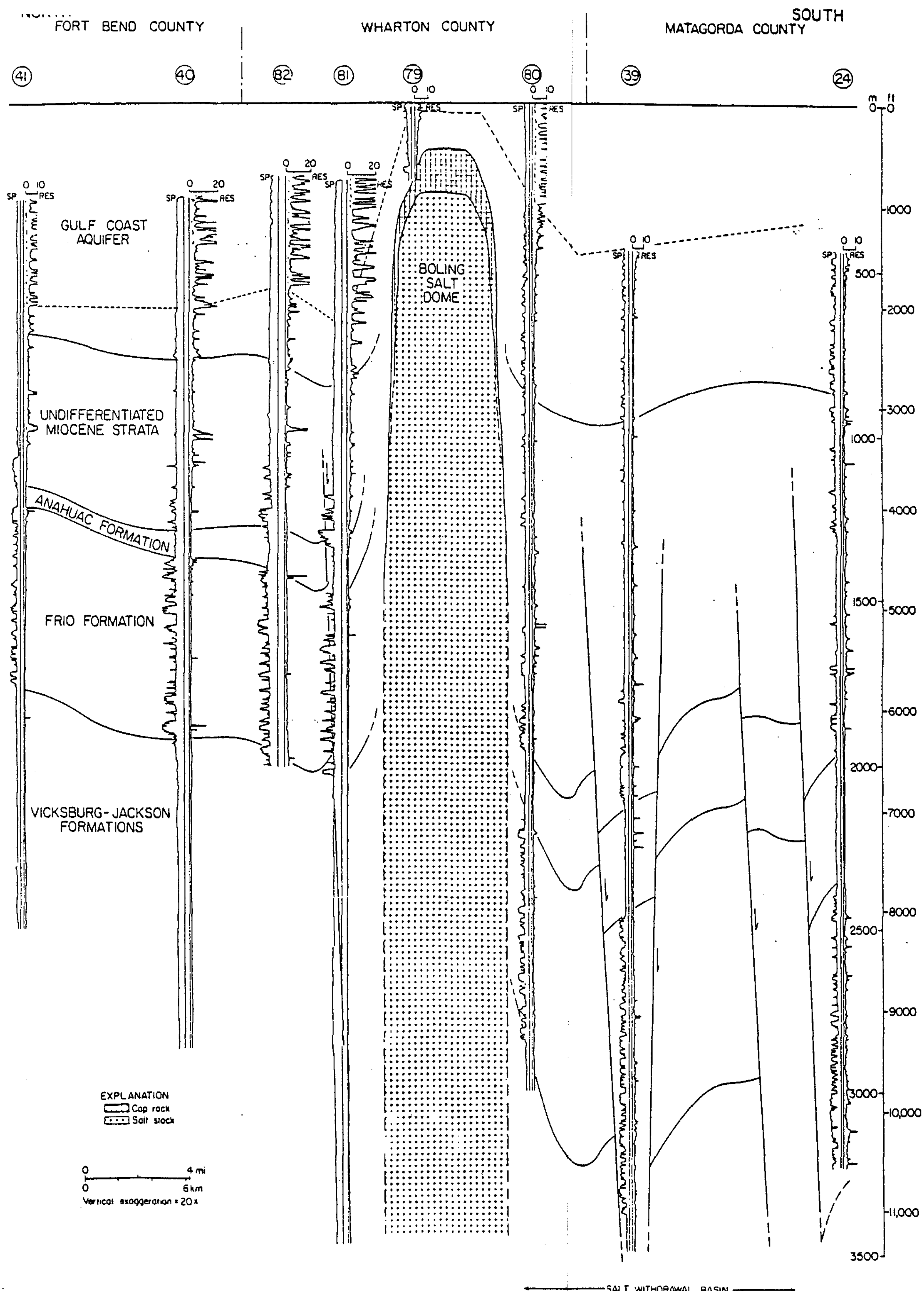

Figure 5. Cross section, Boling dome and flanking strata. Salt-withdrawal basin has abundant faults in Vicksburg, Jackson, Frio, and Anahuac Formations. Top of Miocene is depressed 500 ft over salt-withdrawal basin owing to post-Miocene (younger than 5 Ma) salt flow into Boling dome. Map shows location of wells.

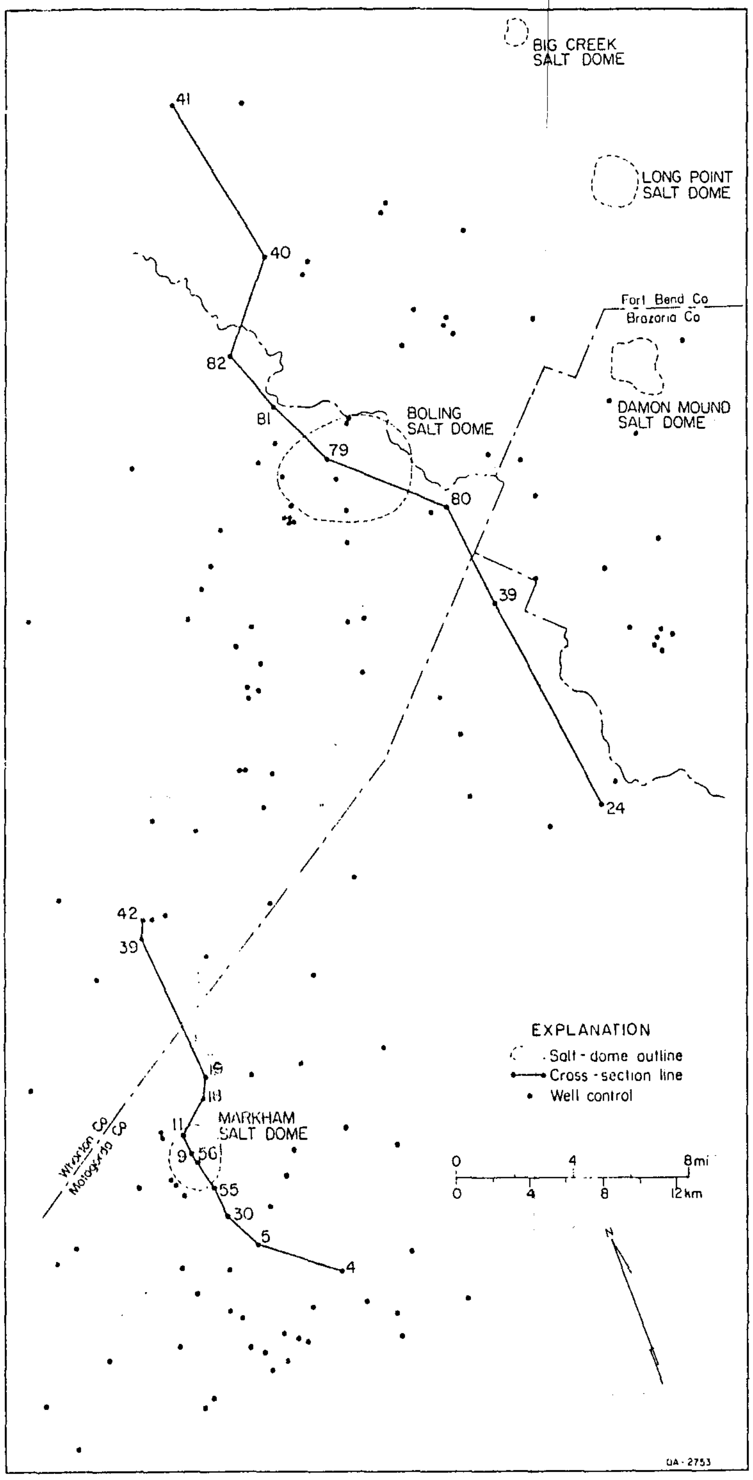
BIG CREEK SALT DOME
LONG POINT SALT DOME
Fort Bend Co
Brazoria Co
DAMON MOUND SALT DOME
BOLING SALT DOME
MARKHAM SALT DOME
Wharton Co
Matagorda Co
41
40
82
81
79
80
39
24
42
39
19
18
11
9
56
55
30
5
4
EXPLANATION
Salt-dome outline
Cross-section line
Well control
0 4 8 mi
0 4 8 12 km
N
DA-2753

(continued)

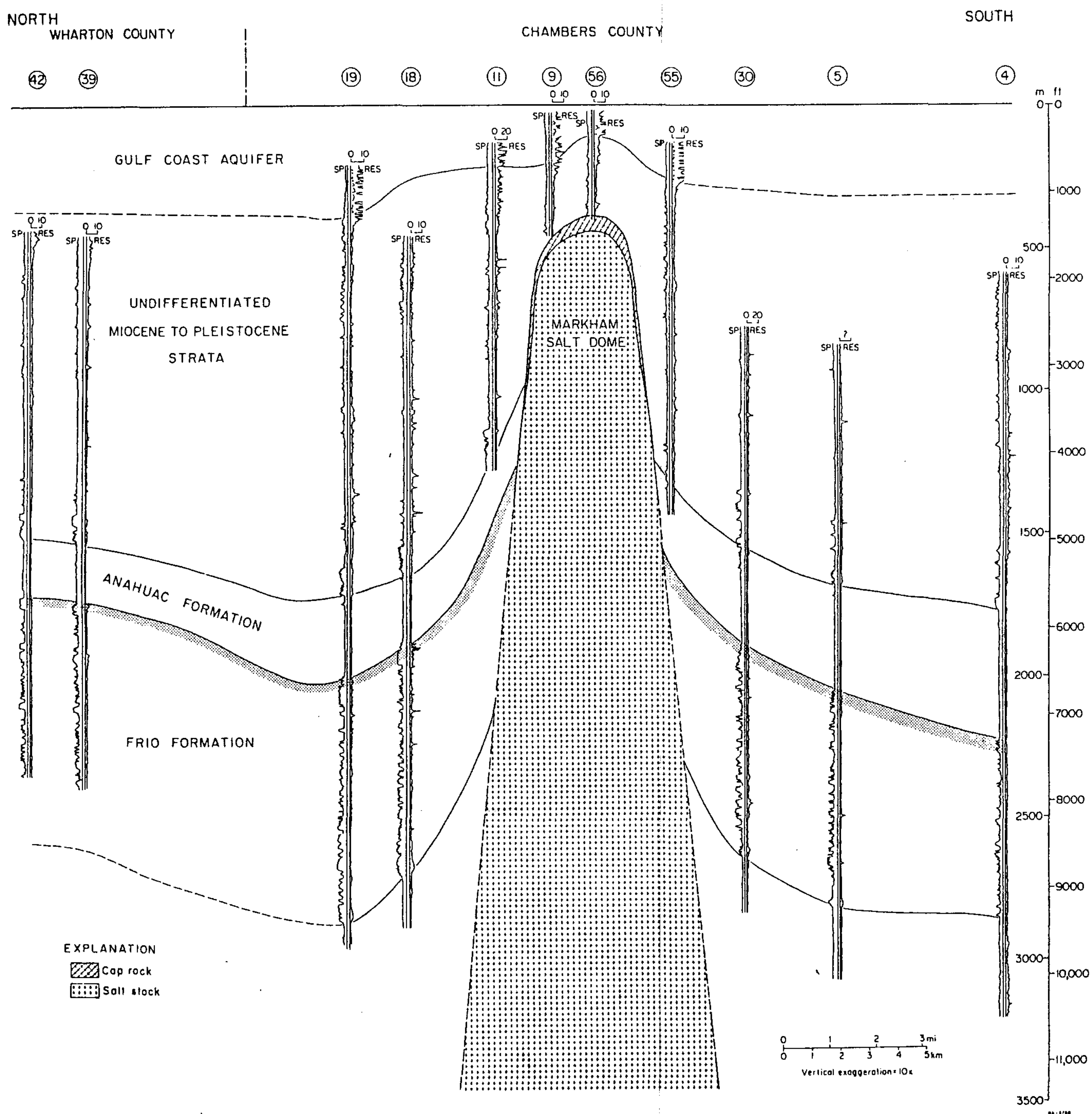

Figure 6. Cross section, Markham dome and flanking strata. Salt-withdrawal basin is a structural sag north of dome. Major faults are absent in this orientation of cross section. See figure 5 for map showing location of wells.

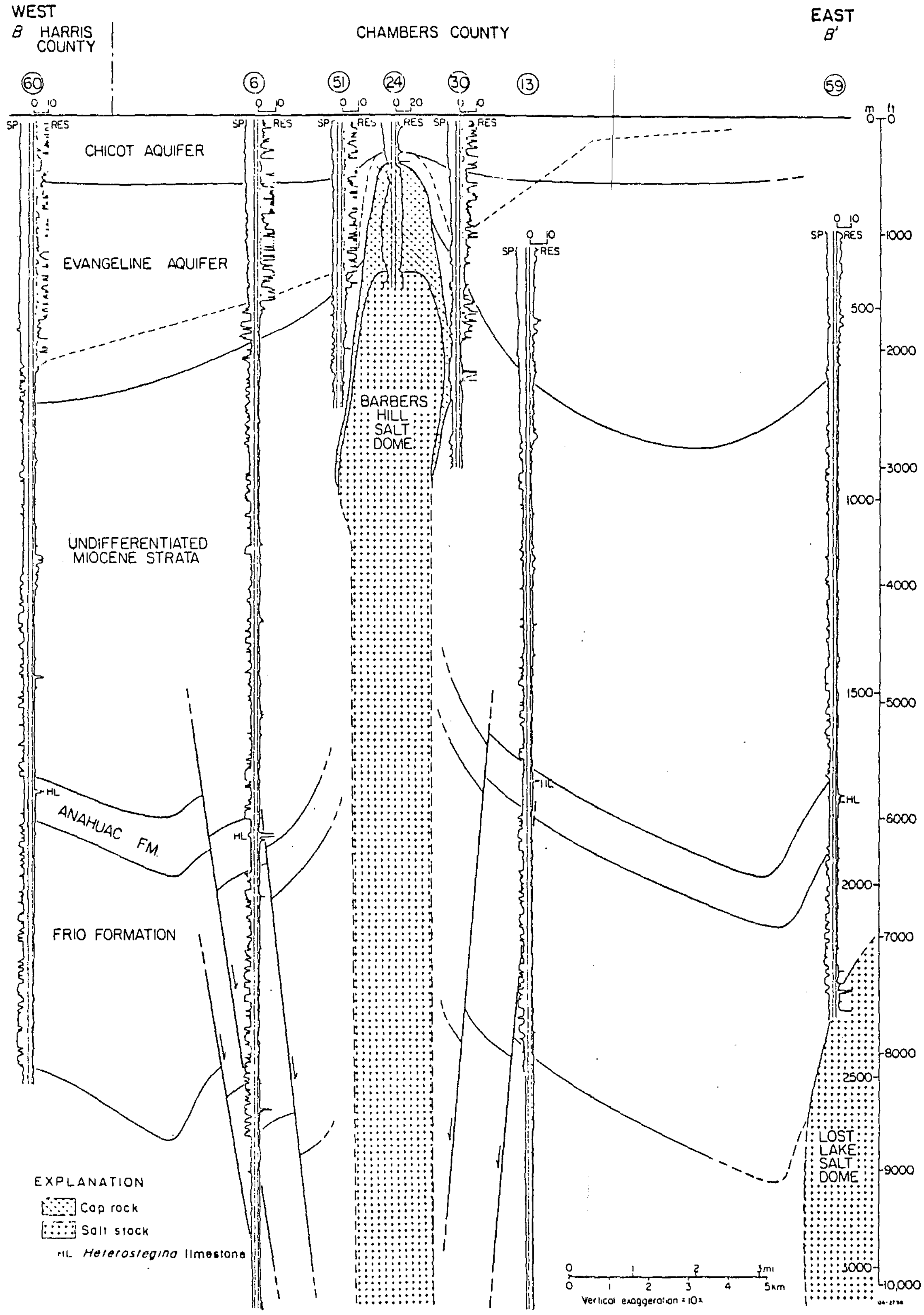

Figure 7. East-west cross section, Barbers Hill dome and flanking strata. Faulting is common through Frio and Anahuac Formations and at base of Miocene strata. Cap rock is surrounded by Evangeline aquifer. Map shows location of wells.

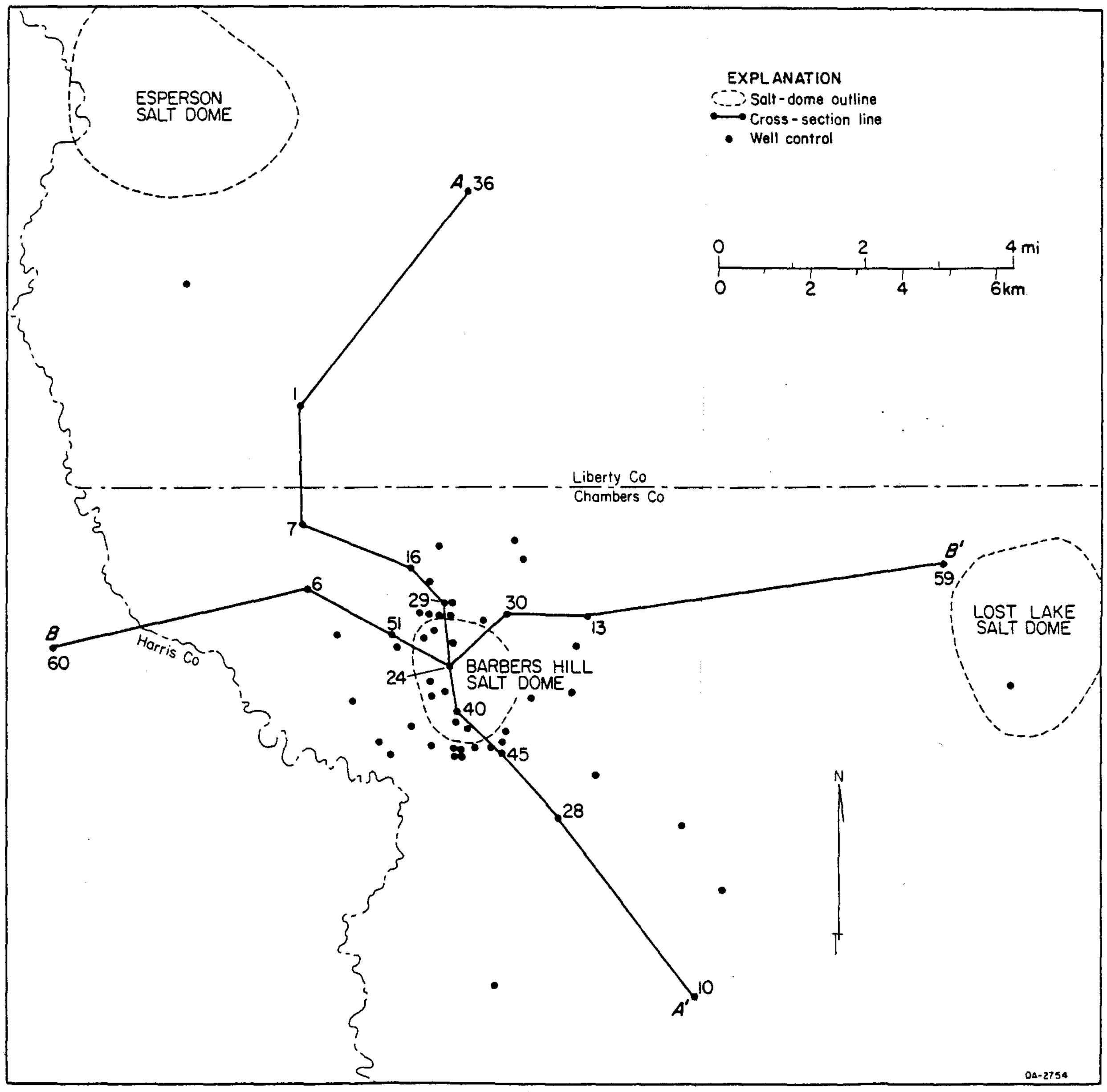

ESPERSON SALT DOME
EXPLANATION
Salt-dome outline
Cross-section line
Well control
A 36
0 2 4 mi
0 2 4 6km
1
Liberty Co
Chambers Co
7
16
B'
59
29
30
13
6
51
LOST LAKE SALT DOME
B
60
Harris Co
24
BARBERS HILL SALT DOME
40
45
28
N
10
A'
OA-2754

(continued)

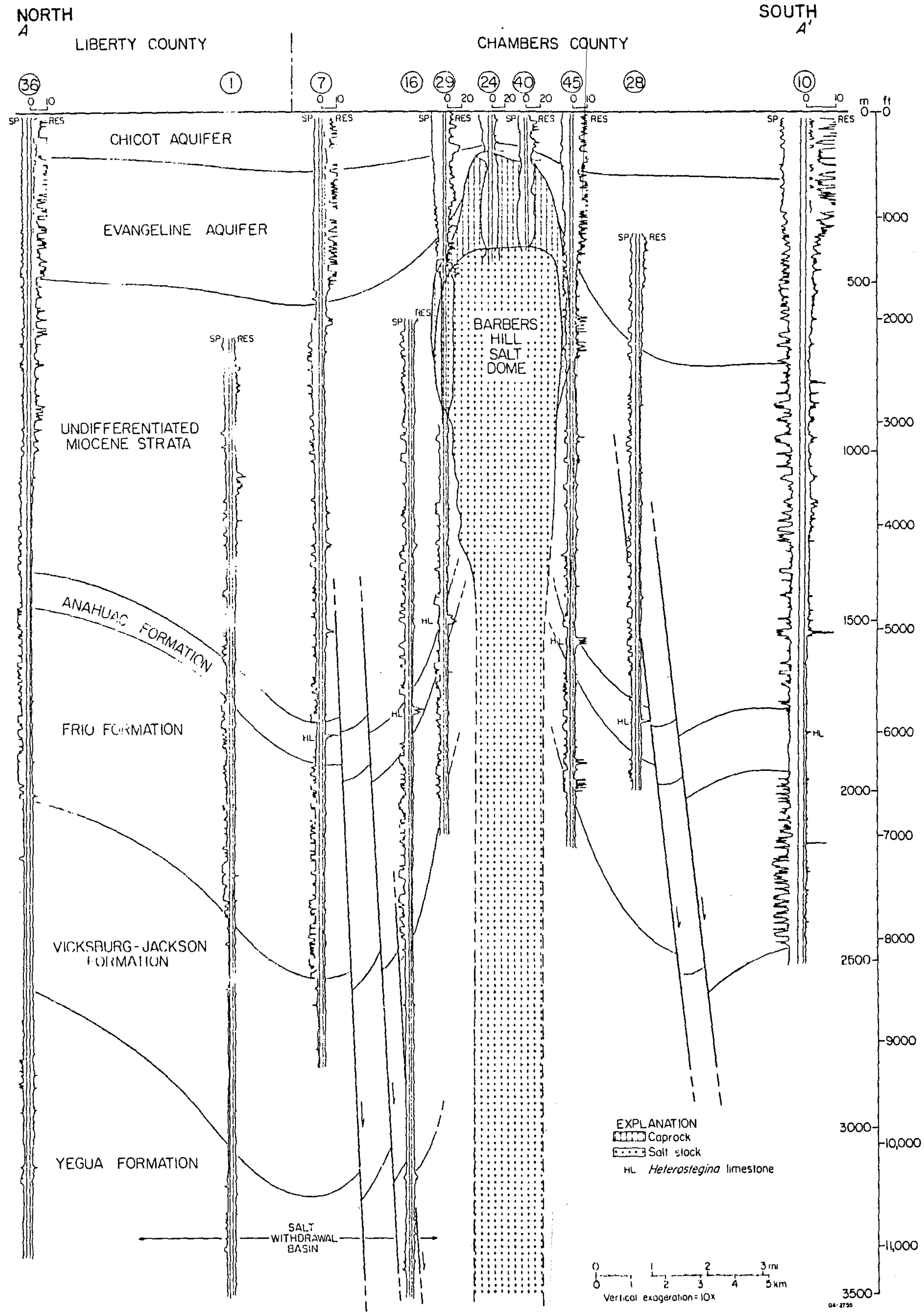

Figure 8. North-south cross section, Barbers Hill dome and flanking strata. Faulting is common from base of Miocene to deepest control. Faults are typical down-to-the-coast (south) regional growth faults. Salt-withdrawal basin is north of dome. See figure 7 for map showing location of wells.

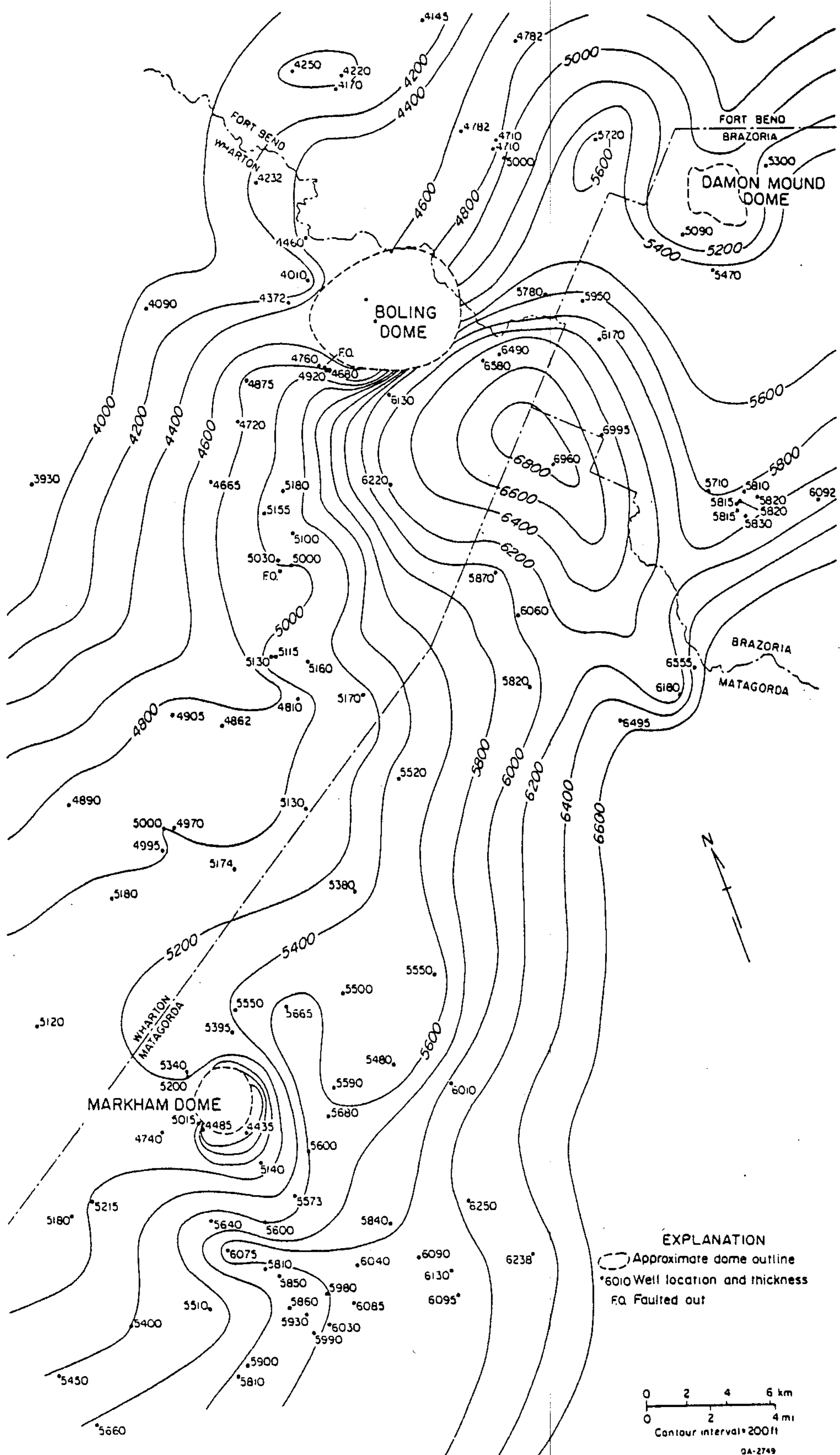

Figure 9. Isopach map, Miocene and post-Miocene strata, area around Boling, Markham, and Damon Mound domes. Miocene and post-Miocene strata are 2,000 ft thicker in salt-withdrawal basin southeast of Boling dome owing to extensive syndepositional salt flow into Boling dome. See figure 4 for mapped area.

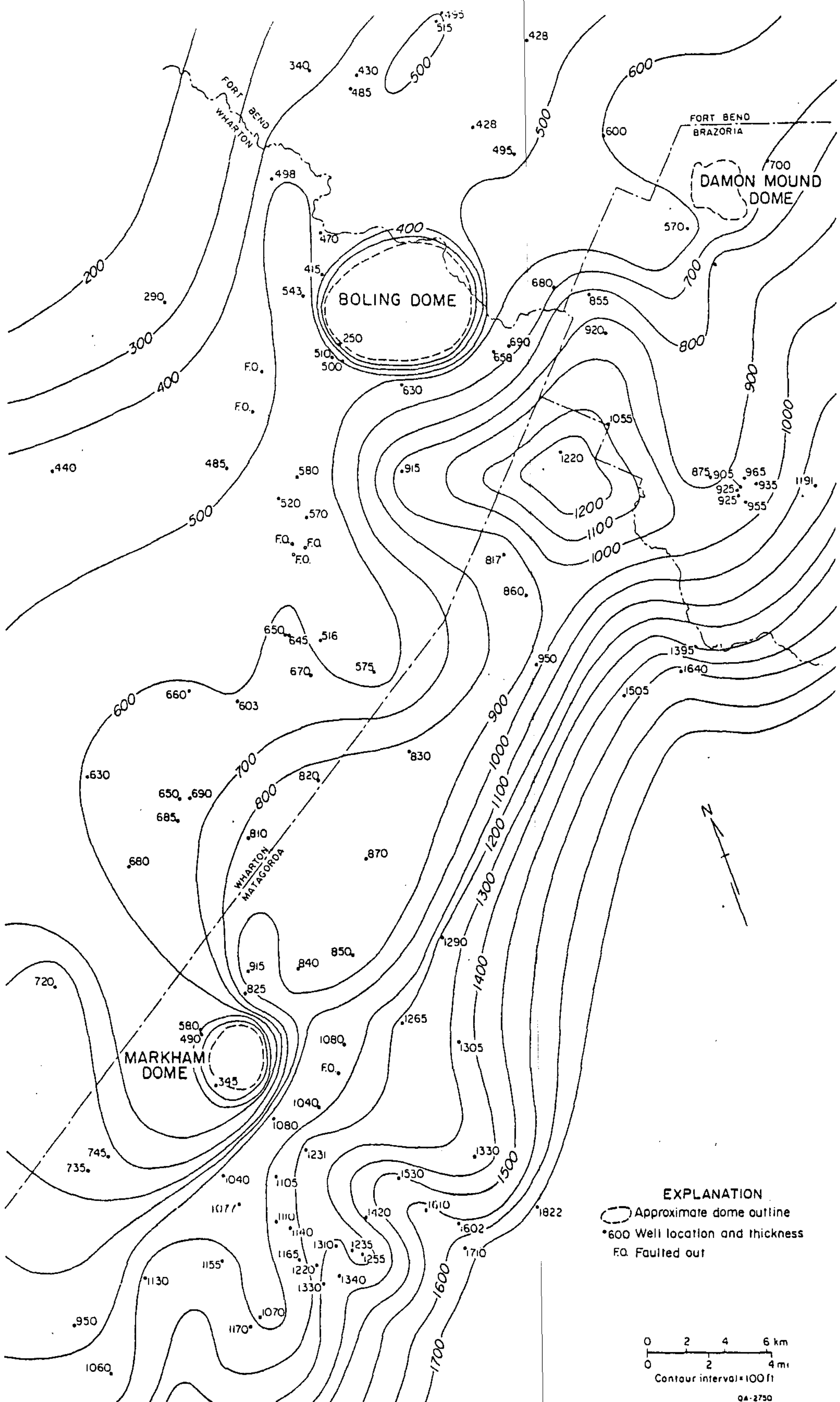

Figure 10. Isopach map, Anahuac Formation, area around Boling, Markham, and Damon Mound domes. Anahuac Formation is approximately 100 percent (600 ft) thicker in salt-withdrawal basin southeast of Boling dome owing to extensive syndepositional salt flow into Boling dome. See figure 4 for mapped area.

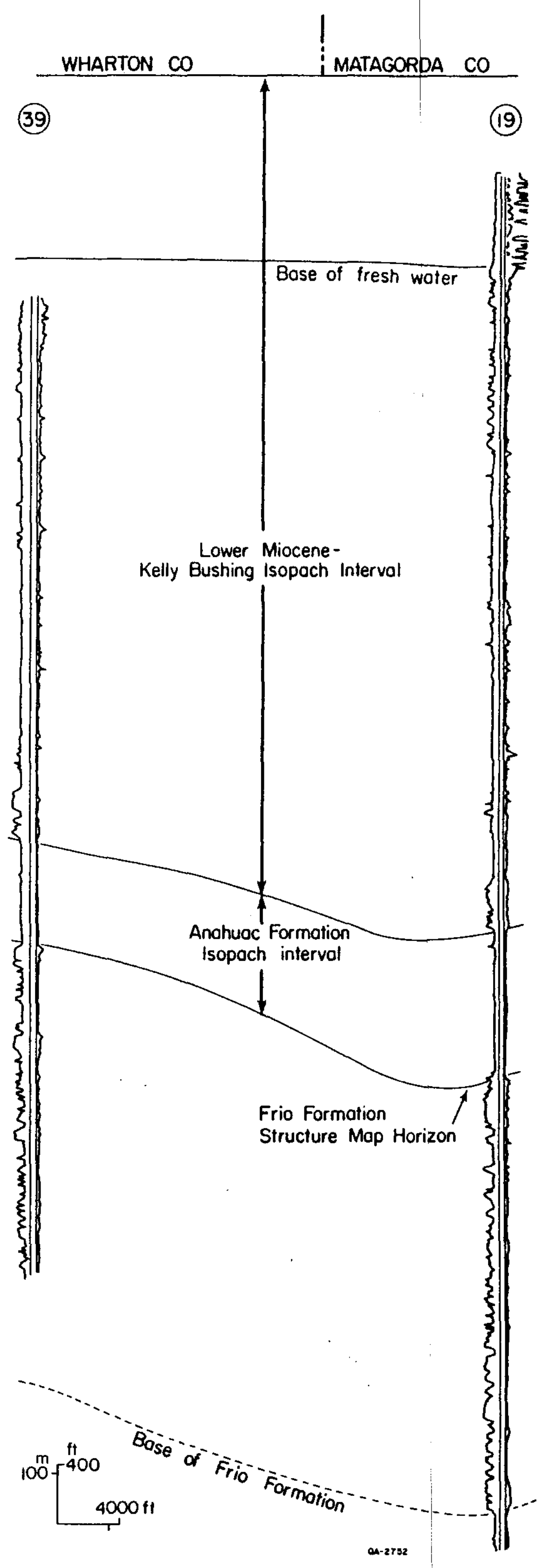

Figure 11. Cross section showing map intervals and correlations.

.050 ft/1000 0.5 ft/10,000 yr 0.3 ft/1000 or 3 ft/10000 Damon Late Pleistocene (2.5 Ma) 2 ft/1000 Miocene rate 0.3 ft/1000 yr

Growth Rates For Boling Salt Dome

Net and gross rates of growth for Boling dome were calculated following the techniques of Seni and Jackson (1983b; 1984). The growth rates are averaged over the entire Miocene and post-Miocene time interval--22.5 millions of years (Ma). This is a relatively long time interval for measuring rates of dome growth. Actual rates of dome growth over shorter time spans will probably be much greater. Long-term growth rates mask the short-term fluctuations of non-steady-state dome growth.

Gross rates of dome growth measure the rate of movement of salt within the salt stock. The gross rates are calculated by equating the volume of sediment in the salt-withdrawal basin with the volume of salt that migrated into the salt stock during that interval of deposition. The vertical rate of movement within the salt stock is determined by dividing the volume of salt mobilized by the cross sectional area of the neck of the salt stock for the duration of deposition (Table 1). During the past 22.5 Ma, 11.9 km^3 (2.6 mi^3) of salt migrated into Boling salt dome. This yields a gross rate of growth for Boling dome of 16 m/Ma (52 ft/Ma). The gross rates of growth for Boling dome are approximately equal to the gross rates for East Texas salt domes in the East Texas salt diapir province during their growth in the Late Cretaceous and Eocene.

Regional rates of sediment-accumulation were 84 m/Ma (276 ft/Ma) in the vicinity of Boling dome during the Miocene to present. Net rates of sediment accumulation were 94 m/Ma (309 ft/Ma) in the Boling dome salt-withdrawal basin. If Boling dome kept pace with the rate of sediment accumulation and stayed at the same relative position with respect to the depositional interface, then net rates of dome growth averaged 94 m/Ma (309 ft/Ma) for Boling dome from the Miocene to the present. The net rate of growth for Boling is comparable to the net rates of growth for the fastest growing domes in the East Texas diapir

Table 1. Growth Rates for Boling Salt Dome

Gross Rate

Volume of salt-withdrawal basin

Contour Interval (ft)	Area (mi^2)	Thickness (ft)	Volume (mi^3)
6200		200	
6400	40.95	200	1.55
6600	22.73	200	0.86
6800	9.00	200	0.34
6960	3.60	1.60	0.11
		Sum	2.86 mi^3 (11.91 km^3)

Area column is average area of two contour interval.

Area of Boling dome neck 12.83 mi^2 (32.84 km^2)

$$\text{Gross growth of Boling dome} = \frac{\text{Salt-withdrawal volume}}{\text{Salt-neck area}} = \frac{2.86\ mi^3}{12.83\ mi^2} = 0.223\ mi = 1{,}177\ ft\ (359\ m)$$

$$\text{Growth rate Post-Oligocene to Present} = \frac{\text{Gross growth}}{\text{Duration}} = \frac{1{,}177\ ft}{22.5\ Ma} = 52\ ft/Ma\ (16\ m/Ma)$$

Net Rate

$$\text{Net rate of growth} = \frac{\text{Domal-sediment accumulation}}{\text{Duration}} = \frac{6960\ ft}{22.5\ Ma} = 309\ ft/Ma\ (94\ m/Ma)$$

$$\text{Residual rate of growth} = \frac{\text{Domal-sediment accumulation - Regional-sediment accumulation}}{\text{Duration}}$$

$$= \frac{6960\ ft - 6200\ ft}{22.5\ Ma} = \frac{760\ ft}{22.5\ Ma} = 34\ ft/Ma\ (10\ m/Ma)$$

province during the peak periods of diapiric activity in the Early and Late Cretaceous. The discrepancy between net and gross rates of diapirism for Boling dome may be due to incorrect assumptions of the size of the diapir neck during the Miocene and post-Miocene interval and/or to the crest of Boling dome not keeping pace with deposition in this time interval or to incorrect assumptions of the size and volume of the salt-withdrawal basin.

Discussion

Domes grow and are emplaced under a variety of conditions, thus effecting a diversity of structural and stratigraphic styles in the sediments that surround them. These structural and stratigraphic relationships provide data that can be used to assess the suitability of domes for toxic-waste disposal.

This report and Seni and others (1984a,b) describe some of the structural aspects that affect dome and cavern stability. Domes with structural features indicating diapiric movement in the most recent geologic span of time are less suitable for isolating toxic chemical waste than domes that were quiescent. Recent structural distortion from dome growth causes a range of mappable features that are expressed in near-surface strata. Two important features are (1) structurally and topographically elevated areas over dome crests and (2) faults in strata over the domes, on dome flanks, and in cap rocks. These structural discontinuities are expressed in strata that are deeply buried around domes with an older history of growth. The stability problems associated with domes having a recent growth history are not confined to fear that continued domal uplift might expose a waste repository. Calculations on the rate of dome uplift for East Texas domes and for Boling dome show that the amount of uplift required to expose a repository has a low probability of occurring in the foreseeable future. Nor is there a great likelihood that natural faulting will breach a repository. Rather, the concerns are centered on how these structural discontinuities will affect near-dome hydrogeology. Ground water plays a primary role in salt dome stability. If wastes were to leak from an underground repository, ground water is the likely agent to transport the waste to the biosphere.

The areas over some of the coastal plain domes are topographically elevated 10 to 75 ft (3 to 23 m) above the surrounding plain. These elevated areas are local ground-water recharge zones centered directly over the crest of the dome. Supradomal radial faults, cap-rock faults, and regional growth faults all may act as conduits funnelling meteoric waters toward the upper parts of salt stocks. The geometry and orientation of these faults and their potential for accentuating or inhibiting fluid flow must be analyzed before properly assessing the suitability of a dome for waste isolation. See the CAP ROCK Discussion section for further information on cap-rock faults and hydrogeology.

Stratigraphic relationships around salt domes provide additional means of discriminating among candidate domes. Again, the hydrogeologic aspects are critical. Dome growth strongly influences lithostratigraphy and depositional facies around a dome. This lithostratigraphic framework in turn influences the directions, rates, and flux of ground water around a dome. A diapir encased in a framework of mudstone of low permeability will retard ground-water flow and be a more appropriate candidate for waste isolation than a diapir surrounded by a sandstone characterized by high rates of ground-water flow. These patterns of lithostratigraphy and their influence on ground-water flow are documented around Oakwood dome in East Texas.

MECHANICAL BEHAVIOR OF SALT

Laboratory research on artifical halite and core samples of bedded and domal salt have resulted in substantial strides in our understanding of the mechanical behavior of salt. Sandia National Laboratories (Herrmann, Wawersik, and Lauson), ReSpec (Senseny, Hansen, and Wagner, under contract to Sandia National Laboratories) and Texas A & M (Carter) are the leaders in this research effort. Despite these advances and advances in computer modeling of salt behavior, as yet there is wide discrepancy between results obtained in the laboratory scale experiments and in situ behavior of rock salt. Baar (1977) asserts much of the technical literature includes erroneous and misleading hypotheses based on laboratory data that cannot be reconciled with the actual behavior of salt rocks around underground evacuations. In fact, many laboratory experiments are plagued by small sample size, inadequate test durations, and an absence of many natural geologic variables such as bedding, impurities, and grain size. Herrmann and others (1982) state it is possible that the restricted information obtainable from triaxial tests is not only insufficient but may not dominate behavior involved in mine closing.

In this section we will focus on a review of the creep behavior of salt. Laboratory experiments, results, and in situ observations and experiments will be discussed. Various laws describing creep behavior and possible creep mechanisms will be compared.

Experimental Procedures

Whether testing artifically prepared halite or natural rock salt, the usual test procedure in designing an experiment is to control all variables but one and observe the effects that changing the variable will have on the behavior of the specimen. According to Paterson (1978), the most frequent types of rock mechanical experiments are:

1. A creep test--An axial differential stress is built up rapidly on the specimen and held constant as the specimen deforms. Strain (change in unit length) is then measured as a function of time.

2. A stress-strain test--The differential stress is applied in such a way that the rate of strain is constant and changes in the applied stress are plotted against strain.

3. A strain rate ($\dot{E}$) test--A constant differential stress is applied and the rate of strain is measured. The results are plotted as differential stress versus strain rate.

Triaxial tests are commonly run on salt samples. The specimen is usually subjected to both confining pressure and axial load. The difference between the axial load and the confining pressure is the differential stress. The axial load is transmitted through a hydraulic jack and confining pressure is supplied by a surrounding fluid, whose temperature can be controlled. Thus, confining pressure, directed stress, and temperature can all be varied.

Creep Behavior of Salt

Salt will undergo deformation by slow creep over long periods of time when subjected to constant load or to differential stress. At low temperatures and low stresses salt will exhibit much less creep deformation than at high temperatures and high differential stress (Hume and Shakoor, 1981). Generally when modeling creep behavior of salt in the laboratory, the following variables are considered: stress--σ--(force per unit area measured in megapascals [MPa], pounds per square inch [psi], or bars), strain--E--(ratio of change in length of specimen to its original length), time, and temperature. Appendix 2 is a conversion table for the various units. Most of the units in this section will be Standard International units (SI), because most of the original research and figures use those units. Where non-SI units are used in a cited figure or text, they will be given preference. Creep data are usually presented as some type of time representation. Natural variations in rock salt such as bedding, impurities, mineral content, moisture content, porosity, permeability, mineral fabric, and grain size are rarely considered. Generally, temperature and stress difference have the greatest effect on creep rate. An increase in either temperature or stress difference increases the creep rate considerably (Le Comte, 1965).

Survey of Creep Properties

Major review articles on creep properties of salt include Le Comte (1965), Odé (1968), Baar (1977), Hume and Shakoor (1981), Herrmann and others (1982), and Carter and Hansen (1983). Government sponsored research for nuclear-waste isolation studies and the Strategic Petroleum Reserve program has produced a wealth of new information often termed "gray literature" because it comes from government laboratories and their contractors. Much of the research on creep modeling is based on laboratory tests and computer modeling of artifically prepared halite and rock salt cores from bedded salts at the Waste Isolation Pilot Project site and domal salt principally from Strategic Petroleum Reserve domes in Louisiana and Texas.

Creep is the basis of salt's ability to flow and heal fractures. Simultaneously, creep causes problems related to closure of mined openings, and surficial and subsurface subsidence. Such plastic behavior is demonstrated by salt glaciers, by flowage patterns within salt domes, and by closure of underground openings in salt.

The idealized creep curve for salt (fig. 12) exhibits four parts:

1. Elastic deformation--An instantaneous deformation which is elastic, thus not time dependent.
2. Transient (or primary) creep--A component of creep deformation that decreases with time.
3. Steady-state creep--A component of creep with a constant rate of deformation.

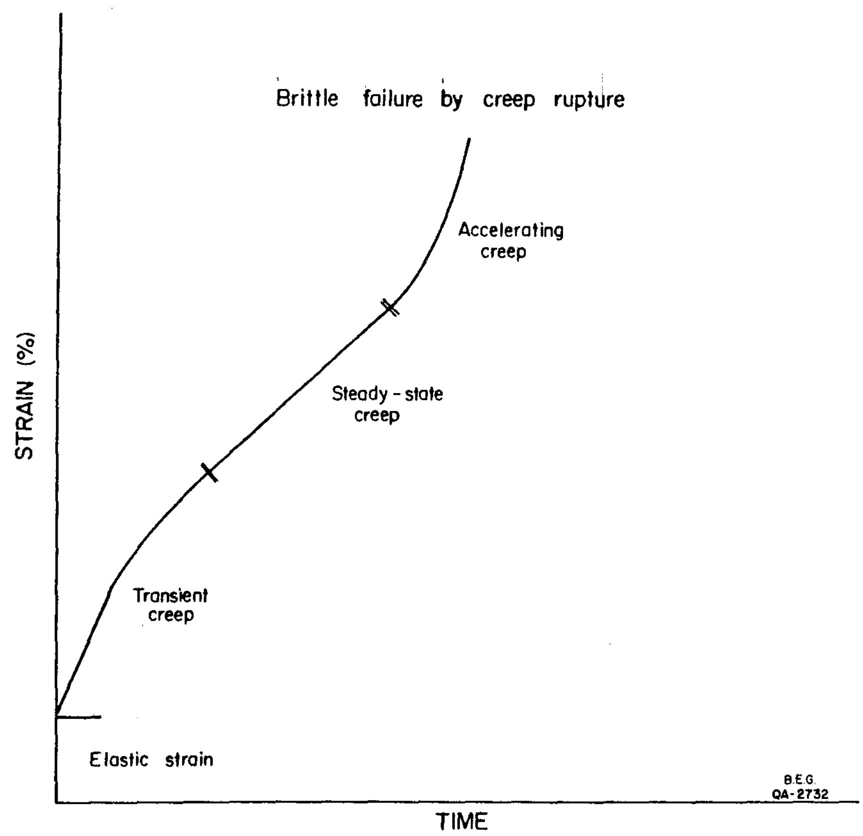

Figure 12. Idealized creep curve depicting behavior of rock salt. Transient (primary), steady-state (secondary), and accelerating (tertiary) stages of creep are separated by inflection points in the curve. The creep curve terminates at the point of brittle (sudden) failure by creep rupture.

4. Tertiary (or accelerating) creep--A component of creep with an increasing rate of deformation leading to brittle failure by creep rupture.

Elastic Properties

Elastic properties of salt include density, compression, Young's modulus, bulk modulus, Poisson's ratio, and wave properties (Hume and Shakoor, 1981). When considering salt properties, from a design viewpoint, elastic properties are of secondary importance because of the extremely low limits of elastic behavior (yield limit) of salt (Odé, 1968). However, shear modulus--the ratio of stress to its corresponding strain under given conditions of load, for materials that deform elastically, according to Hook's Law--is incorporated in various creep laws.

Salt will deform plastically, that is, flow, when the stress difference (σ_1-σ_3) exceeds the limits of elasticity. According to Odé (1968), if salt does have a yield limit, this limit must be low. The reported values for the true elastic limit of salt vary widely and they are the subject of much acrimonious debate (Baar, 1977). Baar (1977) reports a yield limit of approximately 0.99 MPa whereas other researchers give values ranging from 3.94 to 49.25 MPa (Baar, 1977). With advances in test instrumentation the reported values for the limits of elastic behavior have declined. Some calculations of strain rates for Iranian salt glaciers indicate plastic behavior of salt at very low stresses of 0.03-0.25 MPa (Wenkert, 1979; Talbot and Rogers, 1980).

Creep Experiments

Creep experiments are designed to quantify the effect that changes in stress, confining pressure, temperature, and time will have on creep magnitude (strain) or strain rate. At present the literature on salt rock behavior contains results that are conflicting and interpretations that are contradictory (Herrmann and others, 1982; Baar, 1977). Behavioral trends that are in general agreement will be shown as well as the contradictory results. Both laboratory experiments and studies with in situ conditions will be reported.

Temperature has the greatest influence on creep rate (Le Comte, 1965). An increase in temperature always increases the creep rate (fig. 13). Le Comte (1965) experimented with artificial halite at moderately elevated temperatures and his studies are still among the most complete. General observations of his experiments include:

1. An increase in temperature and axial stress increases the creep rate.
2. An increase in confining pressure decreases the creep rate.
3. Increasing the grain size by a factor of six (from 0.1-0.65 mm) decreases the creep rate by a factor of two.
4. The creep activation energy increased from about 12.5 kcal/mole at 29^{o}C to about 30.0 kcal/mole at 300^{o}C.

Le Comte (1965) showed (fig. 14) with constant axial stress (69 bars) and confining pressure (1,000 bars) that an increase in temperature from 29-104.5^{o}C increases creep rate by a factor of four to five, whereas an increase in temperature from 20-198.2^{o}C increases creep rate by a factor of about 22. With the same axial stress (69 bars) and much less confining pressure (1 bar), an increase in temperature from 29-104.5^{o}C increases the creep rate by about 10 times. Note that an increase in confining pressure lessens the effect of temperature on the creep rate. Figure 14 also shows an increase in confining pressure will usually cause a decrease in creep rate.

Although the direction that creep rate will change in as a result of changing variables is often predictable, the magnitude of the change is not. Both Herrmann and others (1982) and Verral and others (1977) note a discrepancy

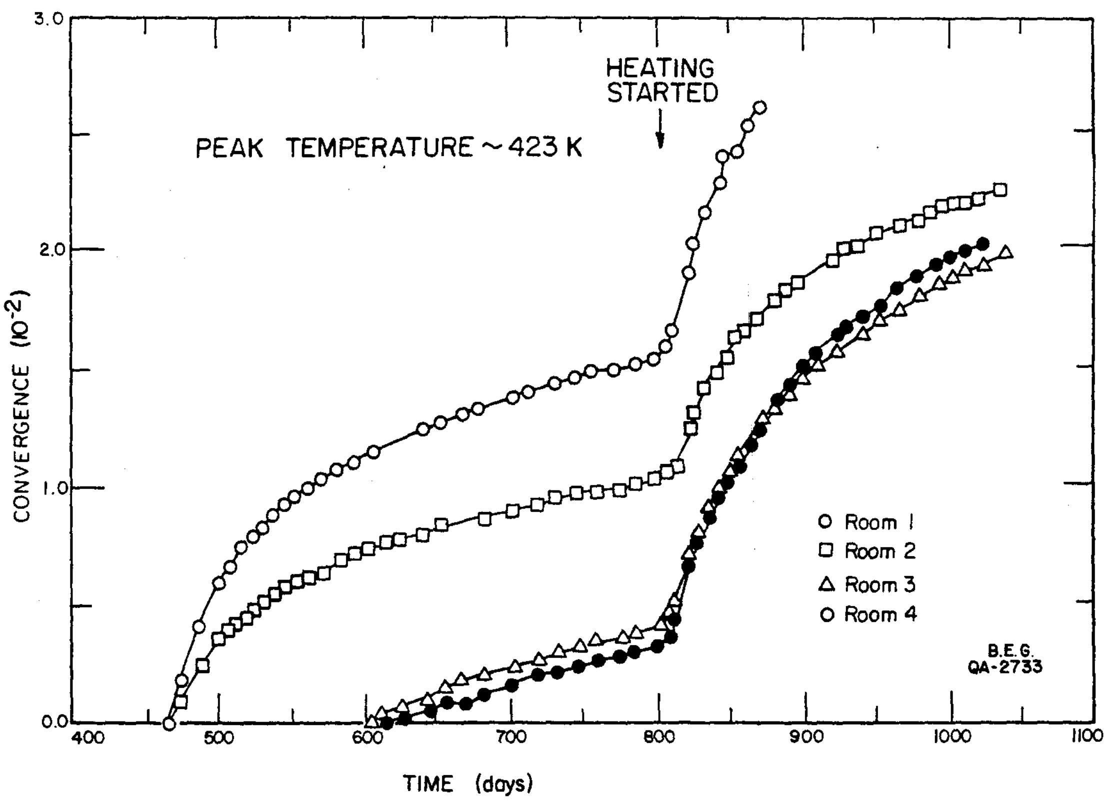

Figure 13. In situ creep shown by convergence of floor and ceiling in an underground salt mine (after Empson and others, 1970). Heating of a nearby mine pillar causes acceleration of the rate of convergence.

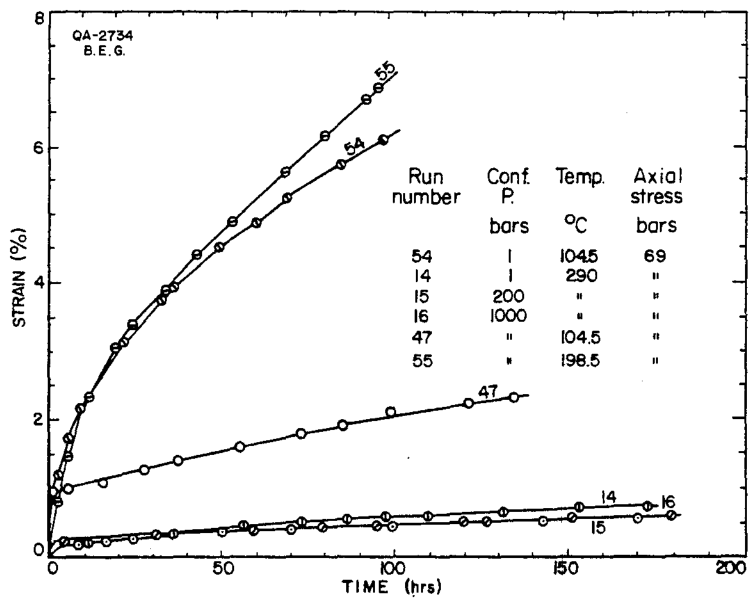

Figure 14. Creep curve for artificially prepared salt showing the effect of temperature, confining pressure, and axial stress (after Le Comte, 1965).

of two orders of magnitude in creep rates between the data of Heard (1972) and Burke (1968).

Strain-rate tests (fig. 15) on natural salt samples from Avery Island salt dome were performed by Hansen and Mellegard (1979) and Hansen and Carter (1980) and are reproduced in Carter and Hansen (1983, their fig. 10). In these experiments a constant differential stress of 10.3 and 20.7 MPa was applied to rock salt at temperatures from 24-200^{o}C. The strain rate curves in figure 15 demonstrate variations in the type of creep behavior with changes in stress and temperature. At differential stress of 10.3 MPa and temperatures less than 115^{o}C the creep is entirely transient, that is, creep decelerates with time. Creep strains are low even as long as ten days (8.6 x 10^4 s). At higher temperatures there is an appreciable increase in creep rate and steady-state creep behavior is attained. Thus, temperature greatly influences creep rate and the timing of the transition from transient to steady-state creep (Carter and Hansen, 1983).

The influence of differential stress on creep behavior is similar to that of temperature. Higher differential stress produces higher creep rates and causes steady-state flow to begin at a much earlier time.

Natural rock salt exhibits wide variations in fabric, crystal size, and impurity content. These variations are especially pronounced between domal salt (relatively nonbedded, highly foliated, and pure) and bedded salt (highly bedded, relatively impure). Recent tests have attempted to quantify differences in creep behavior of natural rock salts including bedded Lyons salt from Kansas, bedded Salado salt from New Mexico, and dome salt from Avery Island and Weeks Island, Louisiana. Results of stress-strain tests on these salts are shown in figure 16. Initial behavior of the salts was nearly identical, except for Lyons salt which is appreciably stronger. The results were unexpected by Hansen and Carter (1980). Lyons salt would have been predicted to be the

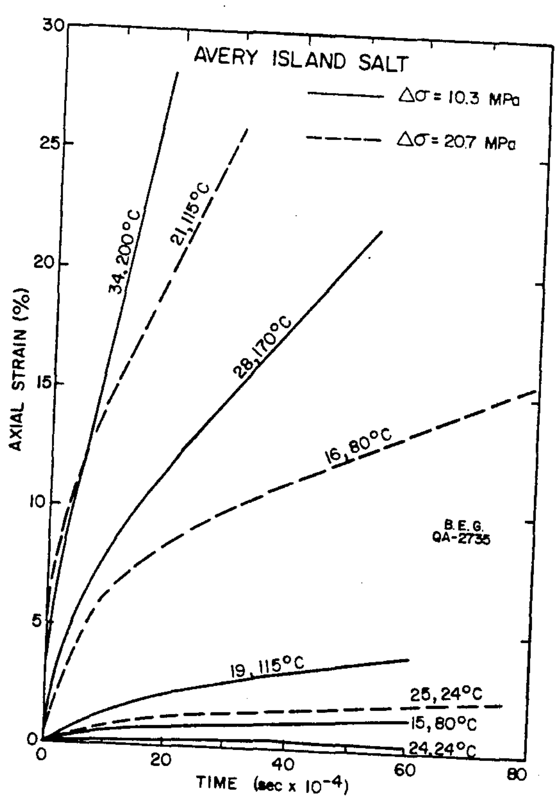

Figure 15. Creep curves for Avery Island dome salt deformed at temperatures from 24°C to 200°C and stresses from 10.3 MPa to 20.7 MPa. Confining pressures were 3.5 MPa or above (data from Hansen and Mellegard, 1979; Hansen and Carter, 1979, 1980; after Carter and Hansen, 1983).

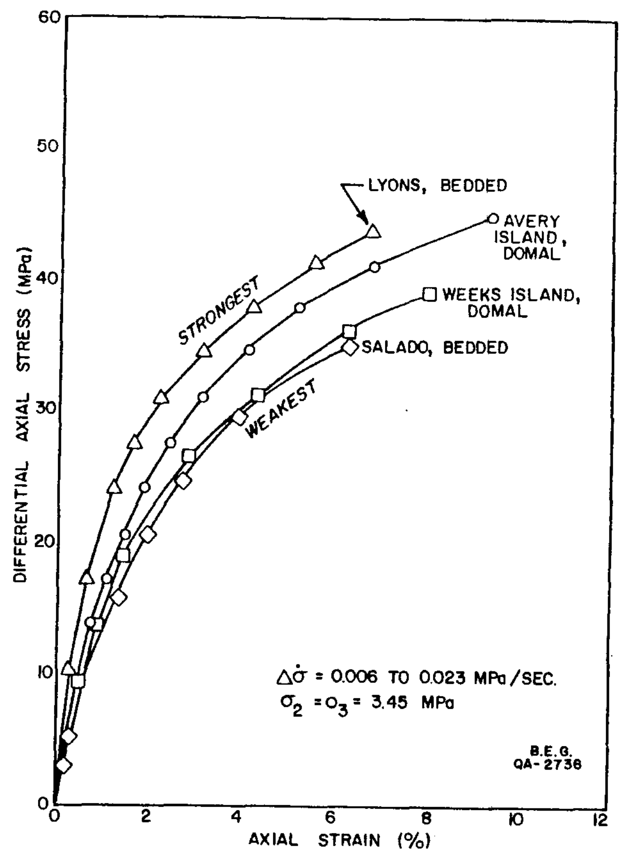

Figure 16. Stress-strain curve for bedded and dome salt deformed by a differential stress rate of 0.006 MPa to 0.023 MPa s^{-1} and a confining pressure of 3.45 MPa. There is no systematic variation in creep behavior between bedded and domal salt. However, bedded salt from Lyons, Kansas, is the most creep resistant salt of those tested (after Hansen and Carter, 1980).

weakest on the basis of the orientation of crystal fabric in which the Lyons salt contained the largest number of primary slip planes oriented with the orientation of high shearing stress.

The influence of grain size on the behavior of salt has been reported by Le Comte (1965), Burke (1968), Reynolds and Gloyna (1961), and Serata and Gloyna (1959). These results are especially contradictory. Le Comte (1965) showed that with all other conditions constant, increasing the grain size by a factor of six decreased the creep rate by a factor of two (fig. 17). Burke (1968) also worked on artificial salt but at higher temperature (1013 K), and his data show the opposite behavior (fig. 18). Increasing the grain size by a factor of 2.5-10 increased the creep rate by about an order of magnitude when the stress is held constant at 1 MPa. The results from in situ observations of mine openings reported by Reynolds and Gloyna (1961) and cited by Odé (1968) documents the exact opposite behavior to that displayed by artificial salt in the laboratory. Reynolds and Gloyna (1961) found that at low temperature fine-grained salt is more creep resistant than coarse-grained salt and that at higher temperatures this effect is reversed (Odé, 1968, p. 584). One possible explanation for the discrepancy between laboratory and in situ results is that under in situ conditions grain-size variations of salt are not the cause of differences in salt behavior but merely a reflection of different stress states which caused the grain-size variations.

In Situ Creep

In situ creep and creep rates have been measured directly in salt and potash mines (Baar, 1977; Dreyer, 1972; Obert, 1964; Reynolds and Gloyna, 1961) and indirectly in boreholes (Thoms and others, 1982; Fernandez and Hendron, 1984), and in solution-mined caverns (Preece and Stone, 1982). Baar (1977) is especially critical of applying laboratory-derived creep curves to in situ

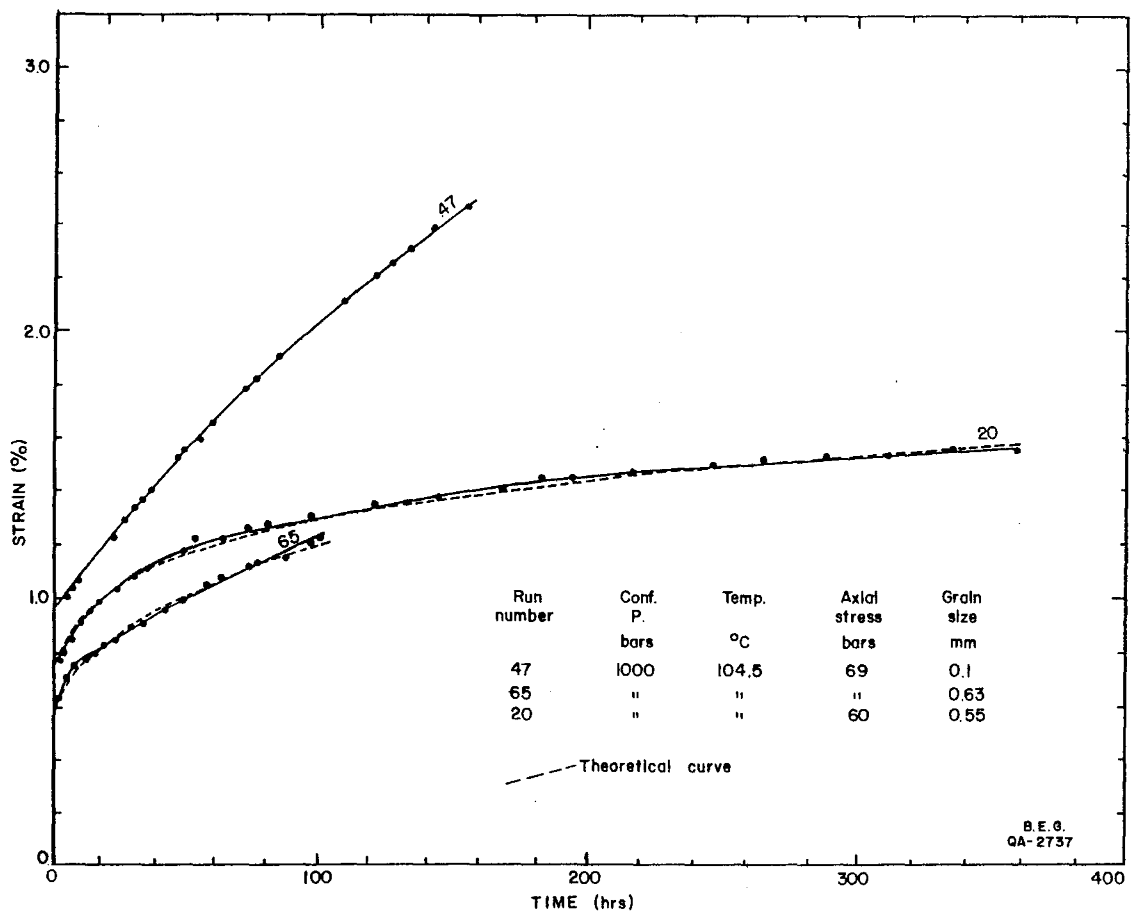

Figure 17. Creep curve for artificially prepared salt showing the effect of variations in grain size and axial stress on the creep behavior (after Le Comte, 1965).

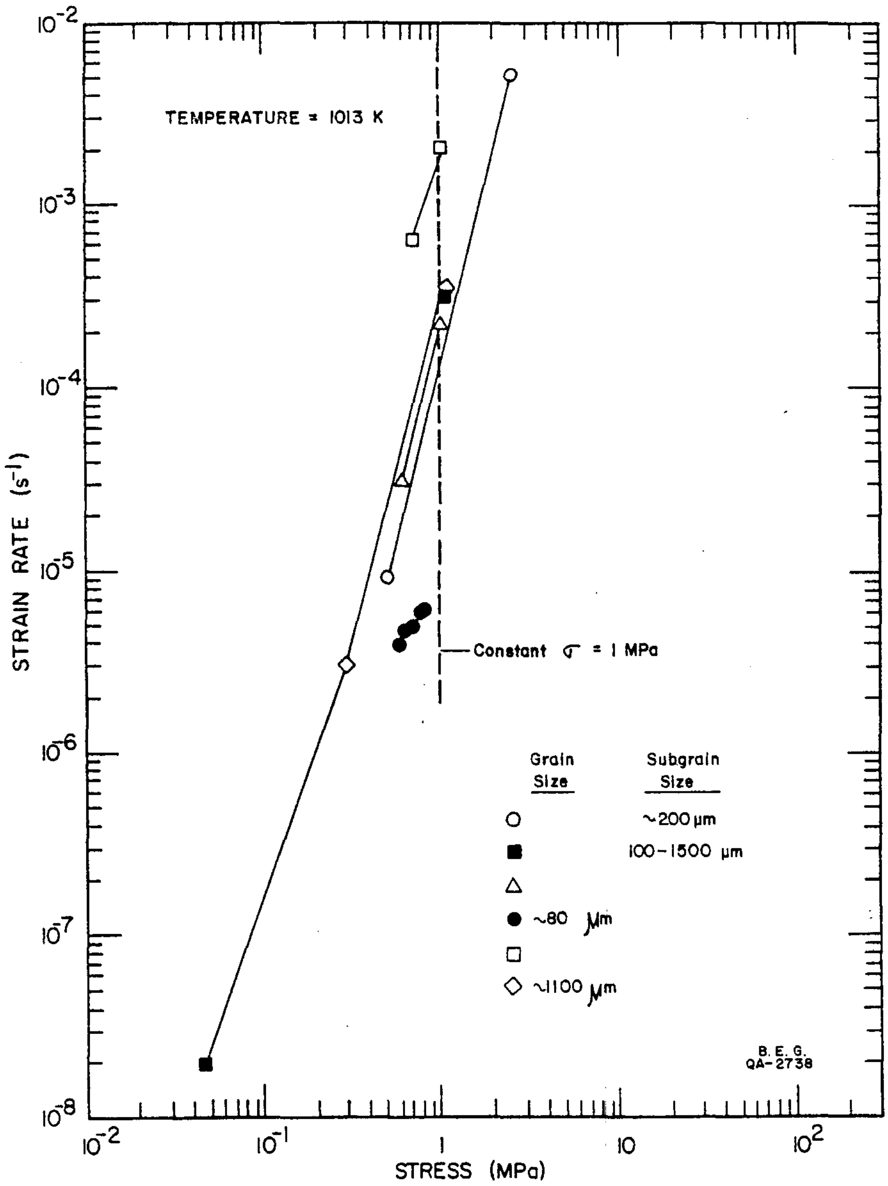

Figure 18. Strain rate curve for artificially prepared salt deformed at high temperature (1013 K). Strain rates with a constant stress show a significant increase due to increases in grain size and subgrain size (cited by Hume and Shakoor, 1981; after Burke, 1968).

conditions. Baar (1977) specifically denies the applicability of the transient part of creep curves to in situ salt behavior. He ascribes the decreasing rate of salt creep with time in laboratory experiments to strain (or work) hardening which he insists only occurs in laboratory scale experiments. A critical review of Baar's data (Baar, 1971, 1977) reveals short initial periods of declining rate of creep with time. This initial period of declining rate is referred to by Baar as "stress-relief creep." Baar (1971, 1977) concentrated on German and Canadian potash mines, and his observations include data of up to five years duration (fig. 19). The results of Dreyer (1972) and Baar (1977) characteristically showed that long-term creep rates are constant. Obert (1964) studied the convergence of rock-salt pillars in Kansas and described both transient and steady-state creep behavior. Reynolds and Gloyna (1961) cited by Odé (1968) summarized convergence measurements from domal salt mines in Louisiana and Texas and from bedded salt in Kansas. Their observations and those of previous workers include:

1. The rate of creep decrease with time.
2. The rate of creep is temperature dependent.
3. The rate of creep depends on the location where the measurement was conducted.
4. The rate of creep increases with depth.
5. Fine-grained materials at low temperature are more creep resistant than coarse-grained material; at higher temperatures the effect is reversed.
6. Impurities can increase the cohesive force of salt.

Borehole closure studies are another potentially powerful means of studying in situ salt behavior (Fernandez and Hendron, 1984; Thoms and others, 1982). Borehole closure at Rayburns and Vacherie salt domes, Louisiana, was studied by simply repeating caliper surveys in a hole filled with saturated

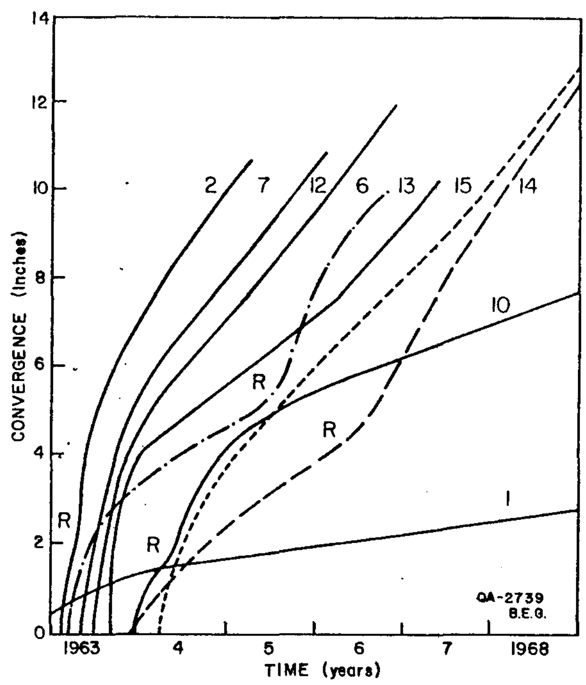

Figure 19. Convergence in Canadian potash mine as a function of time. Long-term convergence is nearly constant (after Baar, 1977).

brine at 387 and 864 days and at 163, 413, and 890 days, respectively, after drilling (figs. 20A, 20B). Note that after 864 days Rayburns borehole closure at a depth of 4,000-5,000 ft was fairly constant, but at Vacherie dome the borehole continued to close throughout the entire depth range. For both domes the closure was very small (percent closure = 0.5) above depths of 2,500 ft.

Borehole closure data for Vacherie dome were recalculated in order to see how strain rates varied with time, stress, and depth and to see how these data compared with data derived from laboratory analysis. The strain rate was calculated by dividing the linear closure (strain) for the borehole (using a nominal hole diameter of 8-3/4 inches) by the duration in seconds of time since drilling. Strain rates were nearly constant at any given depth after a transient initial period of approximately 163 days. The strain rate (fig. 21) clearly increases exponentially with stress and depth and ranges from 7.4 x 10^{-11} s^{-1} at 1,150 ft to 3.5 x 10^{-9} s^{-1} at 4,950 ft. The range of known environmental conditions were temperature (100 to 165°C), axial stress (4.2-18.1 MPa), and strain (0.1 to 27 percent).

Fernandez and Hendron (1984) studied borehole closure over a moderately long term (three test segments of approximately 100 days duration each) in bedded salt at a depth of 6,000 ft. They analyzed wellbore closure of a bedded salt section by daily observation of the volume of saturated brine (stage 1) or oil (stage 2) expulsed from an uncased salt section. The expulsion was inferred to have been due solely to hole closure. Three different levels of constant pressure (9.0, 15.2, and 20.7 MPa) were induced by the weight of fluids in the borehole to evaluate the response to various stress levels. The authors concluded:

1. Creep rates continued to decline for the duration of the test segments.

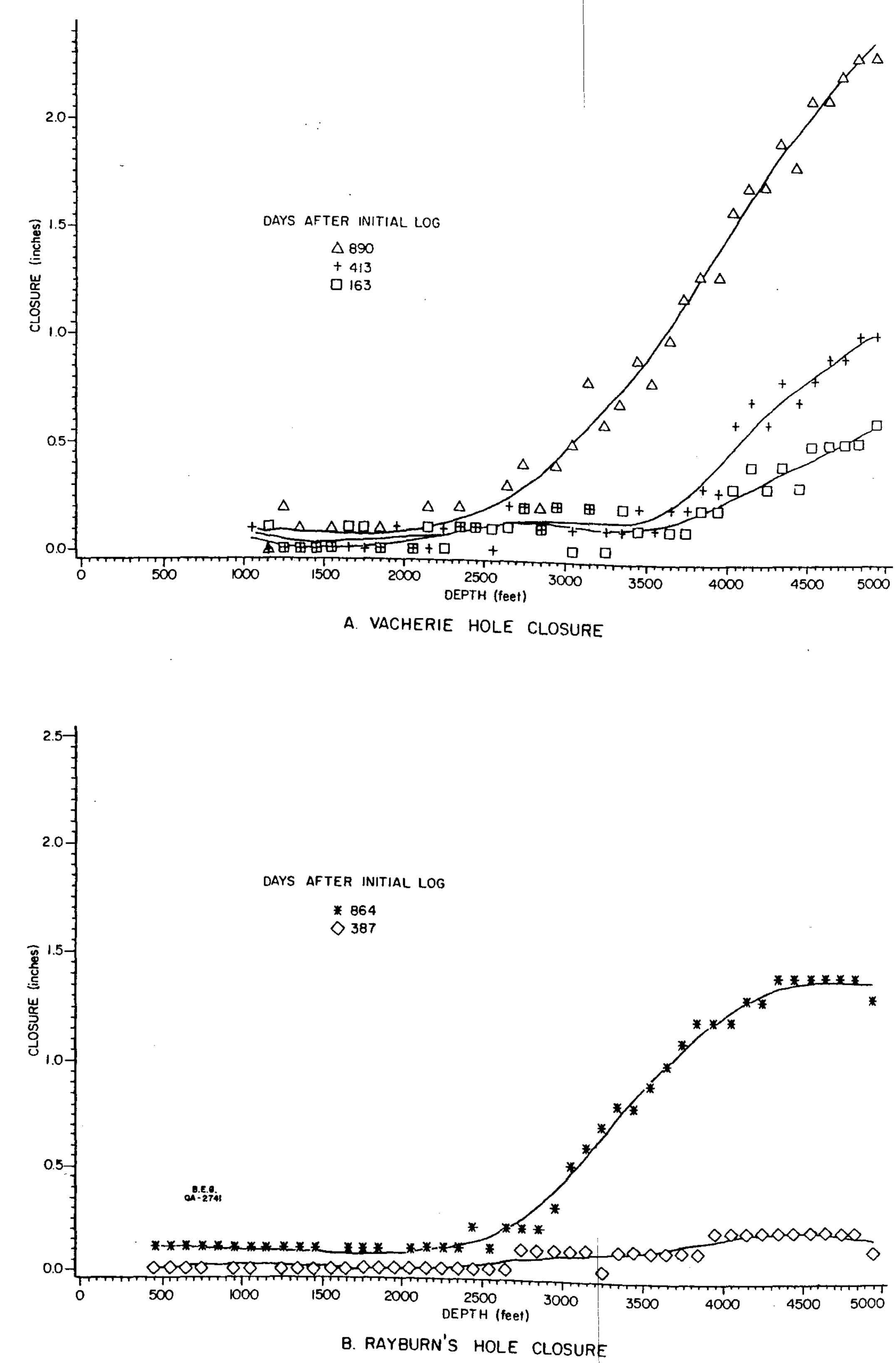

Figure 20. Borehole closure of (A) Vacherie and (b) Rayburns salt domes (after Thoms and others, 1982).

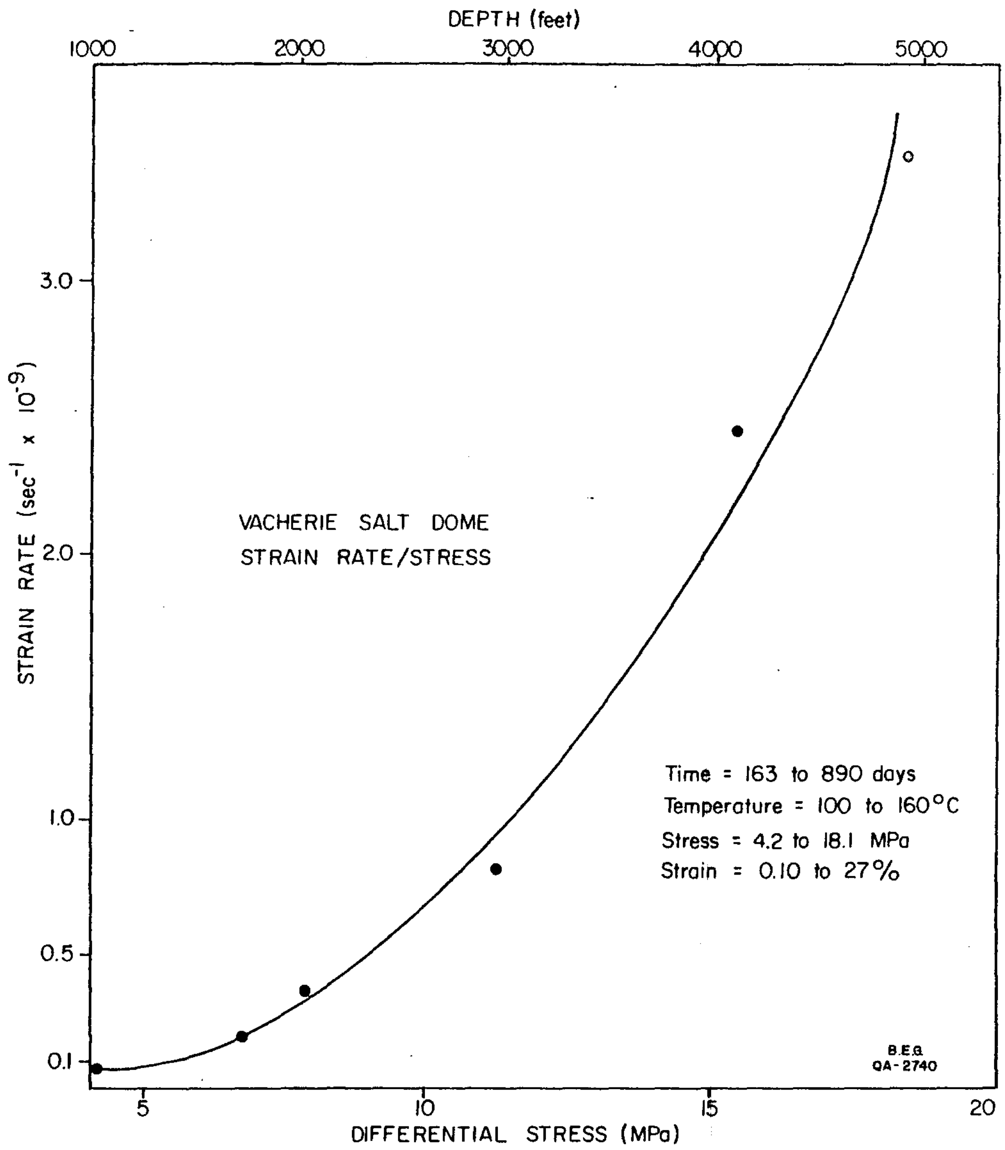

Figure 21. Strain rate curve for borehole closure at Vacherie salt dome based on borehole closure data from Thoms and others (1982). Linear closure data were converted to strain data base on a nominal hole diameter of 8-3/4 inches. Strain rates were derived using four points for time control (that is, 0, 163, 413, and 890 days after drilling; see figure 20). At a given depth, strain rates were remarkably linear. Differential stresses were derived from the difference between the lithostatic load exerted by the salt and the load exerted by the borehole filled with saturated brine. Note the exponential increase in strain rate with increasing differential stress or depth.

1 pascal = 1 newton/m²
1 MPa = 1x10⁶ newton/m²
newton
force gives mass of 1 kg
acceleration ~ 1 m/s²

de of well closure was greater for higher shear stress
al stress).

3. The rate of well closure was greatest for higher shear levels (differential stress).

Comparison of Strain Rates

Strain rates ($\dot{E}$) of domal-rock salt are compared in Table 2 for three fields of data--salt domes and salt glaciers, boreholes and mine openings, and laboratory experiments on rock salt. Only steady-state strain rates were used from laboratory tests (Mellegard and others, 1983; Carter and Hansen, 1983; Spiers and others, 1984). Strain rates for rock salt vary through 11-12 orders of magnitude. Among the fastest strain rates ($1.25 \times 10^{-6}\ s^{-1}$) were those from laboratory runs on Avery Island dome salt with differential stress of 10.3 MPa and a temperature of 200°C. Mean long-term strain rates for fastest growing salt domes in the East Texas salt diapir province were 2.3×10^{-15}-$6.7 \times 10^{-16}\ s^{-1}$ (Seni and Jackson, 1984). Natural stress difference within salt domes is very low, on the order of 0.03-0.25 MPa, thus natural strain rates are expected to be much lower than laboratory rates.

Strain rates for domal salt in laboratory experiments are three orders of magnitude faster than the strain rates calculated from borehole closure and mine closure observations. There is a general equivalence in temperature and stress conditions between these two fields of data. Both sets of data are principally on dome salt. The discrepancy in strain rates is thought to be partially related to differences between in situ and test conditions or observation duration. The duration of laboratory tests usually ranges up to three months. Maximum in situ observations of boreholes and mine openings range from three to thirty years, respectively. Therefore, in situ tests are over a time

Table 2. Strain Rates for Deformation of Rock Salt
(Modified from Jackson 1984)

TEST DATA	STRAIN RATE[a] (per second)
Natural Conditions of Dome Salt	
Diapiric Salt	
Measurement of topographic mound[b]	2×10^{-14}
Comparison of dome profiles[c]	8.4×10^{-13}
Estimates from thickness variations in strata around domes[d]	3.7×10^{-15} to 1.1×10^{-16}
Average growth of Zechstein domes[e]	2×10^{-15}
Glacial Salt	
Direct measure of flow[f]	1.9×10^{-9} to 1.1×10^{-11}
Comparison of glacial profile[c]	6.7×10^{-13} to 9.0×10^{-13}
Estimates from glacial morphology[g]	2×10^{-8} to 2×10^{-13}
In Situ Conditions of Dome and Bedded Salt	
Direct measure of mine-opening closure[h]	1×10^{-9} to 9×10^{-12}
Direct measure of peak-borehole closure[i]	3×10^{-8}
Direct measure of long-term borehole closure[j]	3.5×10^{-9} to 7.4×10^{-11}
Laboratory Strain Rate Tests	
Strain-rate test[k]	1.25×10^{-6} to 9.5×10^{-9}
Strain-rate test[l]	2.04×10^{-9} to 3.61×10^{-9}
Strain-rate test[m]	1.35×10^{-6} to 3.45×10^{-9}
Strain-rate test[n]	4×10^{-4} to 1×10^{-9}

Table 2. (cont.)

a. Conventional strain rate $\dot{E} = E/t$, where elongation E = change in length/original length at t = duration in seconds (s).

b. Ewing and Ewing (1962), Sigsbee Knolls Gulf of Mexico abyssal plain. Calculation based on salt stock height of 1,300 m; duration of strain 3.5×10^{11} s (11,000 years).

c. Talbot and Jarvis (in press) comparison of observed profile of Kuh-e-Namak stock and glacier to profile of numerical model of viscous fluid extruding from a narrow orifice.

d. Seni and Jackson (1984) based on dome growth rates over 9.5×10^{14} s to 1.8×10^{15} s (30 Ma to 50 Ma).

e. Sannemann (1960) based on stratigraphic-thickness data and salt stock height of 4 km; duration of strain 1.14×10^{15} s to 4.1×10^{15} s (35 Ma to 130 Ma).

f. Talbot and Rogers (1980) based on displaced markers on salt duration of strain 2.5×10^{7} s (292 days); calculated stress (σ) $\leq$ 0.25 MPa. Maximum flow after 5 mm rainfall.

g. Wenkert (1979) for five Iranian glaciers, assumed steady-state equilibrium between extrusion and wasting; with erosion rates of 0.08 cm/yr to 0.25 cm/yr; calculated stress (σ) = 0.03 MPa.

h. Serata and Gloyna (1959), Reynolds and Gloyna (1960), and Bradshaw and McClain (1971) based on observations in Grand Saline dome in Texas and Lyons bedded salt in Kansas; upper limit corresponds to wall temperature 100°C; estimated stress difference 10 MPa; duration of strain 3.2×10^{8} s to 9.5×10^{8} s (10 to 30 years).

i. Martinez and others (1978) Vacherie dome, Louisiana; duration 7.8×10^{6} s (3 months).

j. Thoms and others (1982), Vacherie dome, Louisiana; duration of strain 7.7×10^{7} s (890 days); slowest rate at 100°C, 351 m depth, stress difference 42 MPa; fastest rate at 160°C, 1,509 m depth, stress difference 18.1 MPa.

k. Carter and Hansen (1983), from data of Hansen and Carter (1982), Avery Island dome, Louisiana; temperature 24°C to 200°C; differential stress 10.3 MPa and 20.7 MPa; duration 4×10^{4} to 30×10^{4} s.

l. Wawersik and others (1980), Bryan Mound dome, Texas; temperature 22°C to 60°C; differential stress 20.7 MPa; duration 9.72×10^{4} to 1.44×10^{6} s (27 to 400 hrs).

m. Mellegard and others (1983), Avery Island dome, Louisiana; temperature 24°C to 200°C; differential stress 6.9 MPa to 20.7 MPa.

n. Spiers and others (1984), Asse dome, Germany; temperature 150°C; confining pressure 2.5 MPa (SP 124) to 10 MPa (SP 125,129). SP125 brine added, SP129 inherent brine 0.05% only.

period from one to two orders of magnitude longer than laboratory tests. Natural strain rates are very low when measured over the period of dome growth which are up to seven orders of magnitude longer than test durations in the laboratory.

The short duration of laboratory tests may be a serious shortcoming of this type of strain experiment, both from the rapid application of stress and from the inadequate test duration.

Some very exciting data have just come to light (Spiers and others, 1984) which offer a mechanistic explanation for discrepancies observed between previous laboratory data and long-term mechanical properties inferred from geological studies. Salt core form Asse salt dome, Germany, was subjected to laboratory tests exceeding three years duration. Further, brine content, a previously ignored but important variable, was included in the testing. Salt cores were compressed under triaxial load and then studied dilatometrically (under dilation) using stress relaxation techniques. Essentially the conditions may be visualized as a mirror reversal of borehole closure studies. Both "dry" samples with inherent (very small but unspecified) brine concentrations and "wet" (>0.25-0.5 weight percent brine added under pressure of 1.0-10 MPa) samples were evaluated.

The salt deformation was sensitive to both brine content and to strain rates. Above very rapid strain rates of $10^{-7}\ s^{-1}$ (normal laboratory rates), both wet and dry samples exhibited dislocation creep behavior in agreement with previous studies. Dry samples weakened (that is, less differential stress yielded the same strain rate) when subjected to slower strain rates less than $10^{-7}\ s^{-1}$ and when dilatancy was suppressed (σ_3 = 5-10 MPa). Wet samples also displayed weakened behavior at strain rates slower than $10^{-7}\ s^{-1}$, but dilatancy was suppressed naturally (σ_3 = 2 MPa). The weakened behavior of wet salt was due to fluid-film-assisted grain boundary diffusion. The brine greatly facilitated recrystallization. Spiers and others (1984) concluded that flow laws obtained from dry salt at rapid strain rates or low pressures cannot be extrapolated to predict long-term behavior of wet or dry salt. Wet salt under natural low stress conditions displays long-term creep rates much faster than previously predicted particularly if relatively small amounts of brine (>0.25-0.5 weight percent) are present.

Creep Laws

Creep laws are one kind of the many constitutive laws that model the rate-dependent deformation of materials. Creep laws are applied to the design of underground storage caverns, radioactive waste repositories, and to salt mines where the combination of stress, temperature, and time gives rise to significant time-dependent deformation. A number of creep laws have been proposed to describe the behavior of rock salt. These laws have been used in a variety of ways in evolving creep and creep-plasticity theory, creep mechanisms, and in various finite element computer codes for analyzing nuclear-waste isolation studies and in Strategic Petroleum Reserve facilities. Reviews of various creep laws include Dawson (1979), Herrmann and Lauson (1981a, 1981b), Wagner and others (1982), Herrmann and others (1982), Senseny (1981), and Carter and Hansen (1983).

The total strain in any given material is given by Carter and Hansen (1983) as:

$$E = E_e + E_p + E_t + E_s + E_a \qquad (1)$$

where E_e is the elastic strain ($\Delta\sigma/E$) upon loading,

E_p is the plastic strain during loading,

E_t is the transient or primary creep strain,

E_s is the steady state or secondary creep strain, and

E_a is the accelerating or tertiary creep strain.

The contributions of E_t and E_s are expected to contribute the bulk of the creep strain. For the purposes of this discussion, E_e, E_p, and E_a will be neglected, although some creep laws do include terms for these variables.

Most researchers agree that both transient and steady-state creep behavior are likely to be encountered in rock salt at the pressure and temperature range in a waste repository or storage cavern. Various equations used to describe these two aspects of creep behavior will be described and compared.

Steady-State Creep

The Weertman expression (Weertman, 1968; Weertman and Weertman, 1970) is the equation most commonly used to describe steady-state creep behavior of rock salt at 1/4 to 1/2 salt's homologous temperature (the ratio of temperature to the melt temperature in degrees Kelvin). The Weertman expression for creep rate is:

$$\dot{E}_s = A \exp\left(\frac{-Q}{RT}\right)\left(\frac{\sigma}{\mu}\right)^n \qquad (2)$$

where T is absolute temperature, σ is shear stress or principal stress difference under triaxial load, μ is shear modulus, R is the universal gas constant, and A, Q, and n are constants which depend on the creep mechanism that is operating in the given stress-temperature region.

Carter and Hansen (1983) show a somewhat simpler form of the equation

$$\dot{E}_s = A\,\sigma^n \exp\left(\frac{-Q}{RT}\right) \qquad (3)$$

where A is a slightly temperature and structure-sensitive material parameter.

The temperature dependence of the creep rate is strong, being given by the exponential term in both (2) and (3). Similarly, the stress dependence is also strong. The influence of various creep mechanisms will be described in later sections. Both (2) and (3) tacitly imply that steady-state creep is not dependent on the mean stress of hydrostatic pressure.

Transient Creep

Transient creep is not well understood and various creep laws have been proposed to describe and predict creep rates that decrease with time (Herrmann and Lauson, 1981a). These laws include exponential, logarithmic, power law, and Munson and Dawson equations.

Exponential Creep Law

An exponential (on time) creep law is of the form:

$$E = E_e + E_s t + E_\infty (1 - \exp(\xi t)) \qquad (4)$$

where E is strain, E_e is elastic strain, t is time, and

E_s, E_∞, and ξ are fitting parameters.

This equation first proposed by McVetty (1934) for high temperature creep of metals is also widely used for rock salt. It is the baseline creep law used for numerical analysis of potential nuclear repositories in salt (Senseny, 1981).

As t approaches infinity in equation (4) the bracketed term approaches zero. Thus, when the steady-state terms E_e and E_s are ignored, the transient creep rate decays linearly from the initial value of ξE_∞ to zero as the transient creep rate approaches its limiting value E_∞ (fig. 22).

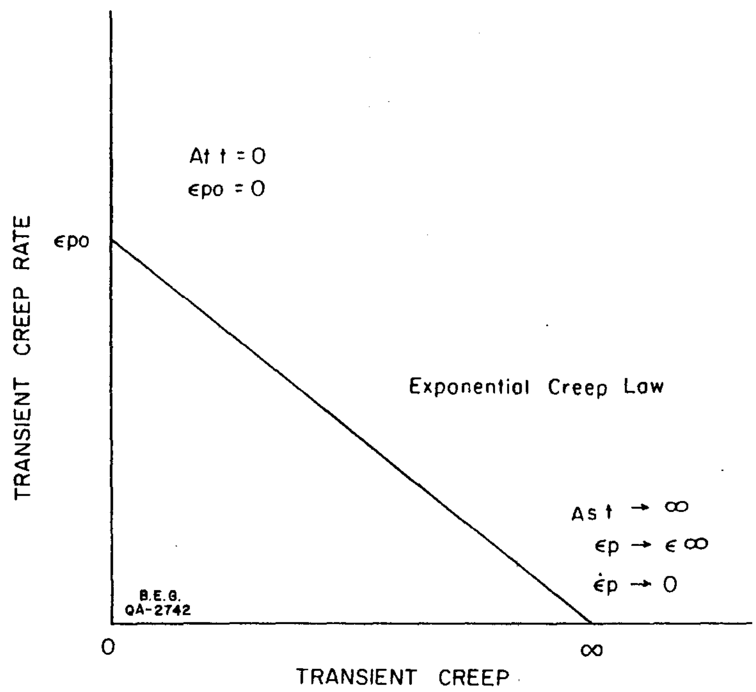

Figure 22. Exponential creep law behavior (after Herrmann and Lauson, 1981a).

Logarithmic Creep Law

The logarithmic (on time) law is given as:

$$E = E_e + \dot{E}_s t = \gamma \ln (1 + \mu t) \qquad (5)$$

where E is strain, $\dot{E}_e$ is elastic strain, t is time, μ is shear modulus, $\dot{E}_s$ and γ are fitting parameters.

The logarithmic law has been used to fit low temperature creep data in both metal and rock salt (Herrmann and Lauson, 1981a). Herrmann and Lauson (1981a) showed the creep rate decays exponentially to zero from its initial finite value with the logarithmic creep law, but the transient creep strain becomes unbounded as t approaches infinity (fig. 23).

Power Creep Law

A power creep law is of the form:

$$E = \dot{E}_e t + K \sqrt{J_2}^{\,m} t^n \qquad (6)$$

where E is strain, E_e is elastic strain, t is time, $\sqrt{J_2}$ is the square root of the second invariant of the deviator stress, and K, m, and n are creep fitting parameters.

According to Herrmann and Lauson (1981a), the transient creep rate is infinite initially and decays to zero with time, whereas the creep strain grows without limit as time goes to infinity (fig. 24).

Discussion of Creep Laws

Both Herrmann and Lauson (1981a) and Wagner and others (1982) applied these creep laws to a single set of laboratory data and compared the resulting fit. Herrmann and Lauson (1981a) also derived the laws and examined interrelations between the laws. In both the articles, the laws were found to fit the data base equally well, although the duration of the laboratory data was quite short (9 to 72 days). Major conclusions were very different. Wagner and

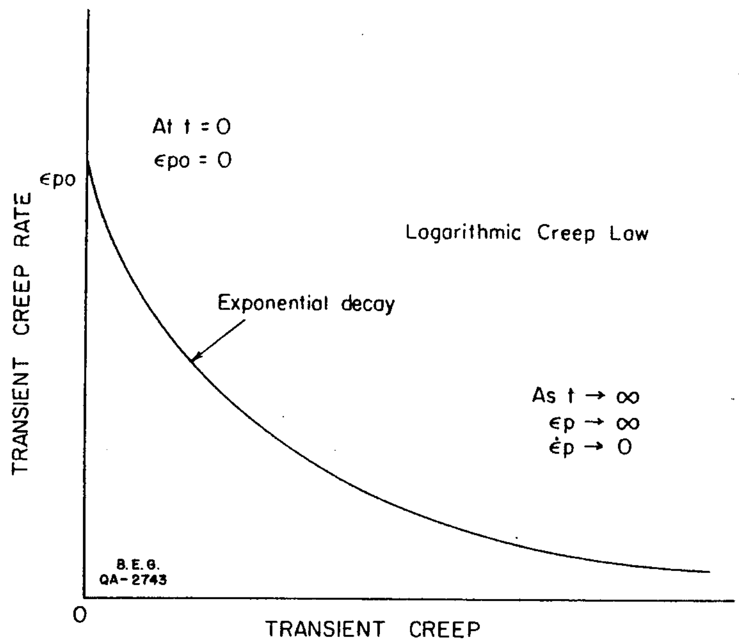

Figure 23. Logarithmic creep law behavior (after Herrmann and Lauson, 1981a).

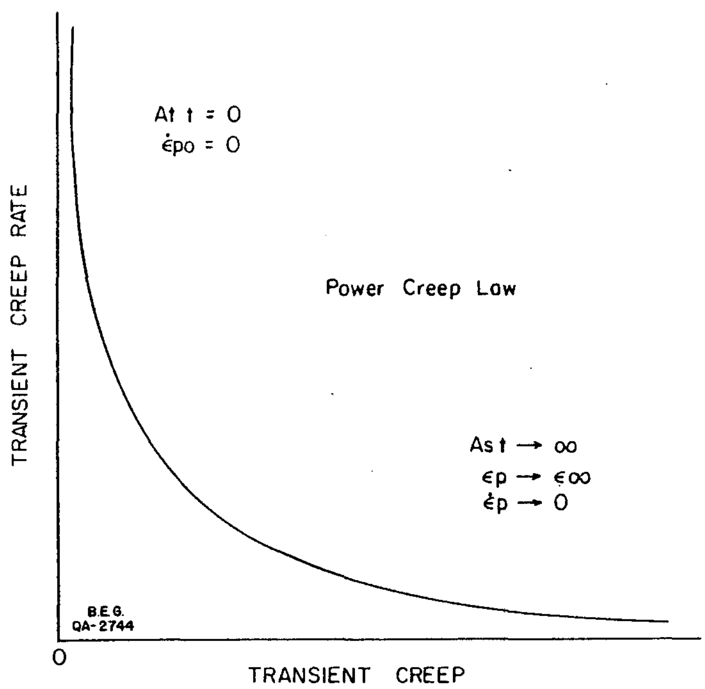

Figure 24. Power law creep behavior (after Herrmann and Lauson, 1981a).

others (1982) emphasized long-term extrapolation of the results (up to 25 years). They found that the amount of predicted closure was very sensitive to the form of the creep law. They found that the exponential (on time) creep law yielded the least closure and the power law the greatest (fig. 25). Herrmann and Lauson (1981a) emphasized the fact that all the creep laws fit the creep data satisfactorily for the duration of the lab tests. Herrmann and Lauson (1981a) used a power law that did not have a steady-state term. Because transient creep became negligible in extrapolations greater than a few months, the three creep laws with steady-state terms essentially coincided while the power law yielded much lower rates of creep. The power law predicted creep strains about two orders of magnitude less than the other laws at 30 years duration. In contrast, Wagner and others (1982) found their power law equation yielded the greatest creep over the long term (4 months) (fig. 25).

Deformation Mechanism

Munson (1979) and Verrall and others (1977) have produced a preliminary deformation mechanism map for salt based on theoretical and experimental results (fig. 26). According to Munson (1979), the deformation-mechanism map is a representation in non-dimensionalized space of regimes of stress (stress/shear modulus) and homologous temperature. Munson defined five stress and temperature regimes where a single deformation mechanism predominates in controlling the strain rate. These regimes include (1) defectless flow, (2) dislocation glide, (3) dislocation climb creep, (4) diffusional creep, and (5) an undefined mechanism. The two high stress regimes (defectless flow and dislocation glide) are controlled by flow processes, whereas the other three regimes (dislocation climb, diffusional creep, and the undefined mechanism) are thermally activated equilibrium processes (Munson, 1979). Although Munson (1979)

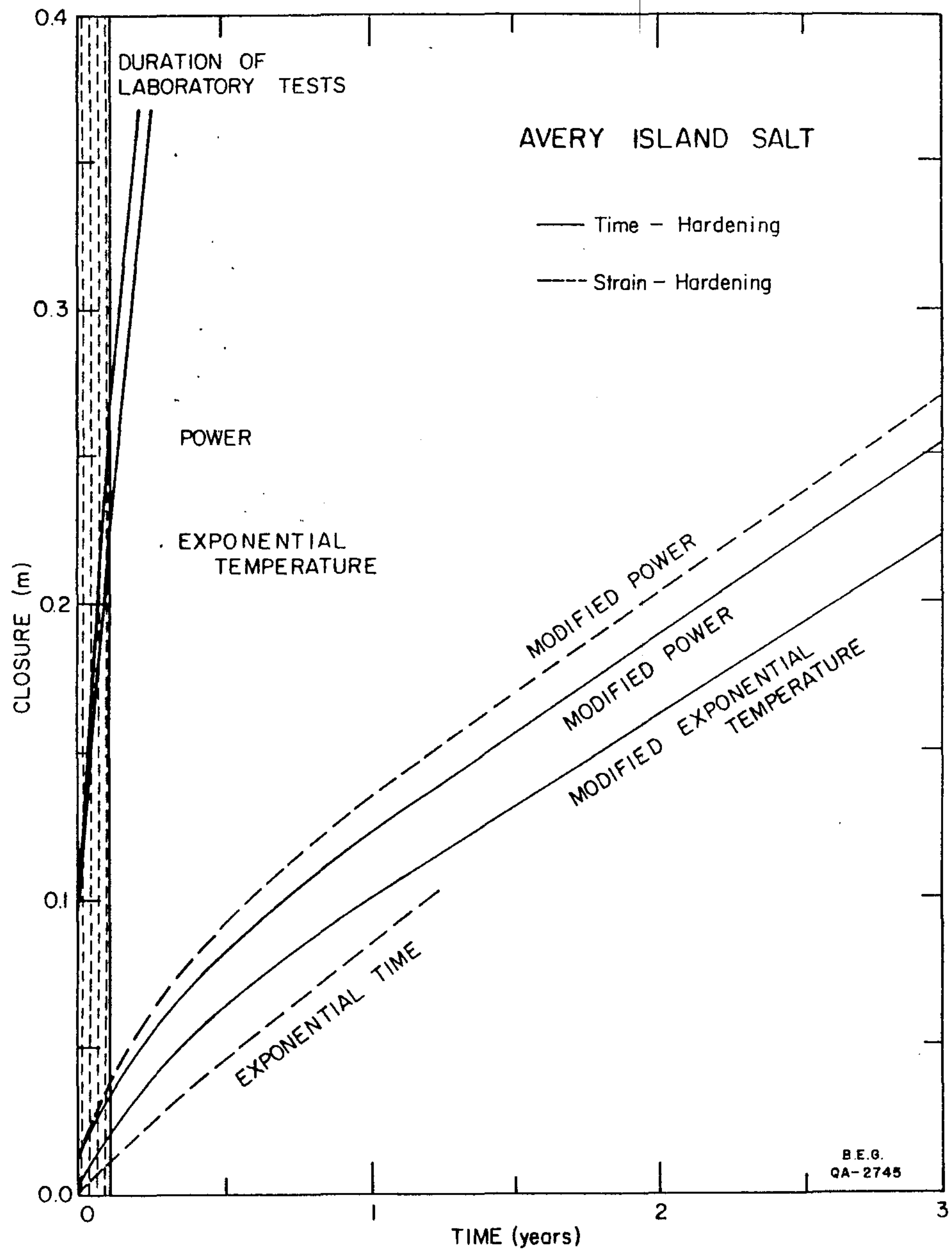

Figure 25. Predicted long-term closures using different creep law forms (after Wagner and others, 1982).

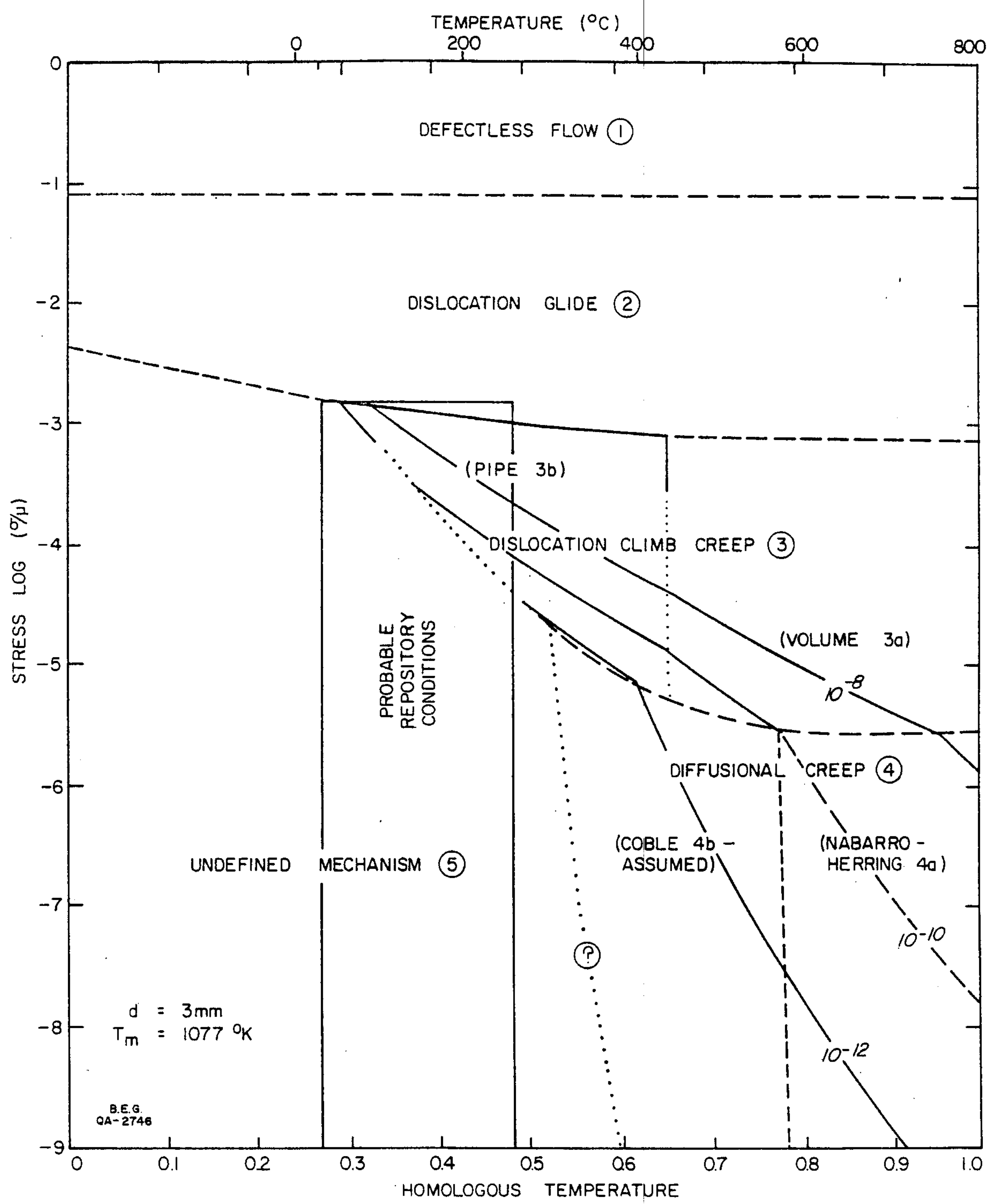

Figure 26. Deformation-mechanism map for salt, including probable repository and storage cavern conditions in cross-hatchured area. Grain size is constant at 3 mm. Solid lines between regimes are confirmed by experimental evidence; boundaries shown as dashed lines are based on calculations of constitutive equations; boundaries shown as dotted lines are based on interpolation or extrapolation; questions marks on boundaries mean the location is based on conjecture only (after Munson, 1979).

provided constitutive equations for each regime, a complete treatment of those equations is beyond the scope of this report and is largely repetitive with the preceding section.

Defectless Flow--Regime 1

At the theoretical shear strength (derived from calculations of atomic bonding strengths), a crystal of salt will deform even though it is initially without defects. Stress above the theoretical shear strength will produce infinite strain rates and therefore deformation will occur simultaneously throughout the crystal. This stress regime is of little consequence to problems of designing salt storage space or waste repositories because of the very high stress levels in regime 1.

Dislocation Glide--Regime 2

Salt deformation by dislocation glide occurs along several slip systems that permit deformation by dislocation motion. Slip systems listed in decreasing order of importance are $\{110\}\langle 1\bar{1}0\rangle$, $\{100\}\langle 110\rangle$, $\{111\}\langle 1\bar{1}0\rangle$. Dislocation glide along these systems is hindered by particles of other mineralogical phases, grain boundaries, and by forest dislocations (Munson, 1979). As glide continues, dislocations stack up at locations where flow is hindered; this results in work (or strain) hardening and an increase in flow stress.

Dislocation Climb Creep--Regime 3

Dislocation climb creep is controlled by the equilibrium processes of dislocation climb and polygonization that leads to steady-state creep. Munson (1979) further defined two subregimes of higher and lower temperatures--volume diffusion and pipe diffusion, respectively. At higher temperatures, the creep processes are controlled by volume diffusion of Cl^- ions. For dislocation climb in salt both Na^+ and Cl^- ions must be supplied to the dislocation jog, but the slower diffusing ion Cl^- controls the rate of the process. This is the reason why the Weertman expression (1) uses the gas constant R in the equation for steady-state creep. At lower temperatures the limiting factor of volume diffusion of Cl^- ions is replaced by a more rapid pipe diffusion of Cl^- ions along dislocations as the controlling process.

Diffusional Creep--Regime 4

Diffusional creep is grain shape changes--strain--by selective transportation of material (Munson, 1979). According to Munson (1979) diffusional creep includes two mechanisms: (1) Nabarro-Herring creep (stress-induced bulk vacancy diffusion of Carter and Hansen, 1983) if transport is by volume diffusion and (2) Coble creep (grain-boundary diffusion of Carter and Hansen, 1983) if transport is by grain-boundary diffusion. Carter and Hansen (1983) note that fine-grained metals and ceramics undergo these processes at low stresses when near melting. However, they say these processes have not been observed in rocks. The boundary between subregimes is a function of grain size. The Nabarro-Herring regime of creep vanishes in favor of Coble creep for grains with a diameter less than 0.33 mm (Munson, 1979).

Undefined Mechanism--Regime 5

The undefined mechanism(s) falls into the low stress, low temperature region of greatest interest to designing storage facilities and waste repositories. The mechanism is difficult to analyze and its boundaries are poorly constrained. There is a clear and pressing need for additional laboratory and in situ studies to understand the nature of the mechanism and the stress/temperature conditions of its activity, especially at the low temperature and stress field of repository or storage cavern conditions.

Discussion

The preceeding section of the behavior of rock salt points out how poorly understood are the mechanical properties of salt and creep mechanisms under in situ conditions. Predictions of cavern closure that were based on empirical calculations are not universally applicable. There is no consensus on how salt grain size, salt-stock permeability, and foliation within the stock influence creep properties. Recently recognized is the critical role that small amounts of intercrystalline water play in weakening salt (that is, accelerating salt creep) by recrystallization through fluid-film-assisted-grain boundary diffusion.

Even the best laboratory experiments are seriously flawed by inadequacies in experiment duration, sample size, and in the ability of the experiment to mimic in situ conditions. There is an obvious need for refined experiments based on in situ and site-specific data. Such data are available from core studies, from analysis of structures and textures within core, and from borehole and cavern closure studies.

SALT STOCK PROPERTIES

The in situ structure, stratigraphy, and physical properties of salt in Texas salt domes are known from a few cores and from observations at two salt mines (Kleer Mine--Grand Saline dome, and Hockley salt mine--Hockley dome). Internal boundary-shear zones, foliation, bedding, associated mineral phases, moisture content, grain size, porosity, and permeability are properties that will influence the geometry and long-term stability of solution-mined caverns. In this section we discuss aspects on internal geometry of salt structures from analysis of core from Bryan Mound salt dome.

Bryan Mound Salt Dome

Thirteen cores (with 610 ft [180 m] of recovered salt) from Bryan Mound dome are housed at the Bureau of Economic Geology Well Sample Library. The U.S. Department of Energy is storing crude oil in preexisting brine caverns at Bryan Mound dome. Future plans include creating 12 additional storage caverns. The cores were recovered for site-specific data on mechanical and physical properties of salt at Bryan Mound dome (Bild, 1980; Wawersik and others, 1980; Price and others, 1981).

Bryan Mound dome is in Brazoria County 0.5 mi (1.2 km) from the Gulf of Mexico. Bryan Mound dome is circular with a nearly planar salt stock--cap-rock interface at a depth of 1,100 ft (335 m). Table 3 lists the core holes and data on foliation, grain size, bedding, and depth.

Salt grain size varied from 0.04 inches (1 mm) to 4.0 inches (100 mm). Bild (1980) reports average grain size is 0.33 inches (8.5 mm). Dark laminations, owing to disseminated anhydrite crystals, were common in cores 1A, 106B, 106C, 109A, 110A, but were rare to absent in cores 104A, 108B, 108C, 109B, and 110C. Bild (1980) reports the cores contain 1.9 to 6.1 weight-percent anhydrite.

The orientation and intensity of foliation (schistosity) of halite crystals were studied to better understand flow patterns within the salt stock and the extent of recrystallization (fig. 27). Two trends are clear: (1) in shallow cores (above a depth of 2,500 ft; 762 m) the foliation tends to be weak or absent, whereas in deep cores (below a depth of 3,000 ft; 914 m) the foliation is strong and (2) preferred orientation of foliation changes from near vertical below a depth of 3,500 ft (1,067 m) to an inclination of 20 to 30 degrees (measured from vertical axis of the core) above a depth of 3,000 ft (914 m). The average dip in the seven deepest wells is 12 degrees, whereas the

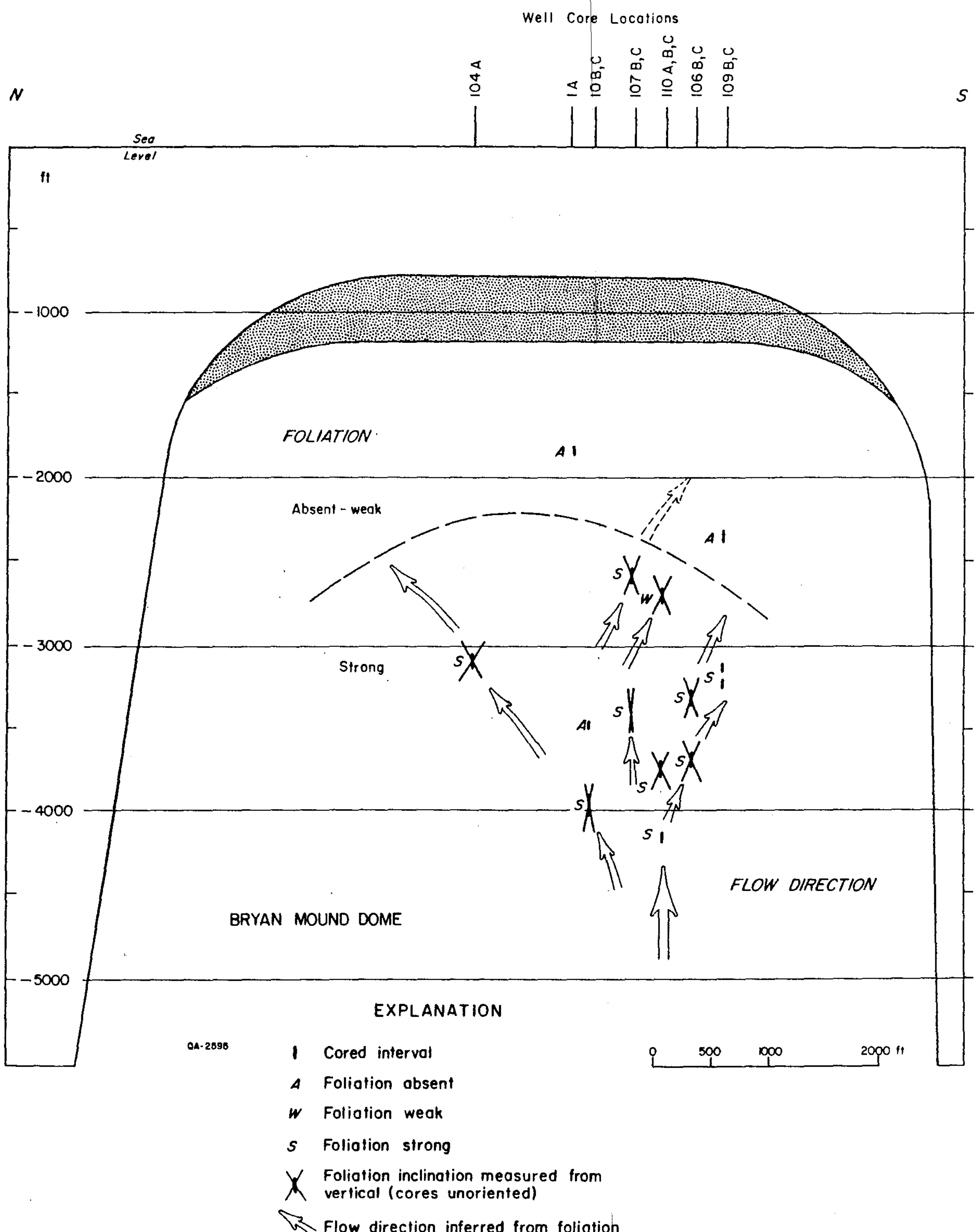

Figure 27. Cross section, Bryan Mound dome, showing core locations and foliation. Angle of foliation decreases from vertical in deepest core to 20 to 30 degrees from vertical (no azimuth orientation) in shallow core. Flow direction is inferred to change from near vertical in deep parts of stock to more lateral flow in upper parts of stock.

Table 3. Analysis of Salt Core--Bryan Mound Salt Dome

CORE	FOLIATION	ORIENTATION (degrees)	GRAIN SIZE Fine = <6 mm Medium = 6-20 mm Coarse = 21-50 mm Very Coarse = > 50 mm	BEDDING	DEPTH (FT)
1A	absent		medium-coarse	dark anhydrite common; inclined 15-30°	1800-1850
104A	strong	30°	coarse	absent	3063-3095
106B	strong	20°	medium	gray anhydrite; vertical	3275-3314
106C	weak-strong	25°	medium	gray anhydrite;vertical	3660-3692
107B	strong	20°	medium-coarse	gray anhydrite; rare, vertical	2520-2589
107C	strong	05°	medium-very coarse	gray anhydrite; rare, vertical	3367-3427
108B	absent		fine	absent	3480-3483
108C	strong	10°	medium	absent	3920-3977
109A	absent-weak	0?	medium	thin, gray anhydrite; inclined 10°	2324-2384
109B	weak to strong	0	coarse-very coarse	absent	3133-3251
110A	weak	25°	medium	thin, gray, anhydrite; inclined 10-35°	2660-2712
110B	strong	25°	medium	rare anhydrite; vertical	3740-3777
110C	strong	0	medium	absent	4139-4180

average dip of the foliation in the three shallowest cores is 25 degrees. Photographs of the whole core illustrate some of these features (fig. 28).

Two processes are considered to be important with respect to foliation in salt domes. Foliation is basically the elongation of individual crystals. The long axis of foliation is oriented along the axis of least principal stress. The direction of salt flow within the diapir controlled the orientation of the resultant foliation. Recrystallization tends to destroy foliation by removing the accumulated strain history.

The record of foliation at Bryan Mound salt dome can be fit into a simple flow model based on near vertical salt flow from deeper areas of the diapir where foliation is near vertical. Lateral spreading of salt at shallower levels near the diapir crest causes foliation to depart from the vertical. Jackson and Dix (1981) presented a more complex model of salt flow at Oakwood dome which is also applicable to Bryan Mound dome. Lateral salt flow near the diapir crest is by multiple emplacement of salt tongues. The salt tongues progressively refold older salt tongues. True azimuth orientation of the foliation at Bryan Mound dome could not be determined because the cores were unoriented. The absence of any definable salt stratigraphy also made it impossible to determine the nature of the folding.

Foliation is absent or weak in shallow salt samples because recrystallization has removed the strain (E). The strong foliation of the deep samples indicates these deep samples are at present still highly strained (elongation may approach 20 percent). The timing of the strain application is unknown. Recrystallization at Bryan Mound dome occurs down to a depth of 2,000 ft (610 m) to 2,500 ft (762 m). This depth is 750 ft (220 m) to 1,250 ft (381 m) below the cap rock-salt interface. A similar recrystallization phenomenon was described for salt core from Oakwood dome (Dix and Jackson, 1982). At Oakwood

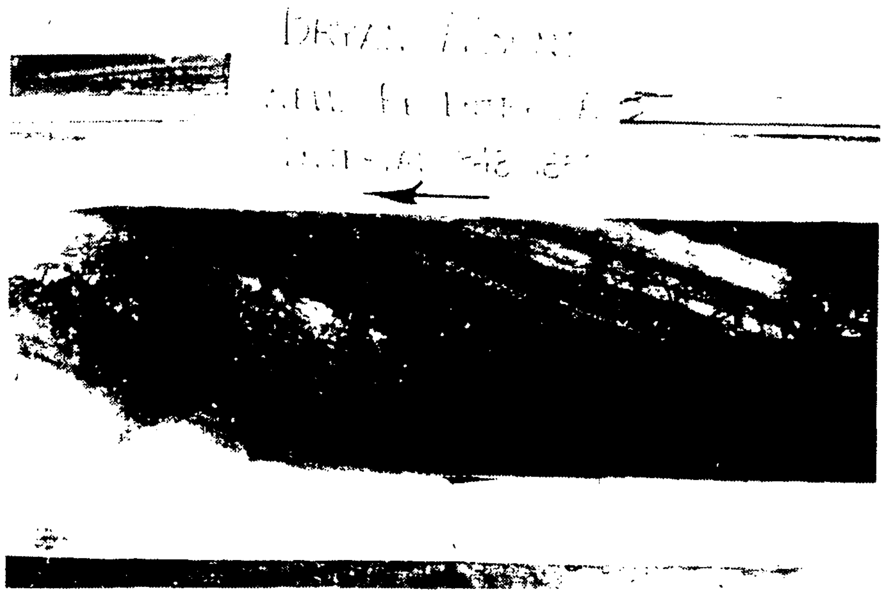

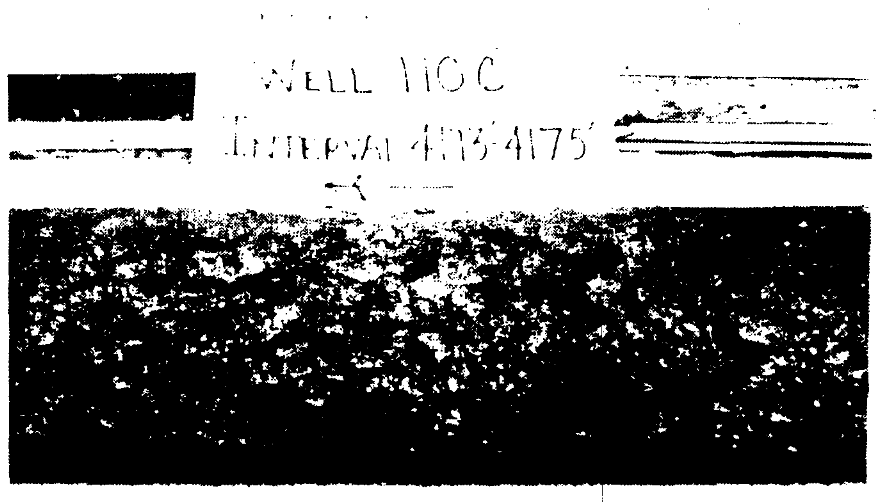

Figure 28. Photographs of core, Bryan Mound dome, showing variations in grain size and foliation. Core 1A at -1,848 ft is well bedded with dark anhydrite layers and unfoliated; core 110C at -4,173 ft shows no bedding and vertical foliation.

dome, recrystallization occurred at depth of 1,168 ft (356 m), only about 2 ft (0.6 m) below the cap-rock--salt-stock interface.

Discussion

The stability of a solution-mined cavern undoubtedly would be influenced by foliation owing to the elongation of grain boundaries and cleavage planes in the direction of foliation. These boundaries and planes are the avenues for fluid flow. However, the magnitude of the influence is unknown. The absence of foliation would seem to be more favorable for stability of underground openings than highly foliated and strained rock salt. The absence of foliation indicates recrystallization under relatively strain-free conditions. Minute amounts of intercrystalline water are thought to promote halite recrystallization by grain boundary diffusion (Spiers and others, 1984). Thus, if recrystallization was facilitated by small amounts of water, then this water must have penetrated a substantial distance through the upper part of the salt stock. Our data indicate that at Bryan Mound dome this ingress seeped down the 750 ft to 1,250 ft from the cap-rock contact or migrated in laterally from the dome flanks. Aufricht and Howard (1961) noted that the addition of small amounts of water to rock salt reduced the permeability in most cases to near zero. However, this positive aspect of moisture content in salt is also saddled with a negative aspect. Water greatly increases the plasticity (creep) of rock salt. Salt glaciers in Iran show peak strain rates of $1.9 \times 10^{-9}\ s^{-1}$ after rainfall events (Talbot and Rogers, 1980). There has only recently been controlled laboratory experiments on the influence of moisture in salt creep and viscosity (Spiers and others, 1984).

CAP ROCK

Domal cap rocks have a significant effect on the stability of a salt dome and an intradomal solution-mined cavern (Dix and Jackson, 1982). Lost-circulation zones especially at the cap-rock--salt-stock interface are among the aspects of cap rocks which could negatively affect dome and cavern stability. In this section we will provide data on cap-rock mineralogy and lost-circulation zones.

Cap rocks are primarily a residual accumulation of anhydrite particles left after a portion of the crest of the salt stock was dissolved. Cap rocks are mineralogically complex and in addition to anhydrite they contain calcite, gypsum, sulfur, celestite, dolomite, Zn-, Pb-, and Fe-sulfides, petroleum, and other minor constituents. This mineralogical complexity stems from a number of cap-rock forming processes (Bodenlos, 1970) in addition to simple salt solution. These processes include (1) hydration of anhydrite to gypsum; (2) reaction of anhydrite and/or gypsum with petroleum and sulfate-reducing bacteria to produce calcite and hydrogen sulfide; (3) vertical migration of metalliferous deep-basin brines into porous cap rock precipitating metallic sulfides (marcasite, sphalerite, pyrite, and other minerals) in reduced zones owing to the presence of hydrogen sulfide (Price and others, 1983); and (4) oxidization of hydrogen sulfide to sulfur.

Examples of the complex mineralogy of domal cap rock are seen in core from Hockley, Long Point, and Boling domes. Massive Zn- and Pb-sulfide concentrations at Hockley dome triggered a significant exploration effort (Price and others, 1983). The Bureau of Economic Geology will receive from Marathon Minerals approximately 40,000 ft (12,000 m) of core from this exploration. Long Point dome was cored for sulfur exploration (M and S Lease Wells 5, 14, 15). These cores show a similar mineralogical complexity with that of Hockley dome. Four mineralogical zones are recognized in core from Long Point dome: (1) a calcite zone with sulfur (depth 628-644 ft; 191-196 m), (2) an anhydrite-gypsum zone with rare sulfur (depth 644-815 ft; 196-248 m); (3) a broken calcite zone containing sulfur and sulfides (depth 815-855 ft; 248-261 m), and (4) an anhydrite sand and gypsum zone (depth 855-865 ft; 261-264 mm).

Banding and fractures in the anhydrite-gypsum zone (depth 719-720 ft; 219.2-219.5 m) are shown in figure 29A. Mineralogical relationships and vuggy fractures in the broken calcite zone (depth unknown) are shown in figure 29B. Vugs and fracture porosity are especially common in the calcite zones. Visual estimates of effective porosity range from 5 to 15 percent. Fractures are 0.02-0.2 inches (0.5-5 mm) wide, but weathering during outdoor storage has enlarged fractures. Some fractures are orthogonal sets oriented 45 degrees to the vertical axis of the core.

Sulfur is a secondary fracture- and vug-filling mineral. Unidentified metallic sulfide minerals are also concentrated in the calcite zones. The paragenesis and diagenesis of cap rocks remain to be examined in detail. An especially critical need is identification of factors controlling formation and distribution of fractures and vugs in the cap rocks.

Cap-Rock--Lost-Circulation Zones

Cap-rock--lost-circulation zones are areas of enhanced porosity and permeability within cap rocks. The porosity in these zones may be either fracture controlled, cavernous, or intergranular. These zones are common in cap rocks of salt domes in the Houston diapir province and are particularly thick in cap rock of Barbers Hill dome. Wells are completed through lost-circulation zones with a series of procedures designed to mitigate the problem of lost circulation. However, 137 storage caverns in Barbers Hill salt dome indicate successful completion through this problem area. The long-term effect of fluids

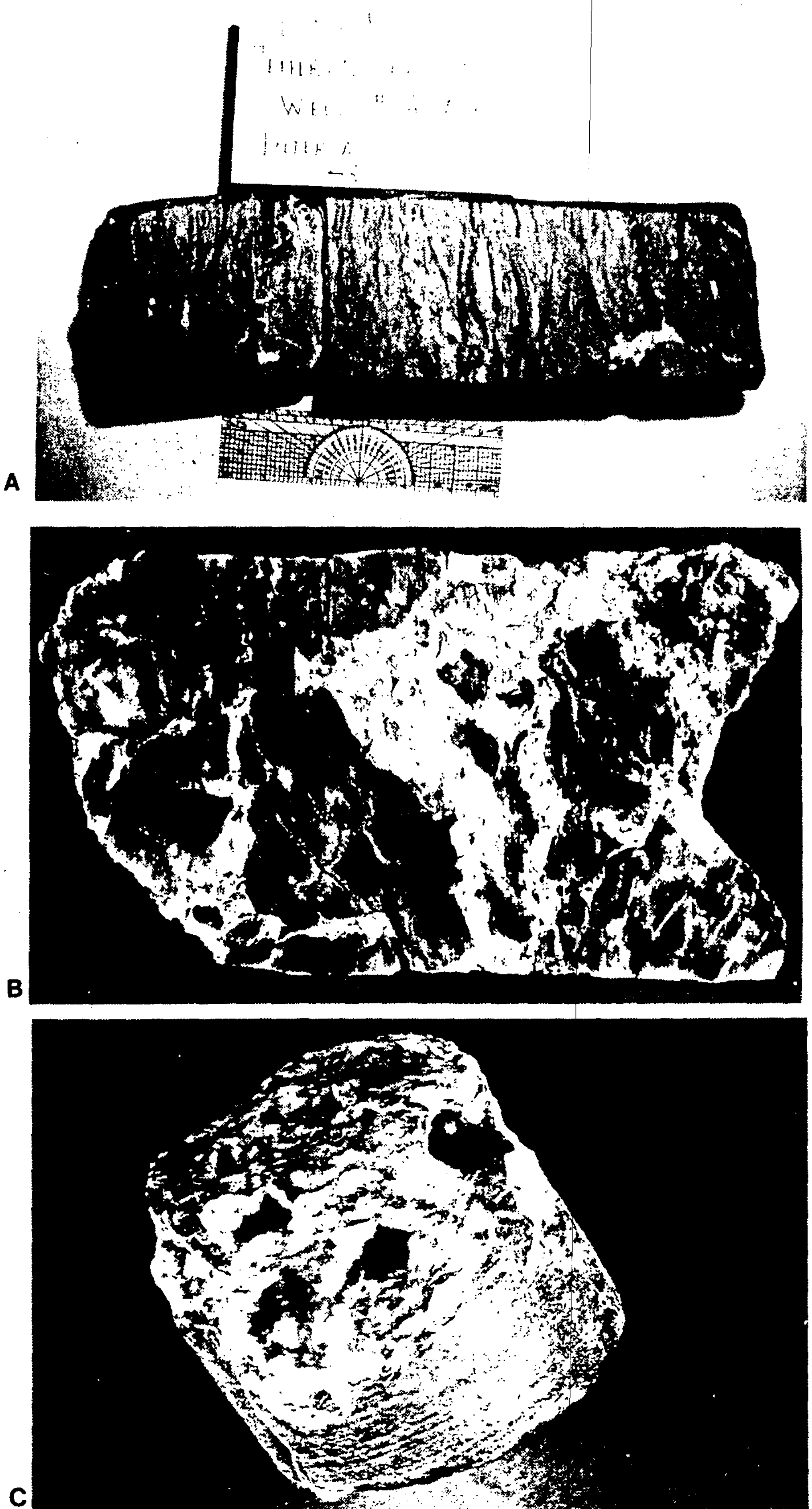

Figure 29. Photographs of core from cap rock, A. Long Point dome, showing mineralogical variations and fractures, B. Long Point dome showing sulfur and fractures, C. Boling dome showing sulfur and vugs.

? Effect is unknown
1.5 Bbls - Barbers Hill

within lost-circulation zones on the cements of casing strings remains unknown. The following section covers lost-circulation zones in Barbers Hill dome cap rock. The information is from cap rock-injection wells for brine disposal. Appendix 3 lists cap-rock injection wells with injection interval and the year the injection permit was approved by the Texas Railroad Commission. Lithology of the actual injection interval is often unspecified. Well depth and location are used to infer the lithology of the injection zone. Most wells clearly inject into cap rock; however, some wells that inject into supradomal or flank sandstones may be included.

Barbers Hill dome is in northwest Chambers County 30 mi (50 km) east of Houston. Barbers Hill dome is nearly circular, with a very planar contact (salt mirror) between the salt and cap rock. A thick (greater than 20 ft; 6 m) anhydrite sand comprises the lost-circulation zone over the flat crest of the salt-cap-rock interface.

An estimated 1.5 billion barrels of salt water have been disposed by injection into lost-circulation zones at Barbers Hill dome. Various zones within the cap rock have been permitted to receive this brine including (1) upper cap-rock gypsum zone, (2) upper and lower cap rock, (3) upper cap-rock gypsum zone and basal anhydrite sand, (4) basal anhydrite sand, and (5) deep flank cap rock and deep flank sandstone. The distribution of these injection intervals is shown in figure 30. The shallowest injection is into the upper cap-rock gypsum zone in the area over the central part of the dome. Brine is injected at a depth of 800-1,560 ft (244-475 m) into the basal anhydrite sand around the periphery of the salt dome. The vertical extent of these lost-circulation zones is shown with stylized cavern geometries in figure 31. Appendix 1C lists well information for caverns and disposal wells.

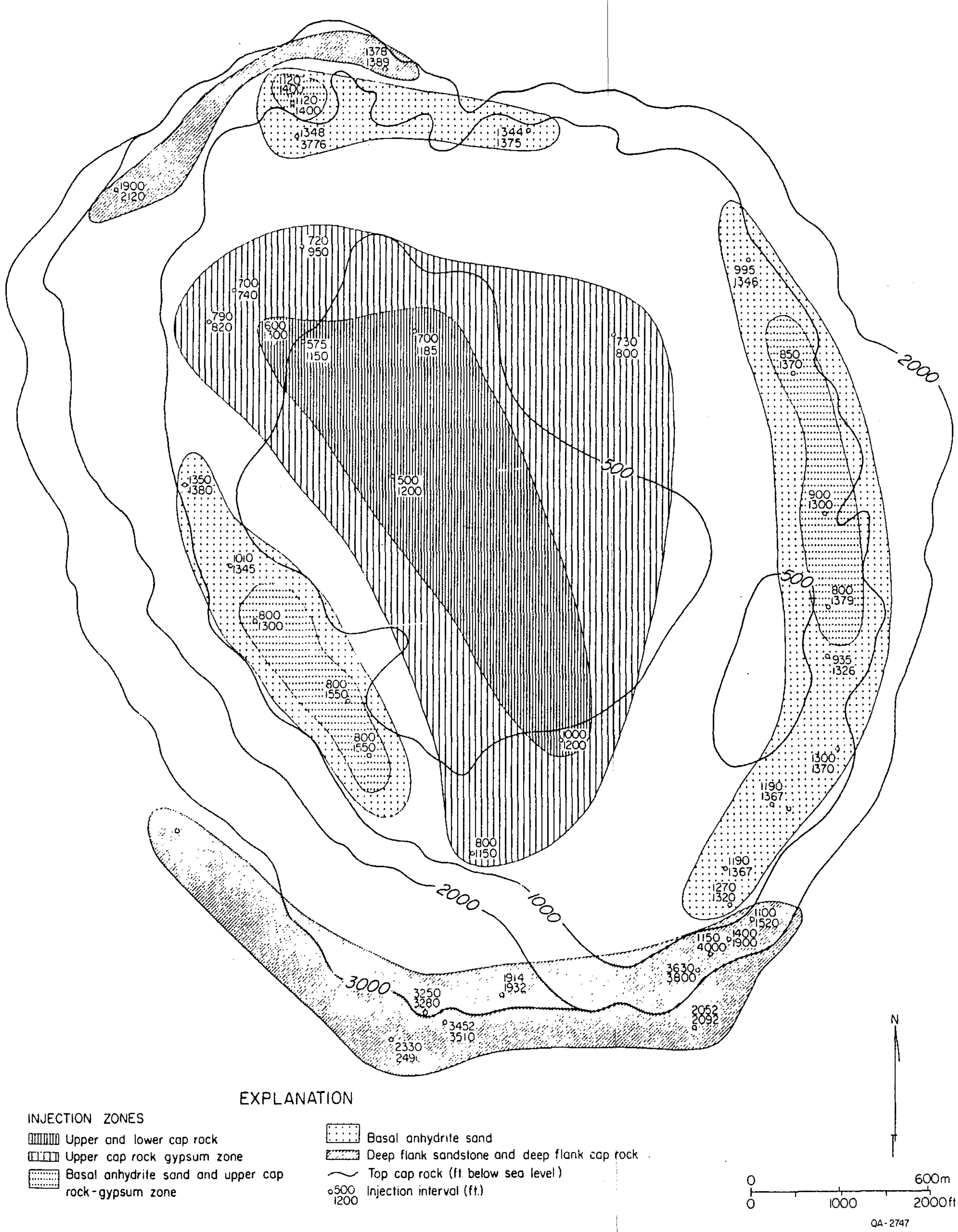

Figure 30. Map of cap-rock injection zones, Barbers Hill dome. Injection into shallow cap rock is over central part of dome, whereas injection into basal anhydrite sand is around periphery of dome.

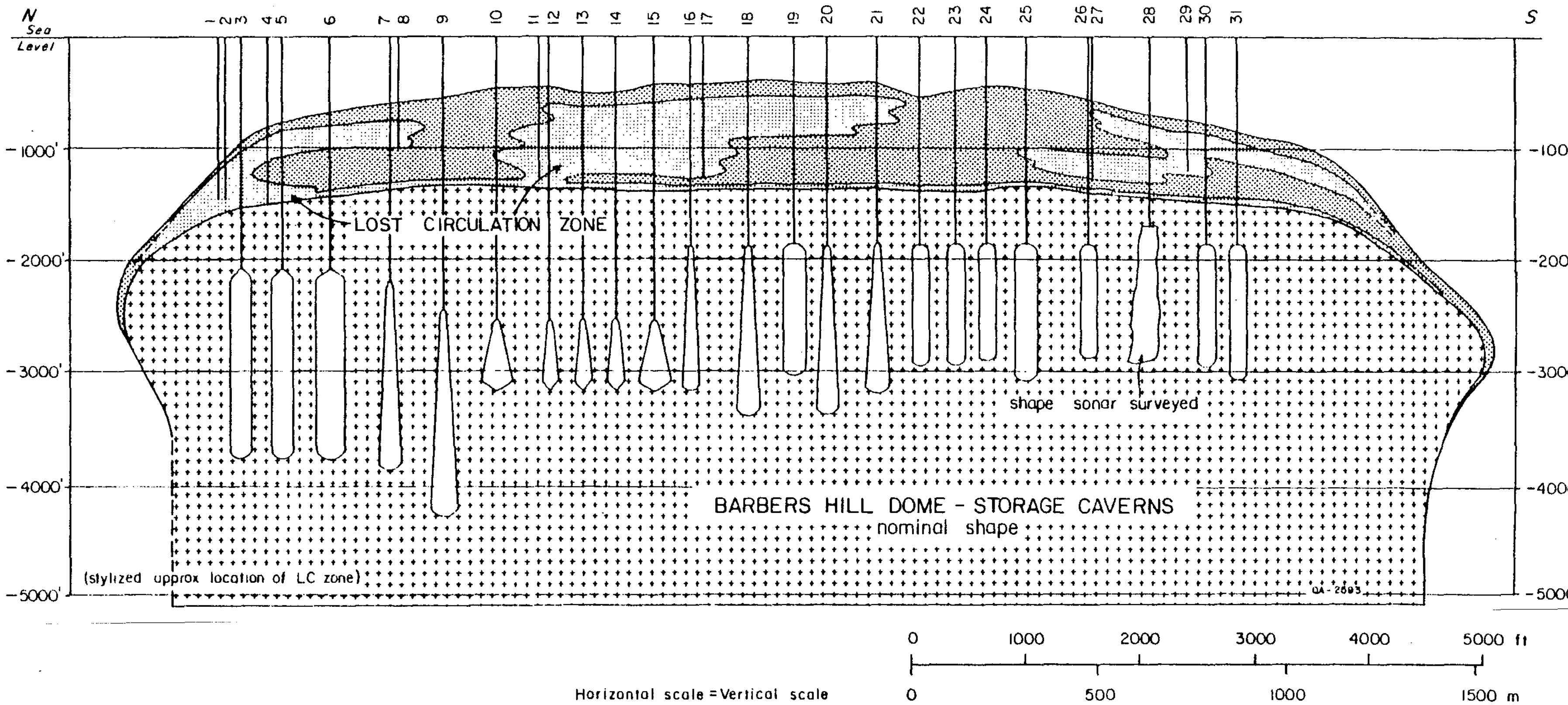

Figure 31. Cross section, Barbers Hill dome, and cap rock showing lost-circulation zones and stylized cavern geometries. Map shows location of caverns in relation to line of section and boundary of salt stock. Appendix 1C lists cavern and injection well names.

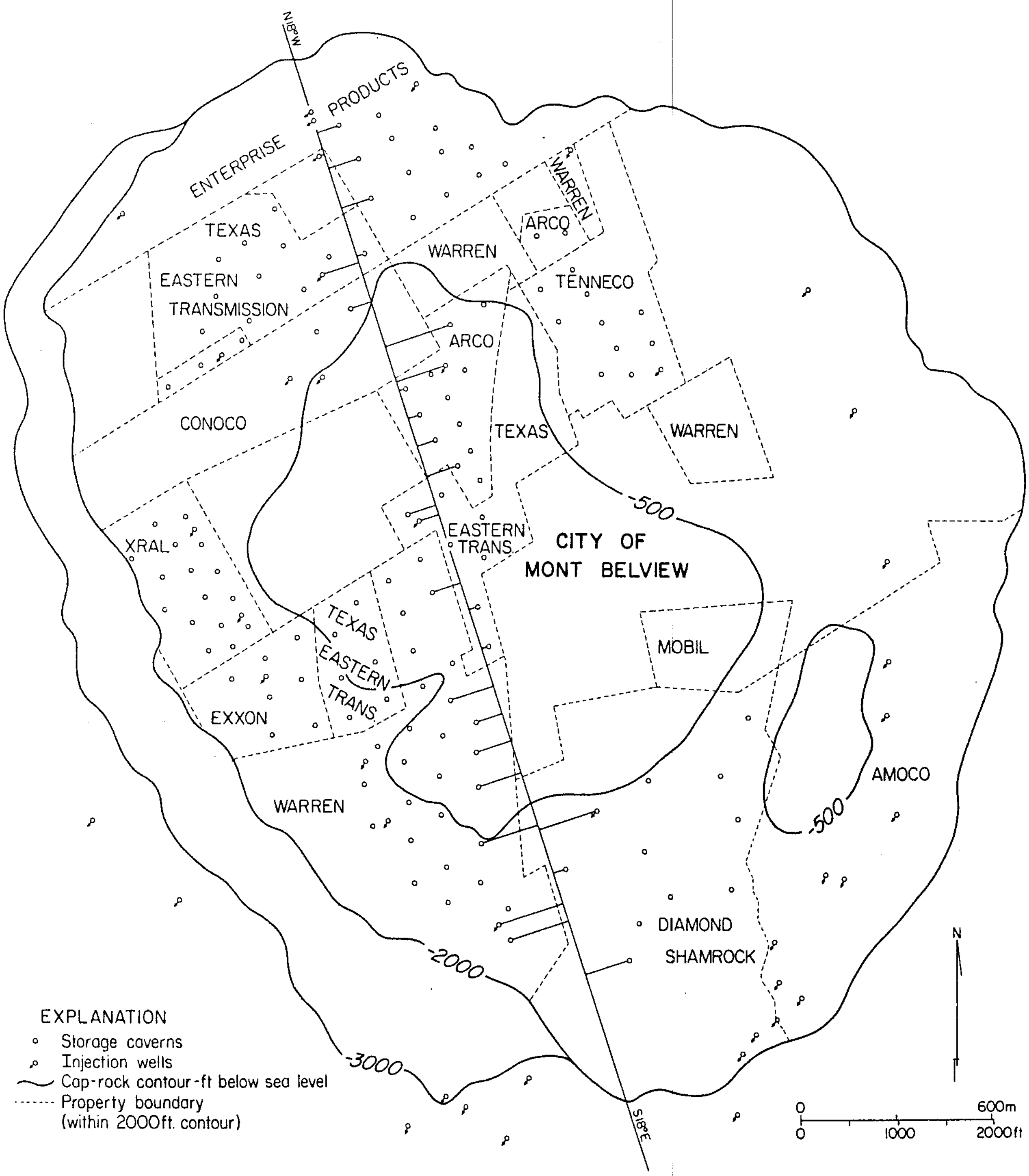

N18°W
ENTERPRISE PRODUCTS
WARREN
TEXAS
ARCO
WARREN
EASTERN
TENNECO
TRANSMISSION
ARCO
CONOCO
TEXAS
WARREN
-500
XRAL
EASTERN
TRANS.
CITY OF
MONT BELVIEW
TEXAS
EASTERN
TRANS.
MOBIL
EXXON
AMOCO
WARREN
-500
DIAMOND
SHAMROCK
-2000
N
EXPLANATION
Storage caverns
Injection wells
Cap-rock contour-ft below sea level
Property boundary
(within 2000ft. contour)
-3000
S18°E
0
600m
0
1000
2000ft

(continued)

The brine is injected either by design or by accident into the upper cap-rock zones over the central part of the dome and is injected into progressively deeper middle and lower cap-rock zones over the peripheral areas of the dome. The influence of this injection scheme on cap-rock hydrogeology and salt dissolution is unknown and unstudied.

Discussion

Cap rocks sheath the upper parts of salt stocks and commonly project into shallow zones where the ground water is circulating most rapidly. Cap rocks are mineralogically complex, and many are faulted, brecciated, highly porous, and permeable. Cap rocks by virtue of their location are the focus of a diversity of geologic processes of which those associated with ground water are of the greatest concern.

Research to date on Texas cap rocks has shown that many Gulf Coast salt dome cap rocks (for example, Barbers Hill and Boling salt domes) are characterized by highly porous and permeable lost-circulation zones, whereas some East Texas cap rocks (for example, Oakwood salt dome) do not have such zones substantiated by a drilling record. Clearly, site-specific data on cap rocks of candidate domes are needed to answer questions on whether cap-rock processes could affect negatively toxic-waste disposal in salt caverns. Such questions include (1) geometry, orientation, and activity of cap-rock faults and (2) the nature and origin of porosity and permeability within cap rocks and within cap-rock lost-circulation zones. Hydrogeologic aspects of cap rocks are clearly one of the highest concerns for toxic-waste disposal. Within cap rocks, potentiometric surface levels, direction of ground-water flow, and interconnection of porous zones are necessary concerns; such data are easily compiled and computed from a series of water level measurements and tests which are in the planning stage.

ACKNOWLEDGMENTS

Funding for this research was provided by the Texas Department of Water Resources under Interagency Contract No. (84-85)-1019. Drs. E. G. Wermund and M. P. A. Jackson critically reviewed the manuscript; their comments are gratefully acknowledged. Thanks are extended to Texas Railroad Commission personnel Mark Browning (Central Records) and J. W. Mullican (Underground Injection Control), who provided easy access to records and files. Discussions with the following industry representatives were very helpful: Kermit Allen, Jose Machado, and Edward Voorhees (Fenix and Scisson, Inc.), Neils Van Fossan (Texas Brine Company), Noe Sonnier and Ferris Samuelson (Texas Gulf Sulfur), Carl Brassow (United Resource Recovery, Inc.), Jack Piskura (Pakhoed, Inc.), and Bill Ehni and Mark Katterjohn (Geotronics Corporation). Word processing was done by Ginger Zeikus, under the supervision of Lucille C. Harrell. Mark Bentley, Tom Byrd, Jeff Horowitz, Jamie McClelland, and Richard Platt drafted the figures, under the supervision of Dick Dillon.

REFERENCES

Aufricht, W. F., and Howard, K. C., 1961, Salt characteristics as they affect storage of hydrocarbons: Journal of Petroleum Technology, v. 13, no. 8, p. 733-738.

Baar, C. A., 1971, Creep measured in deep potash mines vs. theoretical predictions: 7th Canadian Rock Mechanics Symposium, University of Alberta, Edmonton, Canada, p. 23-77.

_______ 1977, Applied salt-rock mechanics I, the in situ behavior of salt rocks: Developments in Geotechnical Engineering, v. 16A, 294 p.

Bild, R. W., 1980, Chemistry and mineralogy of samples from the Strategic Petroleum Reserve: Sandia National Laboratories, SAND-80-1258, 51 p.

Bodenlos, A. J., 1970, Cap-rock development and salt-stock movement, in Kupfar, D. H., ed., Geology and technology of Gulf Coast salt domes: School of Geosciences, Louisiana State University, Baton Rouge, Louisiana, p. 73-86C.

Burke, P. M., 1968, High temperature creep of polycrystalline sodium chloride: Ph.D. dissertation, Stanford University, Stanford, California, 112 p.

Carter, N. L., and Hansen, F. D., 1983, Creep of rocksalt: Tectonophysics, v. 92, p. 275-333.

Dawson, P. R., 1979, Constitutive models applied in the analysis of creep of rock salt: Sandia Laboratories, SAND-79-0137, 47 p.

Dix, O. R., and Jackson, M. P. A., 1982, Lithology, microstructures, fluid inclusions, and geochemistry of rock salt and of the cap-rock contact in Oakwood Dome, East Texas: significance for nuclear waste storage: The University of Texas at Austin, Bureau of Economic Geology Report of Investigations No. 120, 59 p.

Dreyer, W., 1972, The science of rock mechanics, Vol. 1: Tran. Tech. Publications, p. 29-164.

Empson, F. M., Bradshaw, R. L., McClain, W. C., and Houser, B. L., 1970, Results of the operation of Project Salt Vault: a demonstration of disposal of high-level radioactive solids in salt: III Symposium on Salt, v. 10, p. 455-462.

Ewing, M., and Ewing, J. L., 1962, Rate of salt-dome growth: American Association of Petroleum Geologists Bulletin, v. 46, no. 5, p. 708-709.

Ewing, T. E., 1983, Growth faults and salt tectonics in the Houston diapir province--relative timing and exploration significance: Gulf Coast Association of Geological Societies, v. 33, p. 83-89.

_______, compiler, in preparation, Tectonic map of Texas: The University of Texas at Austin, Bureau of Economic Geology, scale 1:750,000.

Fernandez, G. M., and Hendron, A. J., 1984, Interpretation of a long-term in situ borehole test in a deep salt formation: Bulletin of the Association of Engineering Geologists, v. 21, no. 1, p. 23-38.

Hansen, F. D., and Carter, N. L., 1980, Creep of rocksalt at elevated temperatures: Proceedings of the 21st U.S. Symposium on Rock Mechanics, Rolla, Mississippi, p. 217-226.

Hansen, F. D., and Carter, N. L., 1980, Mechanical behavior of Avery Island halite: a preliminary analysis: RE/SPEC, Inc., Rapid City, South Dakota, prepared for the Office of Nuclear Waste Isolation, ONWI-100, 37 p.

Hansen, F. D., and Mellegard, K. D., 1980, Quasi-static strength and deformational characteristics of domal salt from Avery Island, LA: RE/SPEC, Inc., Rapid City, South Dakota, prepared for the Office of Nuclear Waste Isolation, ONWI-116, 86 p.

Heard, H. C., 1972, Steady-state flow to polycrystalline halite at pressures of 2 kilobars, in Heard, H. C., Borg, I. Y., Carter, N. L., and Raleigh, C. B., editors, Flow and fracture of rocks: American Geophysical Union Monograph Series, v. 16, p. 191-210.

Herrmann, W., and Lauson, H. S., 1981a, Review and comparison of transient creep laws used for natural rock salt: Sandia National Laboratories, SAND-81-0738, 62 p.

______ 1981b, Analysis of creep data for various rock salts: Sandia National Laboratories, SAND-81-2567, 96 p.

Herrmann, W., Wawersik, W. R., and Montgomery, S. T., 1982, Review of creep modeling for rock salt: Sandia National Laboratories, SAND-82-2178C, 9 p.

Hume, H. R., and Shakoor, A., 1981, Mechanical properties, in Gevantman, L. H., ed., Physical properties data for rock salt: U.S. Department of Commerce National Bureau of Standards, Monograph 167, p. 103-203.

Jackson, M. P. A., 1984, Natural strain in diapiric and glacial salt, with emphasis on Oakwood Dome, East Texas: The University of Texas at Austin, Bureau of Economic Geology Report of Investigations No. 143.

Jackson, M. P. A., and Dix, O., 1981, Geometric analysis of macroscopic structures in Oakwood salt core, in Kreitler, C. W., and others, Geology and geohydrology of the East Texas Basin: a report on the progress of nuclear waste isolation feasibility studies (1980): The University of Texas at Austin, Bureau of Economic Geology Geological Circular 81-7, p. 177-182.

Jackson, M. P. A., and Seni, S. J., 1984a, Atlas of salt domes of the East Texas Basin: The University of Texas at Austin, Bureau of Economic Geology Report of Investigations No. 140, 102 p.

_______ 1984b, Suitability of salt domes in the East Texas Basin for nuclear-waste isolation: final summary of geologic and hydrogeologic research (1978-1983): The University of Texas at Austin, Bureau of Economic Geology Geological Circular 84-1, 129 p.

Le Comte, P., 1965, Creep in rock salt: Journal of Geology, v. 73, p. 469-484.

Martinez, J. D., and others, 1978, An investigation of the utility of Gulf Coast salt domes for the storage or disposal of radioactive wastes, Volume I: Louisiana State University, Institute for Environmental Studies, Contract Report EW-78-C-05-5941/53, 390 p.

McVetty, P. G., 1934, Working stresses for high temperature service: Mechanical Engineering, v. 56, p. 149.

Mellegard, K. D., Senseny, P. E., and Hansen, F. D., 1983, Quasi-strength and creep characteristics of 100 mm-diameter specimens of salt from Avery Island, Louisiana: Prepared for U.S. Department of Energy, Office of Nuclear Waste Isolation, Battelle Memorial Institute, Columbus, OH, ONWI-250, 210 p.

Munson, D. E., 1979, Preliminary deformation-mechanism map for salt: Sandia National Laboratories, SAND-79-0076, 37 p.

Obert, L., 1964, Deformational behavior of model pillars made from salt, trona, and potash ore: Proceedings of the VI Symposium on Rock Mechanics, Rolla, Missouri, p. 539-560.

Odé, H., 1968, Review of mechanical properties of salt relating to salt dome genesis: Geological Society of America Special Publication 88, p. 543-595.

Paterson, M. S., 1978, Experimental rock deformation--the brittle field: New York, Springer-Verlag, 254 p.

Preece, D. S., and Stone, C. M., 1982, Verification of finite element methods used to predict creep response of leached salt caverns: 23rd U.S. Rock Mechanics Symposium, University of California, Berkeley, California, p. 655-663.

Price, P. E., Kyle, J. R., and Wessel, G. R., 1983, Salt-dome related zinc-lead deposits, in Kisvarsanyi, G., and others, eds., Proceedings, International Conference on Mississippi Valley-type lead-zinc deposits: University of Missouri, Rolla, p. 558-571.

Price, R. H., Wawersik, W. R., Hannum, D. W., and Zirzow, J. A., 1981: Sandia National Laboratories, SAND-81-2521, 46 p.

Reynolds, T. D., and Gloyna, E. F., 1961, Creep measurements in salt mines, in Mining Engineering Series--Proceedings of the 4th Symposium on rock mechanics, 1961: Pennsylvania State University Mineral Industries Experimental Station Bulletin, v. 76, p. 11-17.

Sannemann, D., 1968, Salt stock families in northwestern Germany: American Association of Petroleum Geologists Memoir 8, p. 261-270.

Seni, S. J., Hamlin, H. S., and Mullican, W. F., III, 1984, Texas salt domes: natural resources, storage caverns, and extraction technology: The University of Texas at Austin, Bureau of Economic Geology, report prepared for Texas Department of Water Resources under interagency contract no. IAC (84-85)-1019, 161 p.

Seni, S. J., and Jackson, M. P. A., 1983a, Evolution of salt structures, East Texas diapir province, Part I: Sedimentary record of halokinesis: American Association of Petroleum Geologists Bulletin, v. 67, no. 8, p. 1219-1244.

Seni, S. J., and Jackson, M. P. ., 1983b, Evolution of salt structures, East Texas diapir province, Part II: Patterns and rates of halokinesis: American Association of Petroleum Geologists Bulletin, v. 67, no. 8, p. 1245-1274.

______ 1984, Sedimentary record of Cretaceous and Tertiary salt movement, East Texas Basin: times, rates, and volumes of salt flow and their implications for nuclear-waste isolation and petroleum exploration: The University of Texas at Austin, Bureau of Economic Geology Report of Investigations No. 139, 89 p.

Seni, S. J., Mullican, W. F., III, and Hamlin, H. S., 1984a, Texas salt domes: natural resources, storage caverns, and extraction technology: The University of Texas at Austin, Bureau of Economic Geology, report prepared for Texas Department of Water Resources under interagency contract no. IAC (84-85)-1019, 161 p.

Seni, S. J., Mullican, W. F., III, and Ozment, R. W., 1984, Computerized inventory of data on Texas salt domes: The University of Texas at Austin, Bureau of Economic Geology, report prepared for Texas Department of Water Resources under interagency contract no. IAC (84-85)-1019, 34 p.

Senseny, P. E., 1983, Review of constitutive laws used to describe the creep of salt: RE/SPEC, Inc., Rapid City, South Dakota, prepared for the Office of Nuclear Waste Isolation, ONWI-295, 59 p.

Serata, S., and Gloyna, E. F., 1959, Development of design principle for disposal of reactor fuel waste into underground salt cavities: University of Texas, Austin, Reactor Fuel Waste Disposal Project.

Spiers, C. J., Urai, J. L., Lister, G. S., and Zwart, H. J., 1984, Water weakening and dynamic recrystallization in salt (abs.): Geological Society of America, 97th Annual Meeting, v. 16, no. 6, p. 665.

Talbot, C. J., and Jarvis, R. J., in press, Dynamics, budget, and age of an active salt extrusion in Iran: Journal of Structural Geology.

Talbot, C. J., and Rogers, E. Q., 1980, Seasonal movements in a salt glacier in Iran: Science, v. 208, no. 4442, p. 395-397.

Thoms, R. L., Mogharrebi, M., and Gehle, R. M., 1982, Geomechanics of borehole closure in salt domes: Gas Processors Association, Proceedings of 61st Annual Convention, Dallas, Texas, p. 228-230.

Verral, R. A., Fields, R. J., and Ashby, M. F., 1977, Deformation mechanism maps for LiF and NaCl: Journal of The American Ceramic Society, v. 60, no. 5-6, p. 211-216.

Wagner, R. A., Mellegard, K. D., and Senseny, P. E., 1982, Influence of creep law form on predicted deformations in salt: 23rd U.S. Rock Mechanics Symposium, University of California, Berkeley, California, p. 684-691.

Wawersik, W. R., Holcomb, D. J., Hannum, D. W., and Lauson, H. B., 1980, Quasi-static and creep data for dome salt from Bryan Mound, Texas: Sandia National Laboratories, SAND-80-1434, 37 p.

Wenkert, D. D., 1979, The flow of salt glaciers: Geophysical Research Letters, v. 6, no. 6, p. 523-526.

Weertman, J., 1968, Dislocation climb theory of steady-state creep: ASM Transactions Quarterly, v. 61, p. 681.

Weertman, J., and Weertman, J. R., 1970, Mechanical properties, strongly temperature-dependent, _in_ Cahn, R. W., ed., Physical metallurgy: Amsterdam, North-Holland, p. 983-1010.

Appendix 1A. Well Information for Maps

Well Number	Operator	Fee	Field
		Brazoria County	
1	Sun Co.	#5 Wisch-Saint Unit	Pledger
2	Sun Co.	#6 Wisch-Saint Unit	Pledger
3	Exxon Co. U.S.A.	#2 Pledger Gas Unit 3	Pledger
4	Pennzoil Prod. Co.	#5 McFarland	Pledger
5	Pennzoil Prod. Co.	#3 McFarland	Pledger
6	Pennzoil Prod. Co.	#4 McFarland	Pledger
7	Southwest Gas Prod. Co.	#1 McDonald	West Columbia
8	Humble Oil and Refining Co.	#1 Pledger Gas Unit 7	Pledger
9	Humble Oil and Refining Co.	#1 L. Carter	Pledger
10	Stanolind Oil and Gas Co.	#1 W. T. Robertson	West Columbia
11	Southern Prod. Co. Inc.	#30 Pledger Gas Field Unit Well	Pledger
12	Gulf Oil Corp.	#1 Link Fee	Damon Mound
13	Rowan Drilling Co.	#1 Krause	West Columbia
14	Pan American Prod. Co.	#1 N. W. Hopkins	Damon Mound
15	John F. Merrick	#3 Bryan Estate	Damon Mound
16	Delin Taylor Oil Do.	#1 L. Becker	West Columbia
17	Caroline Hunt Trust Est.	#1 M. T. Pratt	West Columbia
18	Texas Gulf Sulphur Co.	#1 M. T. Pratt	West Columbia
		Chambers County	
2	M. T. Halbouty	#1 Gilbert	Barbers Hill
3	H. S. Cole Jr. and Harrell Drlg. Co.	#1 K. Williams	West Columbia
4	The Texas Co.	#3 Kirby Oil and Gas	Barbers Hill
5	The Texas Co.	#1 Whaley	Barbers Hill
6	General Crude Oil Co.	#1 Nash Fee	West Columbia
7	British Texas Oil Co.	#1 Barber	Barbers Hill
8	Gas Producers Enterprises Inc.	#1 P. C. Ulrich	West Columbia
9	The Superior Oil Co.	#1 O. Z. Smith	Barbers Hill
10	Humble Oil and Refining Co.	#B-1 B. Dutton	West Columbia
11	The Texas Co.	#1 A. A. Davis	Barbers Hill
12	The Texas Co.	#1 Kirby Petroleum Co. NCT	West Columbia
13	M. T. Halbouty	#1 E. Wilburn	West Columbia
14	Kirby Petroleum Co.	#1 Kirby Pet. Co. Fee Tr. 8	West Columbia
15	The Texas Co.	#1 K. Fitzgerald	Barbers Hill
16	The Texas Co.	#2 Kirby Oil and Gas	Barbers Hill
17	Sunray Oil Co.	#C-2 F. W. Harper	Barbers Hill
18	Stanolind Oil and Gas Co.	#33 Chambers County	Barbers Hill
19	Stanolind Oil and Gas Co.	#19 Chambers County	Barbers Hill
20	Marine Contractors Supply Co.	#1 Collier Heirs	Barbers Hill
21	Mills Bennett Estate	#17 E. E. Barrow	Barbers Hill
22	C. L. Chambers	#1 Schilling-Lillie	Barbers Hill

Appendix 1A. (cont.)

Well Name	Operator	Fee	Field
		(Chambers County-continued)	
24	Texas Eastern Transmission Co.	#7 M. Belview Storage Well	Barbers Hill
25	Humble Oil and Refining Co.	#5 L.P.G. Storage Well	Barbers Hill
26	Texas Eastern Transmission Co.	#5-10 Storage Well	Barbers Hill
27	The Texas Co.	#1 Kirby Oil and Gas Co.	Barbers Hill
28	Sierra	#1 Trichel	Barbers Hill
29	Sunray-Mid Continent Oil Co.	#A-8 Barber	Barbers Hill
30	The Texas Co.	#1 J. M. Fitzgerald Est.	Barbers Hill
31	Harrison and Gilger	#2 A. E. Barber	Barbers Hill
32	Otis Russel	#1 Blaffer-Farrish	Barbers Hill
35	Kirby Petroleum Co.	#1 Wilburn	West Columbia
37	Warren Petroleum Co.	#13 M. Belvieu Storage	M. Belvieu Term.
38	Sun Oil Co.	#23 J. Wilburn	Barbers Hill
39	Warren Petroleum Co.	#3 Caprock Disposal	Barbers Hill
40	Warren Petroleum Co.	#11 Mt. Belvieu	Barbers Hill
41	Sunray-DX Oil Co.	#D-5 E. W. Barber	Barbers Hill
42	Texas Gulf Prod. Co.	#3-5 L. E. Fitzberald	Barbers Hill
43	Texas Butadiene Co.	#1 Texas Butadiene	Barbers Hill
44	Humble Oil and Refining Co.	#1 M. Belvieu Storage Facility	Barbers Hill
45	Houston Oil and Minerals Corp.	#12 Chambers County Agricultural Co.	Barbers Hill
46	Sun Oil Co.	#A-1 Higgins	Barbers Hill
47	Humble Oil and Refining Co.	#B-9 Kirby Petroleum Co. Fee	Barbers Hill
48	Texas Eastern Transmission Co.	#11 Storage Well NT	Barbers Hill
49	Humble Oil and Refining Co.	#11 Kirby Fee	Barbers Hill
50	Humble Oil and Refining Co.	#B-14 Kirby	Barbers Hill
51	Texas Gulf Producing Co.	#15 Kirby "A"	Barbers Hill
52	Texas Gulf Producing Co.	#A-11 A. E. Barber	Barbers Hill
53	Pan American Petroleum Co.	#37 Chambers County Agriculture Co.	Barbers Hill
54	R. A. Welch	#2 Barrow Fee	Barbers Hill
55	Mills Bennett Estate	#16 Barrow	Barrows Fee
56	M. T. Halbouty & Hurt Oil Co.	#1 Kirby Oil & Gas	Barbers Hill
57	Lloyd H. Smith Inc.	#1 Claude Williams	Barbers Hill
58	Admiral Drilling Co.	#1 Williams	West Columbia
59	John W. Mecom	#3-B Mayes	West Columbia
		Fort Bend County	
20	John B. Coffee	#4 Texas Gulf Sulphur	Boling
21	Coastal Minerals Inc.	#C-37 J. R. Farmer	Boling
22	Coastal Minerals Inc.	#C-35 J. R. Farmer	Boling
23	Coastal Minerals Inc.	#1 J. Byrne	Boling
24	Grover J. Geiselman	#1 Richter-Warncke Gas Unit	Needville
25	Grover J. Geiselman	#1 Leissner	Needville
26	Acoma Oil Corp.	#1-B Farmer	Boling
27	Callery and Hurt	#1 Kasparek	Boling
28	Allied Minerals	#1 E. C. Farmer	Boling
29	Callery and Hurt	#3 Kasparek	Boling

Appendix 1A. (cont.)

Well Name	Operator	Fee	Field
		(Fort Bend County-continued)	
30	Callery and Hurt	#2 Kasparek	Boling
31	Callery and Hurt	#2 Texas Gulf Sulphur	West Columbia
32	Caddo Oil Co.	#1 Gaidosik	West Columbia
33	Grover J. Geiselman	#1 Steffek Gas Unit	Needville
34	Grover J. Geiselman	#1 Schwettmann	West Columbia
35	Grover J. Geiselman	#1 Hardin-Roesler Gas Unit	Needville
36	H. M. Amsler	#1 Dance	Needville
37	Exxon Co. U.S.A.	#87 Lockwood and Sharp "A"	Thompson
38	Grover J. Geiselman & General Crude Oil Co.	#1 P. Kueck	West Columbia
39	Powers Prod. Co. & T. T. Drlg. Co.	#1 J. R. Farmer	Needville
40	Fort Bend Oil Co.	#1 J. M. Moore Est.	West Columbia
41	Scurlock Oil Co. & M. T. Halbouty	#1 D. Krause	Beasley
42	Bilbo-Redding Drlg. Co.	#1 G. B. Leaman et al.	West Columbia
43	General Crude Oil Co.	#1 Stavinoma	West Columbia
44	Grover J. Geiselman	#1 Schendel Gas Unit	Needville
45	Slade Oil and Gas Inc.	#1 S. B. Kennelly	West Columbia
46	Houston Oil and Minerals	#1 J. M. Moore	West Columbia
47	The Oil and Gas Company	#1 Byrne	West Columbia
		Harris County	
34	The Texas Co.	#1 Mrs. E. K. Busch Est.	West Columbia
60	Pan American Petroleum Corp.	#1 A. Schoeps Oil Unit 1	West Columbia
		Liberty County	
1	M. T. Halbouty	#E-1 Kirby Petroleum Co.	West Columbia
33	General Crude Oil Co.	#B-3 Colby	West Columbia
36	General Crude Oil Co.	#D-1 Moores Bluff	West Columbia
		Matagorda County	
1	Rowan Drlg. Co. & Texas Gulf Prod. Co.	#1 C. Mason	West Columbia
2	So Belle and So Belle	#1 Le Tulle	West Columbia
3	J. M. Huber Corp. & M. S. Cole, Jr. & Son	#1 S. V. Le Tulle	West Columbia
4	M. T. Williams	#1 C. B. Fisher et al.	West Columbia
5	Placid	#1 Le Tulle	West Columbia
6	Bright and Schiff	#1 Camp	West Columbia
7	Texas Gulf Sulphur Co. and Goodell Pet. Co.	#1 W. D. Cornelieus Est.	Markham
8	Shannon Oil and Gas, Inc.	#1 Kountze-Couch	Markham

Appendix 1A. (cont.)

Well Number	Operator	Fee	Field
		(Matagorda County-continued)	
9	Seadrift Pipeline Corp.	#2 Fee	Markham
10	Petroleum Ventures of Texas	#2 Sun Fee	Markham
11	Hamill and Hamill	#1 Sisk and Trull	Markham
12	Shannon Oil and Gas, Inc.	#1 Sun Fee	Markham
13	Holly Energy, Inc.	#1 Hurlbutt	West Columbia
14	The Texas Co.	#1 E. M. Hurlbutt NCT	West Columbia
15	Kennedy and Mitchell, Inc.	#4-207 Buckeye	West Columbia
16	G. P. Johnson and Co.	#1 M. Doman et al.	West Columbia
17	Woodward and Co.	#1 Pierce Ranch	West Columbia
18	The Texas Co.	#1 Hiltpold	West Columbia
19	Robinson Oil and Gas Co.	#1 Anderson	West Columbia
20	Continental Oil Co.	#1 W. W. Fondren, Jr. et al.	West Columbia
21	Michael T. Halbouty	#1 M. E. Crouch	West Columbia
22	Bradco Oil and Gas Co.	#1 E. Burkhart et al.	West Columbia
23	Geier-Jackson et al.	#1 C. C. Sherill	West Columbia
24	Stanolind Oil and Gas Co.	#1 Hawes-Vineyard	West Columbia
25	Falcon Seaboard Drlg. Co.	#1 F. C. Cornelius	West Columbia
26	Lenoir M. Josey Inc. & J. B. Coffee	#1 G. S. Reifslager	West Columbia
27	Sun Oil Co.	#2 St. Louis	West Columbia
28	Lario Oil and Gas Co. and Felmont Oil Corp.	#1 Lewis	West Columbia
29	Natomas North America, Inc.	#1 Cornelius	West Columbia
30	Union Oil	#1 Grady	West Columbia
31	Barron Kidd	#1 E. Krenek	West Columbia
32	J. M. Huber Corp.	#1 A. Copecet	West Columbia
33	Julian Evans	#1 Stasta	West Columbia
34	Davis Oil Co.	#1 Hickl Gas Unit	West Columbia
35	W. M. Harrison	#1 S. Le Tulle Rugeley	West Columbia
36	La Gorce Oil Co.	#1 H. D. Madsen	West Columbia
37	Rowan Drlg. Co. and Texas Gulf Co.	#1 Stovall	West Columbia
38	Goodale, Bertman and Co., Inc.	#1 Northern Ranch	West Columbia
39	Mid-Century Oil and Gas Co.	#1 F. W. Howard "A"	West Columbia
40	Z. W. Falcone and Bay City Drlg. Co.	#1 Kountze and Couch	Arch
41	Phillips Petroleum Co.	#1 Matagorda	West Columbia
42	Ada Oil Co.	#1 G. F. Stovall	West Columbia
43	J. Ray McDermott	#1 H. L. Brown	West Columbia
44	Sun Oil Co.	#4 First National Bank	Midfield
45	Superior Oil Co.	#1 D. K. Poole	El Maton
46	Sun Oil Co.	#1 C. Jumek	West Columbia
47	Coastal States Gas Prod. Co.	#1 H. R. Ferguson	West Columbia
48	Monsanto Chemical Co.	#1 Newmont	El Maton
49	Monsanto Chemical Co.	#2 Fee	El Maton
50	Roy R. Gardner	#1 B. W. Trull	West Columbia
51	Coastal States Gas Prod. Co.	#1 Cornelius	Tidehaven
52	Coastal States Gas Prod. Co.	#2 Cornelius	Tidehaven
53	Humble Oil and Refining Co.	#B-1 J. C. Lewis	Duncan Slough

Appendix 1A. (cont.)

Well Number	Operator	Fee	Field
		(Matagorda County-continued)	
54	The Texas Co.	#1 Denman-Kountze NCT-1	Markham
55	Hamill and Hamill	#20 C. M. Hudson	Markham
56	Claude B. Hamill and C. B. Hamill Trust	#27 Howard Smith	Markham
57	Lenoir M. Josey Inc.	#1 Pierce Ranch	West Columbia
58	Jack W. Frazier and J. B. Ferguson	#1 Pierce Est.	West Codlumbia
		Wharton County	
1	Texas Gulf Sulphur Co.	#41 Abendroth	Boling
2	Texas Gulf Sulphur Co.	#32 O. W. Abendroth	Boling Dome
3	Texas Gulf Sulphur Co.	#33 O. W. Abendroth	Boling Dome
4	Texas Gulf Sulphur Co.	#30 O. W. Abendroth	Boling Dome
5	Texas Gulf Sulphur Co.	#39 Abendroth	Boling
6	Texas Gulf Sulphur Co.	#23 Banker Jr.	Boling Dome
7	Texas Gulf Sulphur Co.	#17-O.W. W. Banker, Jr.	Boling Dome
8	Texas Gulf Sulphur Co.	#18-O.W. W. Banker, Jr.	Boling Dome
9	Texas Gulf Sulphur Co.	#19-O.W. W. Banker, Jr.	Boling Dome
10	Danciger Oil Co.	#3 Mullins	Boling
11	Texas Gulf, Inc.	#18 W. Banker, Jr. "A"	Boling
12	Claude Knight	#2 Fojtik	Boling
13	Otis Russell	#1 M. B. Cloud	Boling
14	Texas Gulf, Inc.	#17-O.W. Chase Trust	Boling
15	Texas Gulf, Inc.	#18 Chase Trust	Boling
16	Texas Gulf, Inc.	#20 Chase Trust	Boling
17	Texas Gulf Sulphur Co.	#16-O.W. Banker Jr. "A"	Boling Dome
18	Texas Gulf Sulphur Co.	#15 O.W. McCarson	Boling Dome
19	Boling Prod. Co., Inc.	#18 A. A. Mullins	Boling
20	Cockburn Oil Corp.	#8 Cockburn Oil Corp.	West Columbia
21	Smith and Smith	#7 Cockburn Oil Corp.	Lane City
22	Goldking Petroleum	#1 M. J. Dupuy	Lane City
23	Prarie Prod. Co.	#5 Blue Creek Ranch	West Columbia
24	Moore and Ahem	#1 Johnson	West Columbia
25	The Atlantic Refg. Co.	#1 Pendergrass	Prasifka
26	Smith and Smith	#1 J. Ziober et ux.	Prasifka
27	Smith and Smith	#1 J. Ziober et ux.	Prasifka
28	Sue-Ann Operating Co.	#1 Vineyard "C"	West Columbia
29	Century Petroleum, Ltd.	#1 Vineyard	West Columbia
30	Chapman Oil Co.	#1 A. M. Brockman	Arrington
31	TexasGulf, Inc.	#20 W. Banker Jr.	Boling
32	Wellco Oil Co.	#3-W F. Sitta	Boling
33	Boling Prod. Co.	#4 M. D. Taylor Est.	Boling
34	Sparta Oil Co. and Mikton Oil Co.	#3 M. D. Taylor	Boling
35	Lyle Cashion Co.	#10 A. A. Mullins	Boling
36	Lyle Cashion Co.	#12 A. A. Mullins	Boling

Well Name	Operator	Fee	Field
		(Wharton County-continued)	
37	Lyle Cashion Co.	#11 A. A. Mullins	Boling
38	Boling Prod. Co.	#8 A. A. Mullins	Boling
39	Texaco Inc.	#3 G. W. Duffy "B"	Blue Basin
40	Danciger Oil and Refining	#1 Mullins	Boling
41	Texas Oil and Gas Corp.	#1 A. Hlavinka "B"	Duffy
42	Texaco Inc.	#4 C. Barton, Jr.	Duffy, South
43	Danciger Oil and Refining Co.	#5 A. A. Mullins	Boling
44	Danciger Oil and Refining Co.	#7 A. A. Mullins	Boling
45	Danciger Oil and Refining Co.	#4 A. A. Mullins	Boling
46	Danciger Oil and Refining Co.	#2 A. A. Mullins	Boling
47	Sparta Oil Co. and Mikton Oil Co.	#2 Taylor	Boling
48	Texas Gulf Sulphur Co.	#11 G. McCarson	Boling
49	Texas Gulf Sulphur Co.	#10 G. McCarson	Boling
50	The Greenbriar Corp.	#4-B J. B. Gary Est.	South Boling
51	The Greenbriar Corp.	#5-B J. B. Gary Est.	South Boling
52	Texas Gulf Sulphur Co.	#A-7 Keller	Boling
53	The Greenbriar Corp.	#3-B J. B. Gary Est.	Boling Dome
54	The Greenbriar Corp.	#1 J. B. Gary Est.	Boling
55	Sisco Oil Co.	#1 E. Hawes	West Columbia
56	Humble Oil and Refining Co.	#B-3 J. B. Gary	Boling
57	W. M. Keck, Jr.	#1 Leissner	West Columbia
58	Brazos Oil and Gas Co. & M. T. Halbouty	#2 Blue Creek Ranch	West Columbia
59	John B. Coffee	#1 G. M. Rauscher	West Columbia
60	Smith and Smith	#D-1 Cockburn Miocene Gas Unit	Magnet-Withers
61	Soloco	#5 Hortman	El Campo North
62	Floyd L. Karsten	#1-B Myatt	Blue Basin
63	Anadarko Prod. Co.	#1 Mangum "A"	West Columbia
64	Humble Oil and Refining Co.	#77 H. C. Cockburn	Magnet-Withers
65	Kilroy Co. of Texas, Inc.	#1 W. H. Banker	West Columbia
66	M. Thompson	#1 J. F. Turner	Boling Dome
67	McKenzie Bros. Oil and Gas Co.	#1 C. Riggs	Boling
68	Gulf Coast Leaseholds, Inc.	#3 Taylor	Iago
69	Layne-Texas Co., Inc.	#1 Trull and Herlin	Water Well
70	Corley and Rice	#1 Gary	West Columbia
71	Mac Drilling Co. and John Mayo	#1 Gary Est.	West Columbia
72	Smith and Smith	#2 Duncan	West Columbia
73	Claude Knight	#1 Fojtik	Boling
74	Neaves Pet. Development Co.	#10 B. M. Floyd	Boling
75	Union Oil Co. of California	#8 C. Riggs	Boling
76	Kirby Petroleum Co.	#1 Dagley	West Columbia
77	Kirby Petroleum Co.	#2 Dagley	West Columbia
78	Roy R. Gardner	#2 R. G. Hawes	Boling
79	J. E. Bishop	#1 E. P. Hawes	Boling
80	Texas Gulf Sulphur Co.	#1 Bassett	Boling
81	The Texas Co.	#1 J. F. D. Moore	West Columbia
82	Davidor and Davidor, Inc.	#1 Moore	West Columbia
83	Standard Oil of Texas	#1 W. M. Meriwether	West Columbia

Appendix 1A. (cont.)

Well Name	Operator	Fee	Field
		(Wharton County-continued)	
84	Getty Oil Co.	#1 Esther Beard	West Columbia
85	Curtis Hankamer	#1 Hobbs and Le Fort	West Columbia
86	The Superior Oil Co.	#1 E. Hawes	West Columbia
87	Sinclair Prairie Oil Co.	#1 Hawes Est.	West Columbia
88	Texas Gulf Sulphur Co.	#2 W. T. Taylor	Boling
89	Cerro De Pasco	#1 Gary Est.	West Columbia
90	Miller and Ritter	#1 C. M. Allen	Boling
91	F. S. Pratt	#1 Fleer	West Columbia
92	Texaco, Inc.	#C-143 Pierce Est.	Magnet-Withers
93	Texaco, Inc.	#C-129 Pierce Est.	Magnet-Withers
94	Humble Oil and Refining Co.	#1 Rogers	Lane City
95	Texas Republic Petroleum Co.	#1 G. R. Hawes	West Columbia
96	R. B. Mitchell	#1 H. C. Cockburn	West Columbia
97	Mac Drilling Co. and John Mayo	#1 Gary Est.	West Columbia

Appendix 1B. Well Information for Cross Sections

Barbers Hill Dome

A - A'

Well No.	Operator	Fee	County
35			Liberty
1			Liberty
7	British Texas Oil Co.	#1 Barber	Chambers
16	The Texas Co.	#2 Kirby Oil and Gas	Chambers
29	Sunray-Mid Continent Oil Co.	A-8 Barber	Chambers
24	Texas Eastern Transmission Co.	#7 Mt. Belview Storage Well S-B	Chambers
40	Warren Petroleum Co.	#11 Mt. Belview	Chambers
45	Houston Oil and Minerals Corp.	#12 Chambers County Agricultural Co.	Chambers
28	Sierra	#1 Trichel	Chambers
10	Humble Oil and Refining Co.	# B-1 B. Dutton	Chambers

B - B'

Well No.	Operator	Fee	County
60	Te		Harris
6	General Crude Oil Co.	#1 Barber	Chambers
51	Texas Gulf Producing Co.	#15 Kirby "A"	Chambers
24	Texas Eastern Transmission Co.	#7 Mt. Belview Storage Well S-B	Chambers
30	The Texas Co.	#1 J. M. Fitzgerald Estate	Chambers
13	M. T. Halbouty	#1 E. Wilburn	Chambers
59	J. W. Mecon	#3-B Mayes	Chambers

Markham Dome

Well No.	Operator	Fee	County
42	Texaco Inc.	#4 C. Barton Jr.	Wharton
39	Texaco Inc.	#3 G. A. Duffy "B"	Wharton
19	Robinson Oil and Gas Co.	#1 Anderson	Matagorda
18	The Texas Co.	#1 Hiltpold	Matagorda
11	Hamill and Hamill	#1 Sisk and Trull	Matagorda
9	Seadrift Pipeline Corp.	#2 Fee	Matagorda
56	C. B. Hamill and C. B. Hamill Trust	#27 H. Smith	Matagorda
55	Hamill and Hamill	#20 C. M. Hudson	Matagorda

Appendix 1B. (continued)

Well No.	Operator	Fee	County
	Markham Dome (continued)		
30	Union Oil Co.	#1 Grady	Matagorda
5	Placid	#1 LeTulle	Matagorda
4	M. T. Williams	#1 C. B. Fisher et al.	Matagorda
	Boling Dome		
41	Scurlock Oil Co. and M. T. Halbouty	#1 D. Krause	Fort Bend
40	Fort Bend Oil Co.	#1 J. M. Moore Est.	Fort Bend
82	Davidor and Davidor, Inc.	#1 Moore	Wharton
81	The Texas Co.	#1 J. F. D. Moore	Wharton
79	J. E. Bishop	#1 E. P. Hawes	Wharton
80	Texas Gulf Sulphur Co.	#1 Bassett	Wharton
39	Mid-Century Oil and Gas Co.	#1 F. W. Howard "A"	Matagorda
24	Stanolind Oil and Gas Co.	#1 Hawes-Vineyard	Matagorda

Appendix 1C. Well Information for Caverns and Salt-Water Disposal Wells at Barbers Hill Salt Dome

Well No.	Operator	Well Name
1	Enterprise Products	Salt-water disposal Well No. 1
2	Enterprise Products	Salt-water disposal Well No. 2
3	Enterprise Products	Cavern Well No. 9
4	Houston Oil and Minerals	Salt-water disposal Well No. 1
5	Enterprise Products	Cavern Well No. 7
6	Enterprise Products	Cavern Well No. 4
7	Texas Eastern Transmission	Cavern Well No. NT-10 LPG
8	Texas Eastern Transmission	Salt-water disposal Well No. 2
9	Conoco	Cavern Well No. 1 UGSW
10	Arco	Cavern Well No. 8 LPG
11	Arco	Salt-water disposal Well No. 1B
12	Arco	Cavern Well No. 3 LPG
13	Arco	Cavern Well No. 4 LPG
14	Arco	Cavern Well No. 6 LPG
15	Arco	Cavern Well No. 11 LPG
16	Texas Eastern Transmission	Cavern Well No. S-8 LPG
17	Texas Eastern Transmission	Salt-water disposal Well No. 1
18	Texas Eastern Transmission	Cavern Well No. S-4 LPG
19	Warren	Cavern Well No. 25 LPG
20	Texas Eastern Transmission	Cavern Well No. S-3 LPG
21	Texas Eastern Transmission	Cavern Well No. S-2 LPG
22	Warren	Cavern Well No. 17 LPG
23	Warren	Cavern Well No. 2 LPG
24	Warren	Cavern Well No. 1 LPG
25	Warren	Cavern Well No. 5 LPG
26	Warren	Cavern Well No. 7 LPG
27	Diamond Shamrock	Salt-water disposal Well No. D-1
28	Diamond Shamrock	Cavern Well No. 2
29	Warren	Salt-water disposal Well No. 3
30	Warren	Cavern Well No. 22 LPG
31	Diamond Shamrock	Cavern Well No. 12

Appendix 2. Conversion tables for stress units, length units (Paterson, 1978), and time.

Example 1 bar = 14 503 pounds per square inch.

	Bars	Kilobars (kbar)	Dynes per square centimeter (dyn/cm^2)	Atmospheres (atm)	Kilograms per square centimeter (kg/cm^2)	Pounds per square inch (lb./in.^{2})	Pascals (Pa)	Megapascals (MPa)	Gigapascals (GPa)
Bars	1.0	10^{-3}	10^{6}	0.9869	1.0197	14.503	10^{5}	10^{-1}	10^{-4}
Kilobars	10^{3}	1.0	10^{9}	0.9869×10^{3}	1.0197×10^{3}	14.503×10^{3}	10^{8}	10^{2}	10^{-1}
Dynes per square centimeter	10^{-6}	10^{-9}	1.0	0.9869×10^{-6}	1.0197×10^{-6}	14.503×10^{-6}	10^{-1}	10^{-7}	10^{-10}
Atmospheres	1.0133	1.0133×10^{-3}	1.0133×10^{6}	1.0	1.0333	14.695	1.0133×10^{5}	0.1013	1.0133×10^{-4}
Kilograms per square centimeter	0.9807	0.9807×10^{-3}	0.9807×10^{6}	0.9678	1.0	14.223	0.9807×10^{5}	0.9807×10^{-1}	9.807×10^{-5}
Pounds per square inch	6.895×10^{-2}	6.895×10^{-5}	6.895×10^{4}	6.805×10^{-2}	7.031×10^{-2}	1.0	6.895×10^{3}	6.895×10^{-3}	6.895×10^{-6}
Pascals	10^{-5}	10^{-8}	10	0.9869×10^{-5}	1.0197×10^{-5}	14.503×10^{-5}	1.0	10^{-6}	10^{-9}
Megapascals	10	10^{-2}	10^{7}	9.869	10.197	145.03	10^{6}	1.0	10^{-3}
Gigapascals	10^{4}	10	10^{10}	0.9869×10^{4}	1.0197×10^{4}	14.503×10^{4}	10^{9}	10^{3}	1.0

Conversion table for length units

Example: 1 meter = 3.281 feet.

	Centimeters	Inches	Feet	Meters	Kilometers	Miles
Centimeters	1.0	0.3937	0.0328	0.01	10^{-5}	6.215×10^{-6}
Inches	2.540	1.0	0.0833	0.0254	2.54×10^{-5}	1.578×10^{-5}
Feet	30.48	12.0	1.0	0.3048	3.048×10^{-4}	1.894×10^{-4}
Meters	100.0	39.37	3.281	1.0	10^{-3}	6.215×10^{-4}
Kilometers	10^{5}	3.937×10^{4}	3281	10^{3}	1.0	0.6215
Miles	1.609×10^{5}	63360	5280	1609	1.609	1.0

Conversion table for time units

	Seconds (s)	Minutes	Hours	Days	Months	Years
seconds	1×10^{0}	6.0×10^{1}	3.6×10^{3}	8.64×10^{4}	2.63×10^{6}	3.16×10^{7}

Appendix 3. Cap-rock injection data for domes in Texas.

Dome	Operator/Well No./Lease	Injection Interval	RRC Permit Date
Day	International Underground Storage, 3 G.P. Day	2450 - 2550	1964
	International Underground Storage, 1 LPG Pure Oil	2400 - 2500	1964
Fannett	Warren, 15 I.R. Bordages, et al. "A"	2115 - 2145	1971
	Gulf, 3 SWD I.R. Bordages, et al. "A"	unknown	
	TX Gulf Sulphur, 1 SWD I.R. Bordages, et al. "A"	unknown	
	TX Gulf Sulphur, 2 SWD I.R. Bordages, et al. "A"	unknown	
Hull	Magnolia, 2 SWD Hull Underground Storage	700 - unknown	1956
	Magnolia, 3 SWD Hull Underground Storage	702 - unknown	1956
	Sinclair, 5-A SWD Dolbear Fee	700 - 800	1962
	J.W. Mecom, 1 Elsie Taylor	1150 - 1181	1967
	Texaco, 2-F H.G. Camp Fee	700 - 860	1969
	R.V. Ratts, 1 Jim Best	800 - 820	1974
	T. True, 1 Fuel Oil Manufacturing Plant	400 - 700	1974
	Gulf, 2 SWD J.W. Canter "A" Fee	700 - 710	1975
Markham	Texas, 7 SWD H. Smith Fee	1594 - 1736	1959
	Texaco, 9 N.N. Meyers "E"	2209 - 2334	1959
	Texaco, 24 SWD N.R. Meyers "C"	1950 - 3060	1960
	Texaco, 9 SWD N.R. Meyers "B"	1500 - 2070	1960
	Seadrift, 2 Fee	1400 - 1510	1961
	Seadrift, A-3 Fee	2874 - 3110	1962
	Seadrift, A-3 Fee	1590 - 1930	1976
	Seadrift, A-3 Fee	1590 - 2575	1979
	Seadrift, 1 SWD Fee	1280 - 3300	1977
Moss Bluff	Moss Bluff Storage Venture, 1 SWD Fee	1320 - 3040	1980
	Moss Bluff Storage Venture, 2 SWD Fee	1320 - 3040	1980
	Moss Bluff Storage Venture, 4 SWD Fee	1320 - 3040	1980
Nash	Humble, 2 Mary Svocek	1470 - 1505	1953
	Humble, 1 SWD P. Meier	1900 - 3850	1955
	(2 post-1975 permits, unknown)		
North Dayton	Texaco, 12 J.A. Deering, Jr. "N"	2590 - 2970	1962
	Texaco, 3 J.A. Deering, Jr. "N"	2300 - 2735	1963
	(1 post-1975 permit, unknown)		
Pierce Junction	J.S. Abercrombie, II J. Ritter	1376 - 1378	1951
	Wanda, 2-B Settegast	860 - 1000	1971
	Sparta, 1 J.C. Calvert	1020 - 1060	1972
	Martin, 6 White Head	2890 - 3300	1975
	Coastal States, 1 Almeda Underground Storage	801 - 1000	1983
Orchard	Gulf, 2 J.M. Moore, et al.	478 - 510	1959
	(2 post-1975 permits, unknown)		

Damon Mound may have cap rock injection, but wells, locations, intervals unknown.

Appendix 3. (cont.)

Dome	Operator/Well No./Lease	Injection Interval (feet)	RRC Permit Date
Barbers Hill	Texas Butadiene (Arco), 1-A Fee	750 - 752	1956
	Texas Butadiene (Arco), 1-A Fee	775 - 779	1956
	Tenneco, 1 SWD Mt. Belvieu Storage Terminal	745 - 820	1956
	Tenneco, 1 SWD Mt. Belvieu Storage Terminal	820 - 823	1962
	Houston O & M, 1 SWD Kirby Pet. "B"	1348 - 3776	1964
	Pyndus, 4 Kirby	700 - 740	1964
	Sinclair, 4 J.F. Wilburn	935 - 1326	1967
	Sinclair, 13 Kirby Pet. "A"	1900 - 2120	1967
	Sinclair, 10 Kirby Pet. "B"	995 - 1396	1967
	Sunray DX, 1 E. W. Barber "B"	1379 - 1389	1967
	Mills Bennett Est., 1 SWD Kirby Pet.	850 - 1370	1967
	TX Ntnl. Bank of Comm. Houston, 17 J.F. Wilburn	800 - 1379	1967
	Sun, 1 SWD Higgins	1190 - 1367	1967
	Mills Bennett Est., 1 SWD Gulf Fee Fisher	1100 - 1520	1968
	Universal Pet., 1 Gulf Fee Lee Brothers	1344 - 1375	1969
	Arco, 10 J. F. Wilburn	1300 - 1370	1971
	Sun, 15 SWD Higgins	1270 - 1320	1972
	Sun, 15 SWD Higgins	912 - 1270	1972
	TX Eastern Transmission, 1 SWD L.P.G. Storage	500 - 1200	1973,1975
	TX Eastern Transmission, 1 SWD Fee	650 - 810	1972
	Exxon Pipeline, 1 SWD Fee	1125 - 1300	1974,1975
	Warren, 3-A SWD Fee	800 - 1550	1974
	Conoco, 1 SWD Fee	600 - 1300	1975
	XRAL, 1 SWD Fee	1020 - 1300	1975
	TX Eastern Transmission, 2 SWD Fee	720 - 950	1976
	Warren, 4 SWD Fee	800 - 1550	1976
	Arco, 1-B Fee	750 - 1185	1977
	Warren, 5 SWD Fee	800 - 1500	1977
	XRAL, 2 SWD Fee	1350 - 1380	1978
	Enterprise Products, 1 SWD Mt. Belvieu	1120 - 1400	1978
	Enterprise Products, 2 SWD Mt. Belvieu	1120 - 1400	1978
	Conoco, 2 SWD Fee	575 - 1150	1978
	Mills Bennett Est., 1 SWD J.F. Wilburn "C"	900 - 1300	1979
	Diamond Shamrock, D-1 Fee	1000 - 1200	1979
	Amoco, 50 Chambers County Ag.	1400 - 1900	1979
Big Hill	Pure, 1 Fee	830 - 845	1956
	Goodale, Bertman, & Co., 7 TX Exploration	1070 - 1475	1965
	Pan Am, 19 TX Exploration	1460 - 3300	1968
	(2 post-1975 permits, unknown)		
Blue Ridge	L.D. French, II Robinson-Bashare	2435 - 2700	1969
	Ramco, I Wist & Schenck	1980 - 2090	1972
Boling	Cecil Hagen, 6 A.C. Mich	2052 - 2085	1950
	(4 post-1975 permits, unlocated & unknown)		